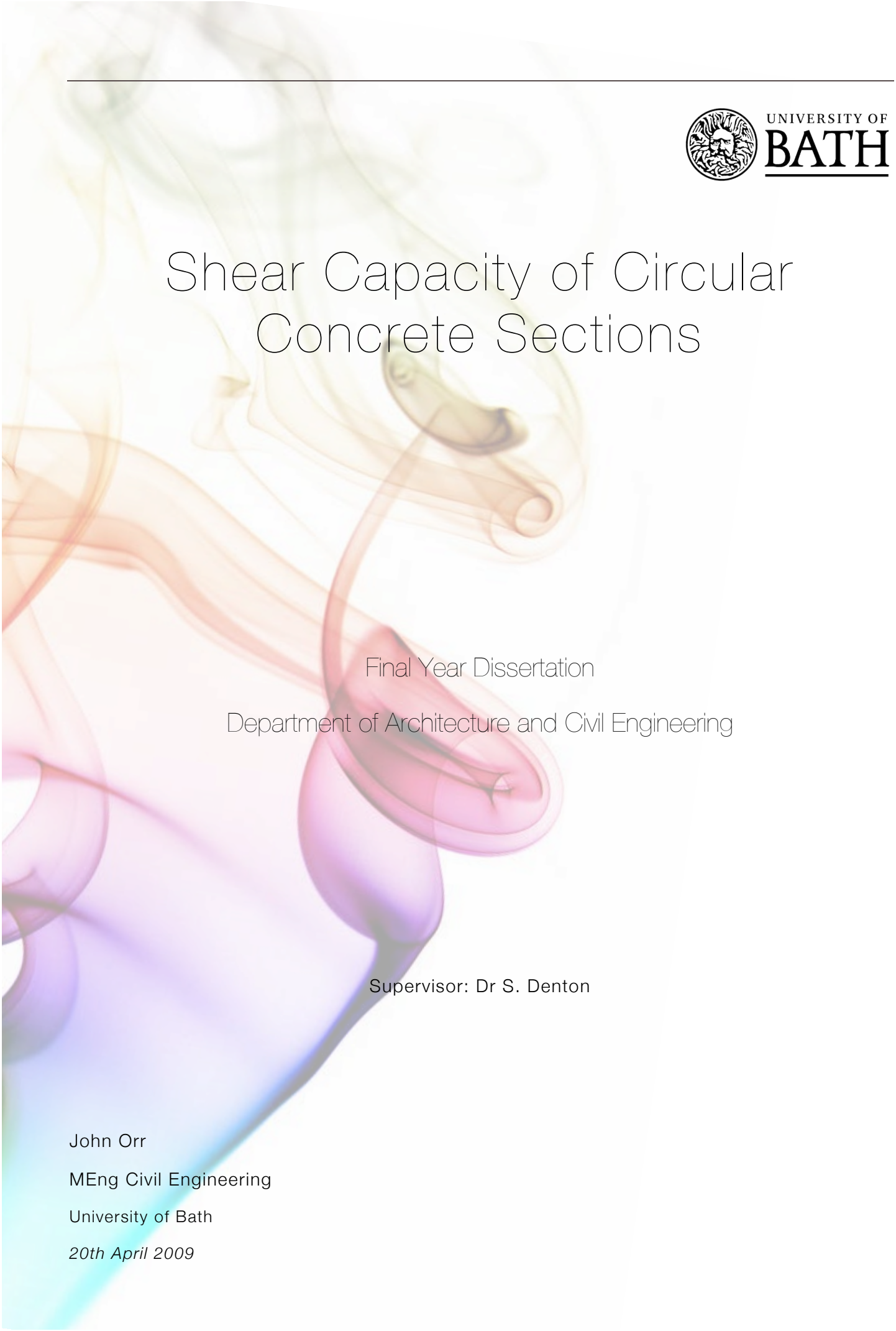

# Shear Capacity of Circular Concrete Sections

Final Year Dissertation

Department of Architecture and Civil Engineering

Supervisor: Dr S. Denton

John Orr

MEng Civil Engineering

University of Bath

*20th April 2009*

# Accompanying CD

john **orr**

| | |
|---|---|
| Email: | jjo20@bath.ac.uk |
| Student number: | 050308794 |
| Year: | 4 |
| Degree: | UEAR-FM07 |
| Unit: | AR 40223 |


*20th April 2009*

# Abstract


## Motivation

The introduction of the Eurocodes for Concrete design will alter the way that shear design is approached for concrete structures. The Eurocodes have adopted the variable angle truss model for shear, a more theoretically consistent approach than that found in the British Standards. The model is confidently applied to rectangular sections, but its applicability to irregular sections is less clear. In particular, the behaviour of circular concrete sections such as those often used as bridge piers is not well defined. A requirement for design guidance on this topic has been recognised by key BSI Committees and this dissertation is intended to help shape and inform future UK design practice.

This dissertation provides a state of the art review of shear design in concrete, followed by detailed analysis of the Eurocode approach. Using both experimental and theoretical data, the Eurocode variable angle truss model for shear design is assessed and extended to circular columns. Previously published test results and guidance are reviewed in the context of the introduction of the Eurocodes and from this new guidance for designers is determined.

### Approach

A brief introduction to concrete design is followed by an analysis of current shear theory, and various approaches to shear design are investigated. Literature spanning 60 years of research and development is assessed and British, European and North American design codes are analysed. A detailed analysis of circular sections follows, where new equations for a variable angle truss model are proposed and alternative design procedures are investigated.

*Chapter summary*

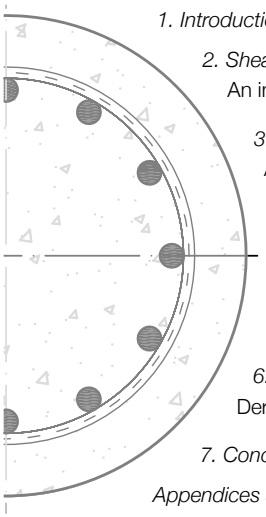

*1. Introduction*

*2. Shear Behaviour*
An introduction to the theories, methods and history of shear analysis

*3. General shear design*
A summary of relevant codes of practice and how they deal with concrete in shear

*4. Eurocode Approach*
The development of the Eurocode model explained, along with derivations

*5. Circular Sections*
A comprehensive review of relevant literature surrounding this topic

*6. Design Approach*
Derivation of a new design approach for circular concrete members in shear.

*7. Conclusions*

*Appendices and References*

### Results

A variable angle truss model is presented for closed and spirally bound circular sections. Equilibrium is satisfied for the stirrups, longitudinal tensile forces and crushing of the concrete struts. The proposed equations are broadly conservative, and simple to implement. Numerous issues surrounding the shear design of concrete to the Eurocode model are highlighted for potential future work. An upper bound plasticity based analysis of circular sections has shown promising results using a simple technique. Comparisons with other existing design procedures have shown that more valid approaches to shear design exist, but are unlikely to be incorporated into the Eurocodes at the present time. Throughout, a lack of experimental data has generally limited the analysis undertaken.



## Acknowledgements

My thanks go to Dr. Steve Denton, Dr. Tim Ibell and Dr. Jon Shave for providing supervision for the duration of this project and to Dr. Anthony Darby and Dr. Mark Evernden who provided additional assistance. Thanks also go to Dr. Trevor Day for his help in writing this dissertation.

# Contents

# List of figures

# List of tables



*Illustration 1: Variety of failures in circular concrete columns (Capon, 1966).*

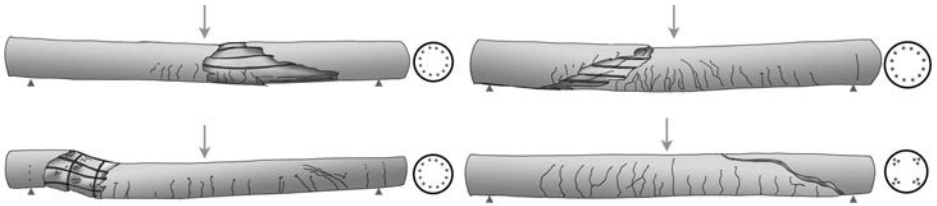

*Design code abbreviations in use throughout:*

| Code | Title | Abbreviation |
|---|---|---|
| BS8110-1:1997 | Structural use of concrete – Part 1: Code of practice for design and construction | BS8110-1 |
| BS5400-4:1990 | Steel, concrete and composite bridges - Part 4: Code of practice for design of concrete bridges | BS5400-4 |
| BS EN 1992-1-1:2004 | *Incorporating corrigendum January 2008*: Eurocode 2: Design of concrete structures - Part 1-1 General rules and rules for buildings | BS EN 1992-1-1 |
| BS EN 1992-2:2005 | Eurocode 2: Design of concrete structures – Part 2: Concrete Bridges – design rules | BS EN 1992-2 |
| S6-06 | Canadian Highway Bridge Design Code | S6-06 |
| ACI 318 (1999) | American Concrete Institute. *Building code requirements for structural concrete* | ACI 318 |

## *Notes*

All analysis presented in this dissertation has been undertaken using Microsoft Excel, and can be viewed in more detail on the enclosed spreadsheets. Trend lines are drawn using Excel's automated functions. 'Linear' relationships are most commonly used to draw general trends in presented data.

## *Accompanying website and CD*

Relevant analysis and data is presented on the enclosed CD. Excel files are presented as '.xls' files and are compatible with most modern versions of Excel (Mac: Excel X, 2008; Windows: 2008). Many relevant files are also available to download from the following website http://people.bath.ac.uk/jjo20/d_a/.

## *Originality*

The work presented herein is my own and, to the best of my knowledge, contains no materials previously published or written by another person, except where explicitly referenced and acknowledged.

*Illustration 2: (Left-right) Spiral links, closed links; multiple spirals in a large diameter section.*

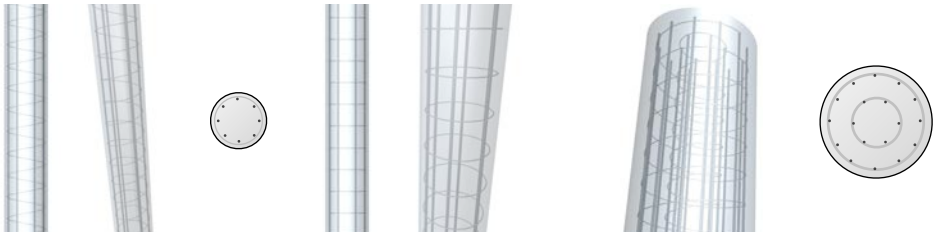

# 1. Introduction

## 1.1. Circular sections

The introduction of BS EN 1992-1-1 will alter the way that shear design is approached for concrete structures. The impetus for this work is to provide a suitable method for the design and analysis of circular sections in shear, making full use of available test data to verify potential approaches. The circular section is widely used in piling and bridge pier design, and its constant strength in all directions makes it useful in seismically active regions. Bridge designers may use circular columns to take advantage of their low coefficient of drag under wind loading. These piers may also be subject to vehicle impact loads, as well as loads applied from the bridge deck due to braking and acceleration forces on the roadway above, Figure 1.1(l).

Shear design in the UK has historically been based on a version of Mörsch's truss model (§2.8.1), while the Eurocodes use a more theoretically consistent 'variable angle model', illustrated in Figure 1.1(r) and discussed in §4. This lower bound solution to shear behaviour provides the basis for this dissertation. Its use, limitations and application to circular sections are considered in detail.

*Figure 1.1: Circular columns – as bridge piers or retaining walls (left). The truss model (right).*

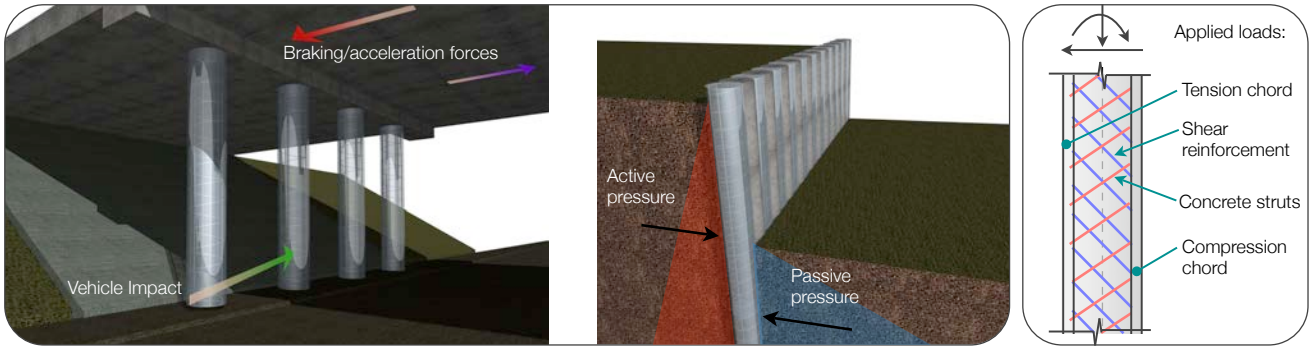


*Table 1.1: A history of codified concrete design in the UK.*

| Published | Code | Design concrete mixes |
|---|---|---|
| 1948 | CP114 *Structural use of reinforced concrete in buildings* | Approx. 31, 26 and 21N/mm$^2$ |
| 1972 | CP110, *The structural use of concrete*. | >20N/mm$^2$ |
| 1985 | BS8110, *Structural use of concrete.* | 20N/mm$^2$ – 40N/mm$^2$ |
| 2010 | BSEN 1992-1-1: *Design of concrete structures.* | 12N/mm$^2$ – 90N/mm$^2$ |

## 1.2. Objectives

The objective of this dissertation is to provide guidelines for the shear design of circular sections. To facilitate this, three main topics are considered:

1) An extension of the variable angle truss model to a circular section, with full derivation of the relevant formulae;
2) Consideration of the BS EN 1992-1-1 limits on truss angles and how these apply to circular sections;
3) An investigation into how the concrete crushing limit is applied to circular sections.

## 1.3. Outline

This dissertation begins by assessing the current body of knowledge surrounding shear design. A wide range of literature is reviewed and discussed throughout the dissertation to support and inform analysis and discussion. Relevant design codes of practice are also assessed and compared. By drawing together the approaches of leading researchers in this field, it is hoped that a more coherent model for the shear design of circular sections is presented. The majority of new work comes in §6 where a variable angle truss model for circular sections is considered in terms of concrete crushing as well as steel yielding equations. To satisfy a lower bound Eurocode model, equilibrium is assessed throughout. A new upper bound plasticity based approach to circular sections is presented, and economic considerations surrounding the use of BS EN 1992-1-1 are discussed and compared to previous design guidance.

# 2. Shear behaviour

## 2.1. Introduction

This chapter provides an investigation into how concrete structures transfer shear, a review of current shear theory, and how these theories relate to current design guidance for circular sections. This should be considered alongside the literature and design codes reviewed in subsequent chapters.

## 2.2. Material properties

### 2.2.1. Concrete

Consider the stress-strain curve for a concrete element under uniaxial compression (Figure 2.1(l)). The stress-strain relationship is almost linear in Zone 1. In Zone 2, the concrete stress due to compression has peaked and the material subsequently expands due to microcrack growth. The 'peak' of the stress-strain curve is sharp for high-strength concrete, while the curves for low-strength concrete tend to flatten out. The tensile strength of concrete is usually ignored in strength calculations, but may be estimated at less than 20% of the uniaxial compressive strength (Park, 1975). In practical situations uniaxial compression is rare, as concrete is more often stressed in multiple directions and so the biaxial stress condition, where principal stresses act in one plane only, should be considered (Figure 2.4). Kupfer et al. (1969) concluded that the biaxial strength of concrete may be up to 27% higher than the uniaxial strength, although the tensile strength remains approximately equal in both cases. Work by Bresler (1958) showed that the compressive strength of concrete is reduced in elements subject to direct stress in one direction and an associated shear stress (Figure 2.1(c)). Finally, concrete subject to triaxial compression (Figure 2.1(r)) has been found to display improved strength and ductility (Park, 1975).

*Figure 2.1: Uniaxial stress-strain plot (l); Direct stress and shear (c); Triaxial stress state (r).*

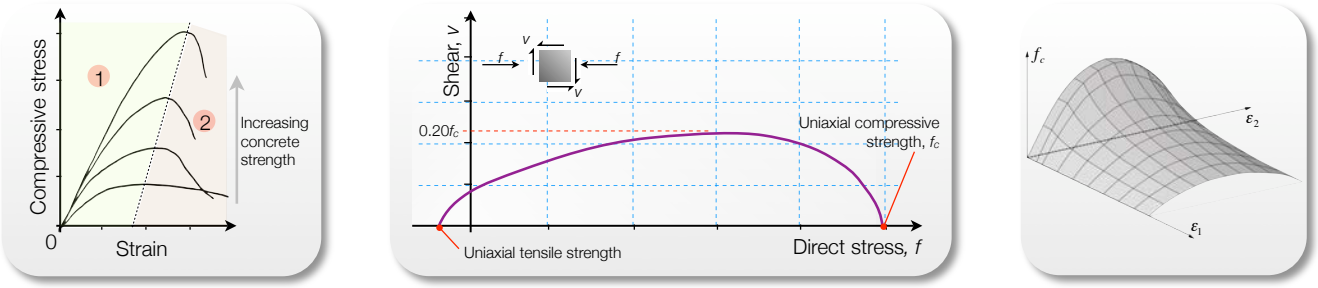


### 2.2.2. The role of fibre reinforced concrete (FRC).

Shear is a brittle mode of failure primarily because plain concrete displays very little ductility (Figure 2.2). FRC shows greater compression capacity, with increases of up to 23% recorded when compared to steel-reinforced sections (Zia et al., 1994). The great advantage of FRC is its improved tensile capacity, and the general effect of fibres is to improve the resistance of a section against crack opening and propagation (Zia et al., 1994). Figure 2.2 highlights the differences between plain and fibre reinforced concrete. Fibres have been found to be more effective in high strength concrete (*>60MPa*) with increases in both ultimate capacity and ductility recorded (Zia et al., 1994). SIFCON (Slurry infiltrated concrete) uses fibre volumes of >12% to provide excellent ductility (see Fritz et al., 1992) and SIMCON (Slurry infiltrated mat concrete) uses a mat of high aspect ratio fibres (ratios up to 500) to provide similar properties but using a fibre volume half that of SIFCON (Zia et al., 1994).

*Figure 2.2: Behaviour of FRC (after Zia et al., 1994).*

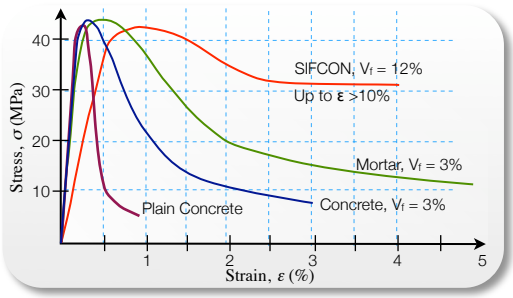


### 2.2.3. Steel reinforcement behaviour

A typical stress-strain curve for steel is presented in Figure 6.1(f). The initial linear elastic behaviour is followed by a yield plateau and subsequent strain-hardening of the steel. High yield steel bars in use today have yield strengths of around *500N/mm²*. Steel exhibits a Bauschinger effect under reversed (tension-compression) loading, so that the stress-strain curve becomes non-linear earlier than expected under repeated loading. Park (1975) provides a more detailed discussion of this effect.

## 2.3. Shear capacity and shear stress

The shear capacity of a concrete element is widely recognised as one of the more difficult aspects of reinforced concrete design. Shear failures are characterised by brittle action and are thus particularly critical in seismically-active regions where ductility at the ultimate limit state is a key design requirement. Loads applied to a concrete section in shear are carried to the supports by a synthesis of six mechanisms, Figure 2.3 (Stratford, 2008).

*Figure 2.3: Six mechanisms to carry shear.*

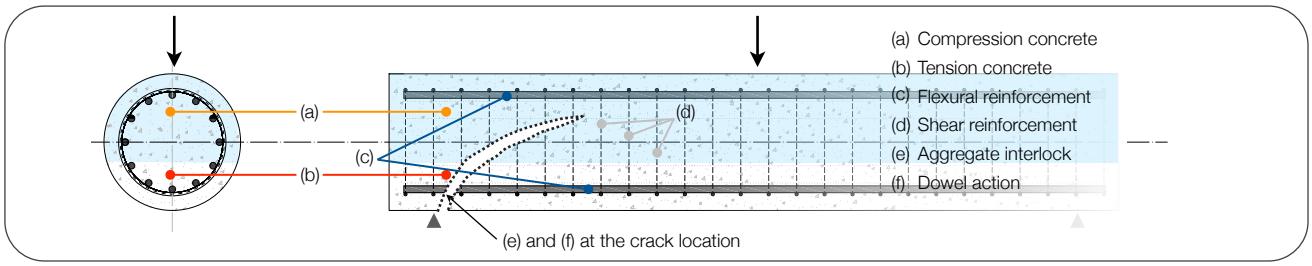


This dissertation considers both upper bound and lower bound approaches to shear design (§2.9). The truss analogy is a lower bound plasticity approach; therefore equilibrium must be satisfied at all locations. The derivation of shear stresses through equilibrium considerations of a homogenous uncracked and isotropic beam is relatively straightforward, but the behaviour of the reinforced section is more complex. In a reinforced section, cracks will form when the principal tensile stress exceeds the tensile capacity of concrete (§2.4.2) and these diagonal cracks typically propagate from the tension face of the member towards the neutral axis (Figure 2.3). Initial cracking often occurs at 45º to the neutral axis, and develops as applied loads are increased. The six mechanisms to carry shear are now considered, before the effect of axial load is analysed.

## 2.4. Mechanisms to carry shear

### 2.4.1. Concrete compression zone

The uncracked compression zone is often considered to provide significant shear resistance in concrete sections (Park, 1975), although the depth of this zone is highly dependent on the properties of the longitudinal steel (FIB, 2007). It has been shown (for rectangular sections) that the neutral axis depth reduces rapidly after the longitudinal steel has yielded (Taylor, 1970), Figure 2.5(r). This causes a reduction in the effective compression area, which in turn leads to a reduction in the available shear resistance of the member. This must be borne in mind when considering circular sections, but it should be noted that the fundamentally different reinforcement layout of a circular section is likely to reduce the magnitude of this effect. It is generally understood that the concrete section carries shear by a combination of the force in the concrete and in the shear stirrups that confine it. Stratford (2008) argues that there are two mechanisms by which the compression concrete zone can carry shear, with these being a variation in axial force along the beam length and variation in the compressive force path depth. However, quantifying the degree to which axial force variation can carry shear is difficult.

### 2.4.2. Concrete tension zone

The tension zone contribution to shear strength is commonly assumed to be zero in design. However, Figure 2.4 shows the results of extensive biaxial testing on plate sections, whereupon the small tensile capacity of concrete is evident. In codified design, it is only the Modified Compression Field Theory that fully considers concrete tensile strength, as discussed in §2.8.3. The tensile capacity of the concrete also influences the ability of a section to carry shear by aggregate interlock (§2.4.3).

*Figure 2.4: Biaxial tests on concrete. Strength plot (l); tension zone (r) (After Kupfer, 1969).*

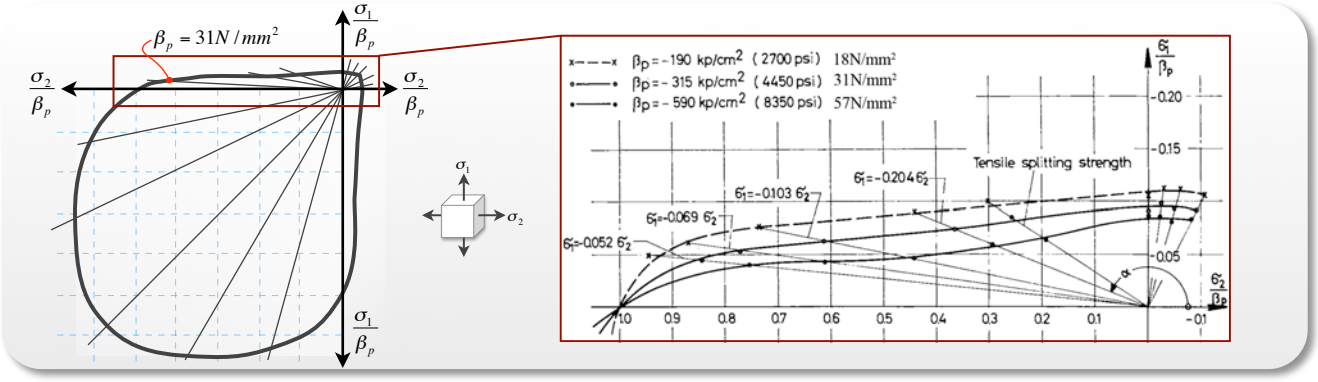

### 2.4.3. Aggregate interlock

The interlock between aggregate particles (which account for typically 60-75% of the concrete volume) has been shown to carry significant shear force in comparison to the capacity of the uncracked concrete, with Taylor (1970) estimating it to be between 33 and 50% of the shear capacity of the uncracked section. Walraven (1981) has shown that the contribution of concrete in the tension zone reduces with increasing crack width as the capacity to transfer stresses normal to the shear direction reduces, Figure 2.5(l).

*Figure 2.5: Aggregate-crack interaction (l); Decrease in neutral axis depth (FIB, 2007) (r).*

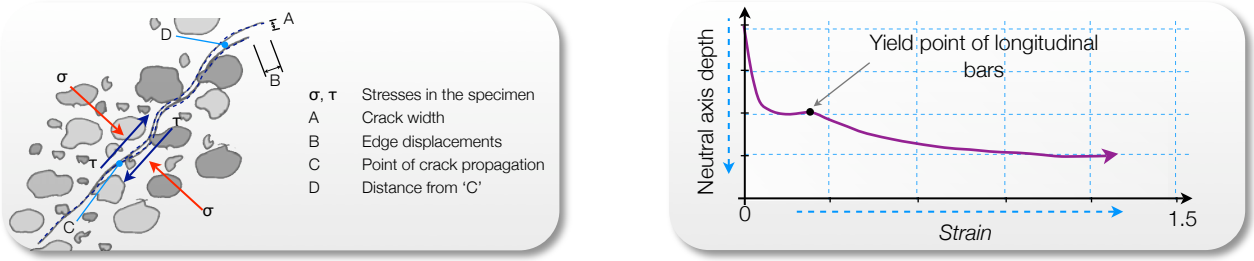


The interaction between shear and aggregate interlock is complex and is not considered in codified design. In Figure 2.5(l) two locations are shown where there is zero capacity to carry shear. At the crack tip (point *C*) rotation of the crack will be the only relative movement between surfaces and thus there is no interlock to generate a shear resistance. Moving along the crack in the direction of propagation there comes a point whereupon the crack width (*A*) is sufficiently large to ensure that the two internal surfaces no longer interact and hence shear cannot be carried by this behaviour.

### 2.4.4. Shear reinforcement and dowel action

Shear reinforcement carries stress over cracks in the section as these cracks open under loading. It is important to define how many bars intersect such a crack to determine the resistance provided against shear. In addition to carrying shear, links both confine the concrete and resist dowel failure in the longitudinal steel. Confinement of the compression zone increases shear capacity by improving the rotation capacity of the section, and the links also prevent the section from splitting along the longitudinal reinforcement, Figure 2.6(l) (Stratford, 2008). Chana (1988) provides a method for calculating these splitting forces.

*Figure 2.6: Dowel action. Beam behaviour with and without shear links (l); Longitudinal reinforcement slippage (r).*

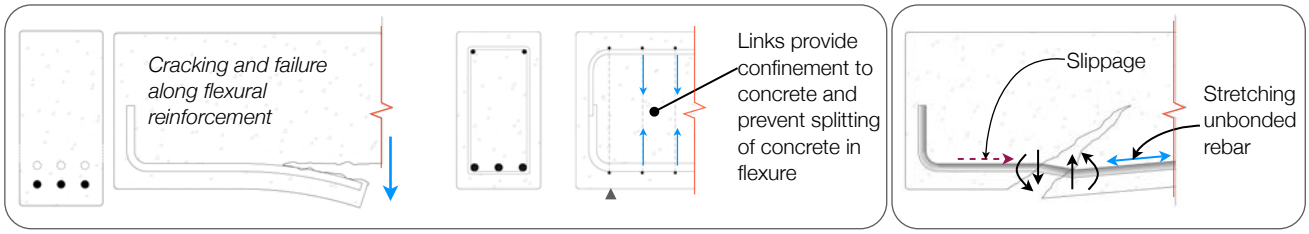


### 2.4.5. Flexural reinforcement and dowel action

Longitudinal reinforcing bars provide shear resistance to the section through compatibility of the crack opening mechanism. This applies to deflections and rotations at the crack/bar interface, both parallel and perpendicular to the reinforcement (Stratford, 2008). In the axial direction, compatibility is ensured by the mechanisms illustrated in Figure 2.6(r). In design it may be assumed that the bars yield at ULS and hence extension of the deformed steel bar dominates the amount of slippage in the system. The component of force acting in shear in the flexural reinforcement is most commonly attributed to the effects of dowel action in the bar and the actual load carried in this mode has been shown to be small to the point of being negligible (Kotsovos, 2006). The complex nature of dowel action, as well as the fact that it is extremely difficult to measure experimentally, means that it is not generally relied on in design.

Work by Kani (1964) showed that the use of plain bars increases shear capacity, because poorly bonded sections have wider crack spacing than well-bonded sections. Therefore the concrete 'teeth' (§2.6) are bigger, and can thus provide greater load capacity according to Eq. 2.1. Experimental work by Leonhardt and Walther (1961) supports this theory.

$$M_{CR} = M_0 \frac{\Delta x}{s} \frac{a}{d} \qquad \text{Eq. 2.1}$$

Where: $M_{cr}$ = capacity of concrete tooth; $M_0$ = moment dependent on cross section properties (see Kani, 1964); $a$ = distance to load; $d$ = effective depth; $s$ = crack length; $\Delta x$ = width of concrete tooth.

## 2.5. Axial Load

The influence of axial load on shear capacity is complex. Poor design can be catastrophic, as seen in the combined compression-shear failure of the Sleipner offshore platform in 1991, where economic losses totalled over a billion dollars (Gupta, 2001). Theoretically, the application of axial compression flattens crack inclination in the section, thereby increasing the number of stirrups intersected, which increases shear capacity. It is therefore generally considered conservative to design a section for zero axial load in the assumption that applied axial loads will increase the capacity of the section. Conversely, axial tension reduces the number of links intersected (Hawkins et al., 2005), reducing shear capacity. However, Gupta (2001) showed that above a compressive stress of approximately *17MPa*, the rate of increase in shear capacity due to axial compression reduces, and in some cases becomes negative, meaning that simple linear equations to predict shear enhancement under axial load may be non-conservative at high values of compressive stress. This effect is discussed further in §2.8, §3 and §4. Axial tension is less common in design, although it may be seen in some piles, or beams subject to restrain during thermal shrinkage.

## 2.6. Size effects

Size effects describe the reduction in strength of a concrete member as it increases in size. Work by Kani (1967) first discovered size effects in non-shear reinforced RC beams and a simple 'tooth' model for the concrete section was proposed wherein the cracked section is considered as a series of short cantilevering concrete teeth which resist applied loads from the flexural reinforcement. Initial tests, which showed a large variation in strength due to member size, have since been refined and it has been shown that the size effect may be reduced through proper scaling of test pieces. Tests at the University of Stuttgart also revealed that the loss of shear strength in large sections was less significant when deep beams with web reinforcement were compared (Bhal, 1968). Consider now a cracked concrete section, Figure 2.7(l). Here, the concrete teeth in the cracked zone may behave as shown in Figure 2.7(r) to ensure equilibrium of the section given the change in stress in the longitudinal reinforcement ($\Delta F$), which causes bending stresses in the tooth. Bending stresses at the intersection must therefore increase as the size of the beam (and so stresses on the tooth) increase, creating the 'size effect'. Shear reinforcement across the tooth provides resistance to these bending stresses, and so in a shear-reinforced section the size effect is less pronounced.

The size effect can also be considered in terms of the concrete crack width at failure, which is often found to be a fairly constant *1mm* irrespective of section size, implying that larger elements are more brittle. Fracture mechanics and dimensional analysis can also be applied to show the presence of the size effect. The sketched graph in Figure 2.8(l) shows that failure loads decrease as 'size' (typically measured as member depth) increases. There are two zones of behaviour, with the initially flat line attributed to a linear relationship between nominal stress and section yield stress. Linear-elastic fracture mechanics is then used to consider the critical stress intensity factor ($K_{IC}$) and analysis provides a 1:2 gradient relationship. The real section behaviour does not follow a perfectly plastic, brittle linear-elastic path; instead quasi-brittle behaviour is seen, as highlighted in Figure 2.8(l).

*Figure 2.7: Cracked concrete section(l); Concrete 'tooth' (r).*

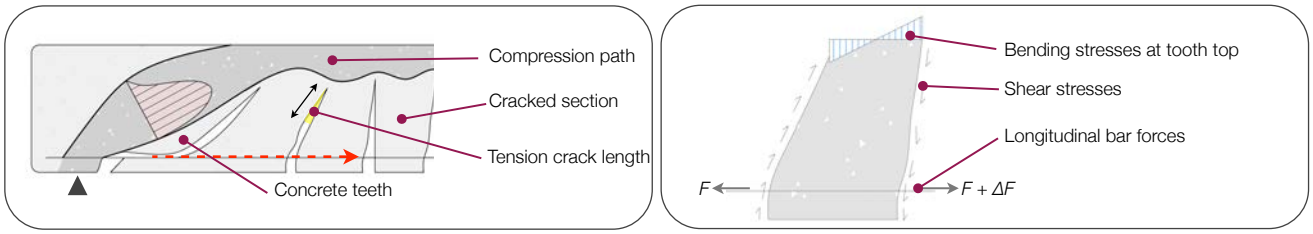


## 2.7. Shear failure modes

With the principles of shear behaviour and size effect now established, more general statements can be considered as to the shear strength of columns and beams. Shear failures are found to occur over a relatively small range of values of *a/d* (*shear span/effective depth*) as shown in Figure 2.8(r), with a critical load position at approximately *2.5d* (Kani, 1967). Deeper sections exhibit larger reductions in capacity. This famous 'Shear Valley' is obtained by dividing the moment from Eq. 2.1 by the flexural failure moment to obtain what is termed the relative beam strength, $r_u$. Relative beam strength depends only on the crack length, $s$, since $\Delta x$ (Eq. 2.1) remains constant. Since crack lengths increase with beam depth, there is a reduction in strength as the section gets deeper. Figure 2.8(r) is an approximation of the shear valley, adapted from work by Bazant (1993) and Brown et al. (2006), with a range of *a/d* from 1.0 to what is termed the transition point (the point at which full flexural failure is attained). In very deep sections, the transition point is often unobtainable and the section will always fail in shear.

However, where $a/d < 2.5$ there is an increase in capacity (shear enhancement) which must also be provided for in design. The enhancement of shear at supports is primarily due to changes in the load path, but the extent to which this applies to circular sections is unclear as there is limited test data available for circular sections loaded close to their supports.

*Figure 2.8: Size effect limits (generalised) (l); Kani's Shear Valley (r).*

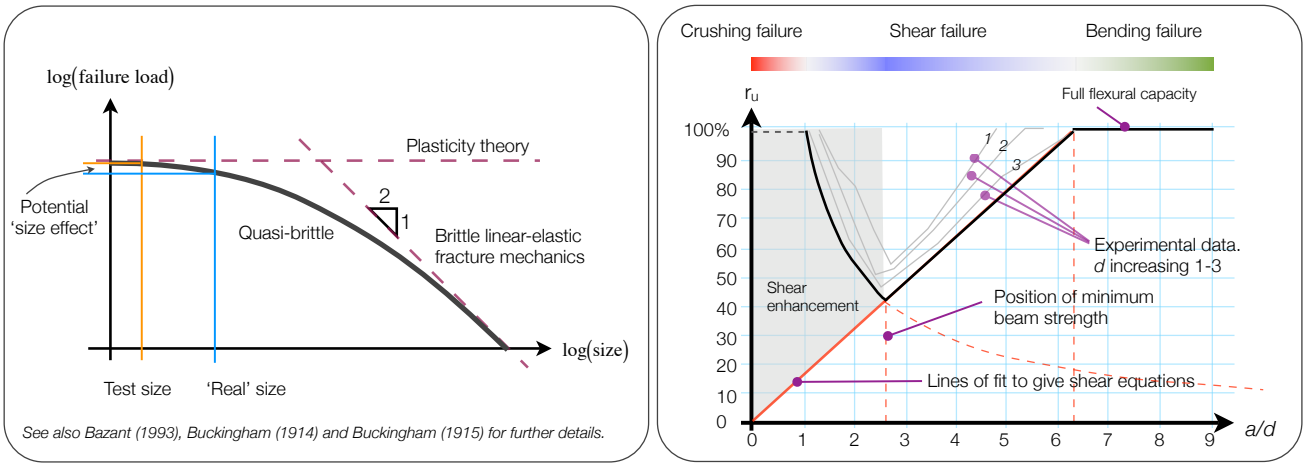


## 2.8. Shear theories

Using five different codified approaches, Bentz et al. (2006) showed that shear strength predictions between codes can vary by up to 200%, while the same codes provide flexural strength predictions within 10% of each other. This illustrates the degree to which design approaches for shear vary, and these differences are discussed further in §3 and §4. Three design models (the truss analogy, compression field theory, and the compressive force-path method) are now briefly investigated.

### 2.8.1. Truss analogy

Modelling shear flow in a reinforced section as a truss was first proposed by Ritter (1899) and Mörsch (1908) as a convenient design method. Mörsch's 45°-truss model has been improved upon since this time and Kupfer (1962) showed that the model underestimates shear capacity by up to 25%. The basic premise of the model is that cracked concrete in the web of the section resists shear by a diagonal compressive stress in a concrete strut which pushes the flanges apart and causes tension in the stirrups which are then responsible for holding the section together, Figure 1.1(r). The Mörsch model assumes that the angle from shear reinforcement to the beam axis is *90°* and the angle of the compression strut from the beam axis is *45°*.

The diagonal compression in the truss model is continuous (as opposed to discrete, Figure 2.9(l,c)) and forces in the stirrups are easily determined from equilibrium considerations. Early researchers (Talbot, 1909; Withey, 1907) found that shear strength predictions according to the force in the stirrups underestimated the section shear strength by a fairly consistent value when using a *45°* concrete strut model. To correct this, a 'concrete contribution' to shear resistance was added, Figure 2.9(r).

*Figure 2.9: Discrete truss (l); Continuous compression (c); Components of shear resistance (r).*

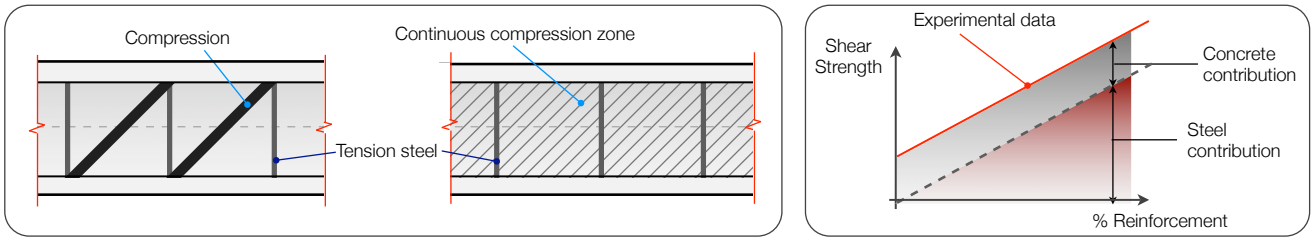


The empirical concrete contribution factor is not used in the Eurocode model (§4). Instead, it is assumed that once cracked, shear capacity comes solely from the links and the concrete is ineffective. However, the model allows the designer to choose the angle of the compression strut *(θ)*. A flatter strut angle ensures that more links are intersected, thus providing more capacity. However, the compressive stress in the strut increases as $\theta$ decreases, and the strut angle is limited by a concrete crushing limit in the inclined strut. This is shown in Figure 2.10(r), where a Mohr's circle for the inclined strut is drawn for decreasing strut angles. The variable angle model is generally considered to be a more theoretically consistent approach, better predicting the failure mode of the actual section, which is likely to occur with a compression strut angle of less than 45°.

The truss model takes the internal condition of the section as a continuum, which is a convenient simplification. However, this means that the models are inconsistent with the reality of reinforced concrete sections which consist of discrete steel bars within a concrete matrix. Link spacing (§5.3.4) is critical in the use of a continuum truss model, and once link spacing is reduced sufficiently, any error found when compared to a discrete truss model is negligibly small. Kim (2007) also showed that for both constant and variable angle truss models, rectangular sections have a higher cracked elastic shear stiffness than circular

sections. Therefore, attempts to simplify circular sections as an 'equivalent rectangle' may be unable to properly account for the behaviour of the circular section, and this approach is not recommended for design. Some design issues that arise when using the truss analogy are now considered (§2.8.2), before alternative design theories are introduced.

*Figure 2.10: Simplified truss model (l); The effect of a variable strut angle (r).*

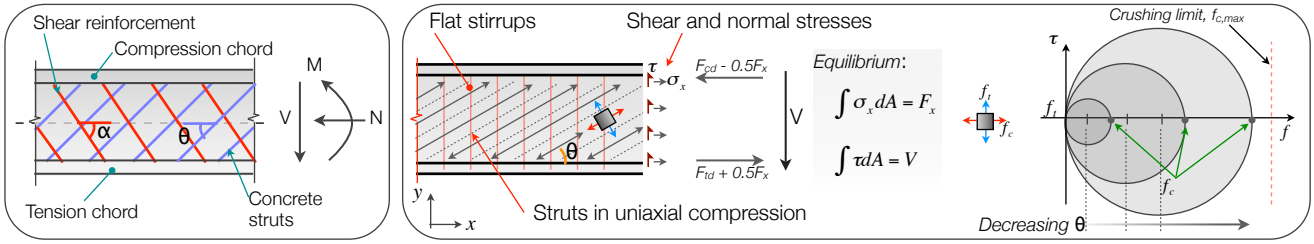


## 2.8.2. Truss analogy design

Kotsovos (2006) determined that current rules for earthquake design do not necessarily prevent brittle failure, and the research suggested that the primary cause of this lack of ductility was the use of the truss analogy in design, which ignores the fact that concrete is brittle and assumes that the concrete can plastically redistribute the applied stresses into the imaginary truss.

A further problem with the truss analogy is seen when cracking is considered. Under loading, microcracks form within an RC element and these cracks interconnect to eventually become visible on the surface once peak loading is reached. The truss analogy relies on the fact that the concrete has sufficient post-peak strength to form the compression struts of the truss and this strength may be attributed to strain-softening behaviour of the concrete which comes about through aggregate interlock (Kotsovos, 2006). However, the cracking behaviour of concrete is such that cracks extend in the direction of principal compressive stress and open in the orthogonal direction (Kotsovos, 2006), a mechanism which is incompatible with a reliance on aggregate action since this requires a shearing movement of the crack faces relative to one another. Therefore, the concept of aggregate interlock behaviour might be considered as conflicting with the true behaviour of concrete.

Fibre reinforced concrete may be the solution, as it has been shown to exhibit both strain-softening and aggregate interlock behaviour, making it more appropriate to use the truss analogy in design (Zisopoulos et al., 2004). However, both compressive force path (§2.8.4) and compression field (§2.8.3) theories better allow for the brittle nature of concrete and are therefore perhaps more valid approaches for the design of concrete in shear.

## 2.8.3. Compression Field Theory, Modified Compression Field Theory (MCFT) and Simplified MCFT

Compression field theory originates from work by Wagner (1929) on the post-buckling behaviour of metal beams with very thin webs. It was determined that post-buckling, the web of the beam no longer carries compression but instead resists shear by a field of diagonal tension. In concrete, the behaviour is reversed such that post-cracking the section no longer carries tension, instead resisting shear by a field of diagonal compression (Collins, 1978). In the development of the truss model, Mörsch was unable to calculate the angle of compression since there are four unknowns and three equations (Hawkins et al., 2005) as illustrated in Figure 2.11. This problem has now been overcome in compression field theory by assuming that the principal compressive stress and principal compressive strain directions are coincident (Hawkins et al., 2005).

*Figure 2.11: Equilibrium: beam section (a); diagonal force equilibrium (b); Shear stirrup forces (c).*

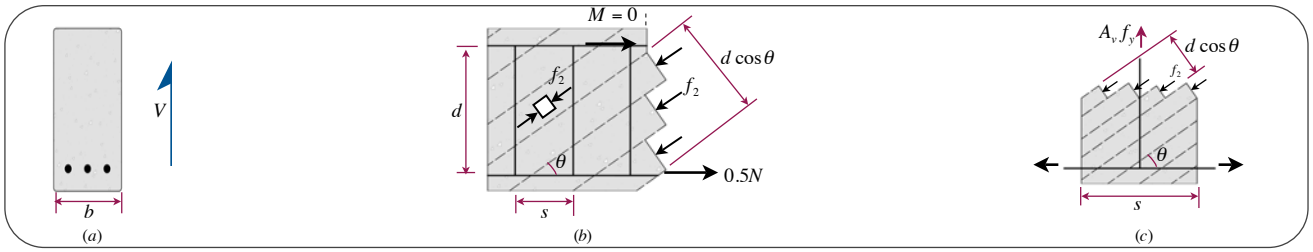


Compression field theory in concrete was first developed for members in pure torsion (Mitchell, 1974) and then later for members in pure shear (Collins, 1978). For both problems the cracked sections have their own stress-strain relationships, distinct from those for the uncracked section, allowing equations for equilibrium and compatibility to be formulated. Equilibrium equations are found for the concrete, stirrups and longitudinal steel in a section by considering a location where the bending moment is zero, Figure 2.11. A Mohr's circle for strain is then considered to assess strain compatibility of the section, Figure 2.12(l). A key result is shown in Eq. 2.3 (Duthinh, 1996) where, assuming the longitudinal steel is elastic (Eq. 2.2) and the shear stirrups and concrete have just reached their plastic limit, the same result as a lower bound plasticity approach is obtained

without requiring the use of strain compatibility (Nielsen, 1984 and §2.9). A fuller explanation of compression field theory can be found in Vecchio (1986) or Collins et al. (2008).

*Figure 2.12: Mohr's circle of strain (l); Mohr's circle of stress (r) for compression field theory. (Collins et al., 2008).*

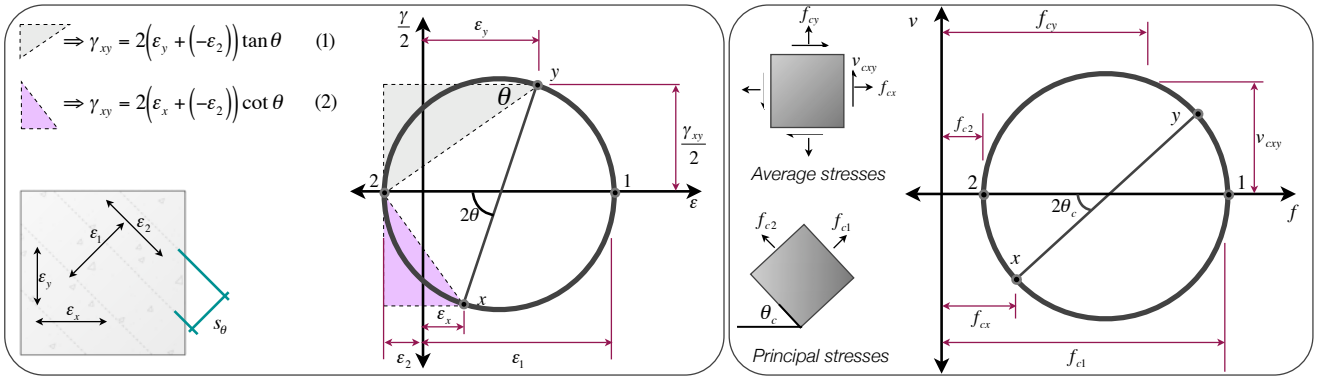


$$f_{longitudinal} = E\varepsilon < f_y \qquad \text{Eq. 2.2}$$

$$f_v = f_y \;;\; f_2 = f_c \qquad \varepsilon_y = \varepsilon_{yield} \;;\; \varepsilon_2 = -\varepsilon_c \qquad \text{Eq. 2.4}$$

$$\tan\theta = \sqrt{\psi/1-\psi} \qquad \text{Eq. 2.3}$$

$$\text{Where: } \psi = \frac{A_v}{bs}\frac{f_y}{f_c} \qquad \text{Eq. 2.5}$$

The modified approach (MCFT) simplifies the concrete-steel boundary condition by allowing no slip to occur between the two materials (and since the prediction of slip is empirical and not well understood, this is an acceptable simplification) and thus by compatibility any deformation (strain) in the steel is matched by equal strains in the concrete. Bentz et al. (2006) determined relationships between the principal concrete stress and principal compressive and tensile strains, giving the MCFT equations as shown in Figure 8.1. The MCFT approach is analysed for circular sections in §6.9. The *simplified* MCFT approach was developed to provide a set of equations for the AASHTO LFRD design code, which had previously relied on a tabulated version of the MCFT equations. The simplifications are described in Mitchell (1974) and are primarily based on strain limits in the steel and concrete. The simplified MCFT method is also used in the Canadian Bridge Design Code (§3.4.2).

### 2.8.4. Compressive force path method (CFPM)

Kotsovos (1988) first introduced the compressive force path method as a new approach to concrete design. The basic premise of the method is that the '*shear resistance of an RC beam without shear reinforcement is provided by the region of the path along which the compressive force is transmitted to the supports*' (Kotsovos, 1988, p74), Figure 2.13. Experimental results (Kotsovos, 1988) suggest that positioning shear stirrups in the centre span of a simply supported beam under two point loading can significantly increase capacity, even though the critical section approach would require shear links within the shear span. Similar tests on deeper beams revealed that shear stirrups do not have to be provided throughout the shear span in order to allow full flexural capacity to be reached.

*Figure 2.13: Compressive force path method. Reality (l); Model (r) (Kotsovos, 1990).*

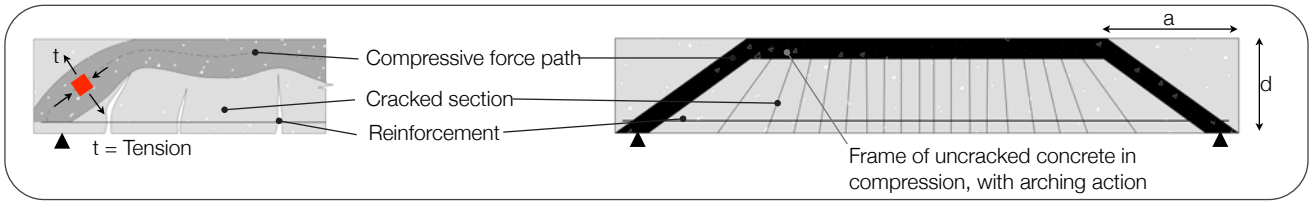


Beams tested with only partial shear reinforcement cannot conform to the truss analogy since there is no continuous vertical (or inclined) tension member (Figure 2.10(l)) but such sections are able to sustain higher load than that predicted by the truss analogy (Kotsovos, 1988). Therefore '*truss behaviour of a section is not a necessary condition for a beam to attain flexural capacity once shear capacity is exceeded*' (Kotsovos, 1988, p.74). Further details may also be found in Kotsovos, 1990.

## 2.9. Plasticity theory

Plasticity theory is concerned with the ultimate strength of members, and whereas in elasticity theory member stiffness is the driving factor in design, plasticity theory is more concerned with strength and ductility. There are two theorems which need to be considered. The lower-bound theorem states that:

> *If any stress distribution throughout the structure can be found which is everywhere in equilibrium internally and balances certain external loads and at the same time does not violate the yield condition, those loads will be carried safely by the structure (Calladine, 1969, p.96).*

And the upper-bound theorem states that:

> *If an estimate of the plastic collapse load of a body is made by equating internal rate of dissipation of energy to the rate at which external forces do work in any postulated mechanism of deformation of the body, the estimate will be either high, or correct. (Calladine, 1969, p.104).*

Therefore, a lower bound approach such as the truss analogy will provide a collapse load estimate less than or equal to the actual collapse load. An upper bound approach (§6.6) equates internal and external work done for a particular collapse mechanism, and provides an estimate equal to or higher than the correct failure load. The correct collapse load is found when both give the same collapse load factor, and hence satisfy the uniqueness corollary.

The use of plasticity theory requires that a number of assumptions be satisfied. The two most significant are that displacements should be small (to avoid affecting equilibrium in the lower-bound approach and compatibility in upper-bound approaches) and that all materials should be perfectly plastic. It is evident that concrete does not display perfectly plastic behaviour and hence is given a factored effective strength. This is discussed in further detail in §4.3 and §6.6.

In contrast to compression field theory, the approach of plasticity theory does not describe the shear behaviour through the cracked section to failure. This means that in a typical case, either the concrete or the reinforcement may be at their limiting stress, whereas in compression field theory neither material is at its limiting stress (Collins, 1978). It should also be borne in mind that whilst the assumptions made in plasticity theory are of questionable validity for concrete structures, which have limited plastic behaviour, good design potential has been realised in upper bound analyses (Ibell et al., 1997).

## 2.10. Elastic stress behaviour

The elastic shear stresses on any section can be derived by considering the general shear flow formula, Eq. 2.6. Here, circular sections are considered, and it is reasonably assumed that *M/z* remains constant along the length of the cross section under consideration. Vertical shear stresses may be found at any location from a suitable reference point by considering the width of the section at that location. In an uncracked circular section, these stresses will be distributed as shown in Figure 2.14(l). Once cracked, and assuming linear elastic behaviour for both the concrete and steel, the stress distribution may be more similar to Figure 2.14(r), with the actual distribution being heavily dependent on the relative magnitude of applied axial load and moments.

$$Q = \int \frac{Vcy}{I} dA \quad \text{Therefore: } \tau = \frac{V}{Ib}\int ydA \quad \text{where } \int ydA = \frac{2}{3}r^3 \qquad \text{Eq. 2.6}$$

For an uncracked circular section, $\tau_{xy} = \frac{S_z V_y}{I_z b}$ *(When M/Z assumed constant)* Eq. 2.7

Where: $S_z$ = first moment of area (mm$^3$); $V_y$ = shear (kN); $I_z$ = second moment of area (mm$^4$) and $b = 2r$ (mm).

Therefore in an uncracked circular section, $\tau_{xy,\max} = \frac{4V_y}{3\pi r^2}$ (Figure 2.14(l)) Eq. 2.8

*Figure 2.14: Shear stresses on an uncracked circular section (l); Shear on cracked circular section (r).*

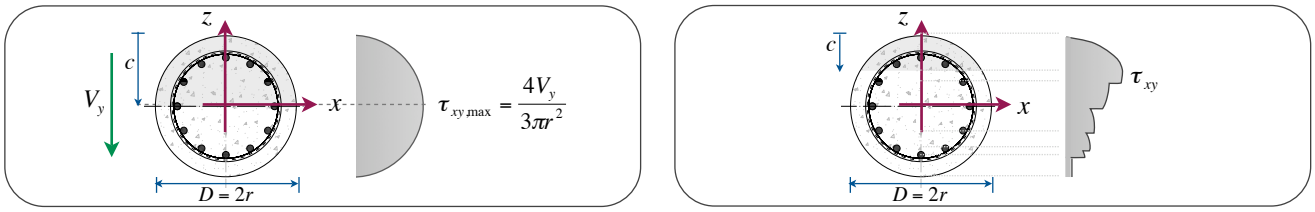


## 2.11. Summary

§2 provides a comprehensive review of the mechanisms by which concrete carries shear, a topic which has occupied researchers for many decades and remains unsatisfactorily dealt with in design codes. New design guidance for circular sections must take all of the above into consideration, and apply this knowledge to the truss model developed by Ritter and Mörsch well over 100 years ago. To facilitate the development of a design procedure for circular sections in shear, current shear design procedures are analysed and reviewed before both theoretical and experimental work on circular sections is considered in more detail.

# 3. General shear design

## 3.1. Introduction

Chapter 3 introduces general approaches to shear design, before the Eurocode design model (§4) and specific issues surrounding circular sections (§5) are analysed in more detail. From the UK, BS8110-1, BS5400-4 and Highways Agency's *BD* series documents are considered, and the Canadian CSA S6-06 and American ACI 318 approaches are then contrasted to these. In all cases, additional information is found in the relevant code documents, and this chapter is intended to present only the fundamentals of each design approach. Eurocode and British Standard axes definitions are presented in Figure 3.1(l) to avoid potential confusion.

*Figure 3.1: (l-r): Eurocode and British Standards axes definitions; Definitions for BS8110 ($a_v$, d).*

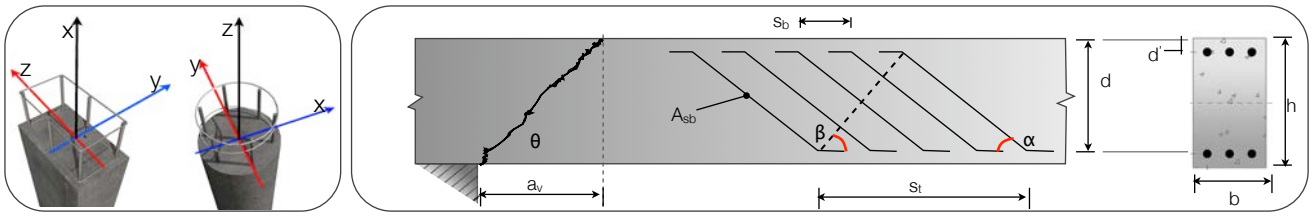


## 3.2. British Standards

The basic model for shear design in the British Standards is the 45º-truss model, where total shear capacity is given by a concrete contribution and a steel contribution (Eq. 3.2, see also §2.8.1). Shear design is undertaken by considering the shear stress, $v$, on a section (Eq. 3.1). This is compared to the concrete shear resistance, $v_c$, of the section at the point under consideration. Where $v$ is greater than $v_c$, shear links may be required.

BS8110-1 allows zero links when $v$ is less than 50% of the concrete shear capacity, $v_c$ (as given by Eq. 3.3). This is rarely the case, and it is more common to provide either minimum or design links (Eq. 3.4), determined by the limits shown in Table 5.2. Shear enhancement is applied in BS8110-1 where $a_v$ is less than $2d$ (Figure 3.1(r)) by factoring $v_c$ by $2d/a_v$. Further details given in BS8110-1 cl.*3.4.5.8*, *3.4.5.9* and *3.4.5.10* should also be considered. For axially loaded sections $v_c$ is replaced with a factored value of shear resistance, $v'_c$, as described in Table 5.2.

$$v = V/(b_v d) \quad \left(\not> 0.8\sqrt{f_{cu}} \not> 5MPa\right) \qquad \text{Eq. 3.1}$$

$$v_{total} = v_c + (v_s) \quad (MPa) \qquad \text{Eq. 3.2}$$

$$v_c = \frac{0.79}{\gamma_{ms}}\left(\frac{100A_s}{b_v d}\right)^{1/3}\left(\frac{400}{d}\right)^{1/4}\left(\frac{f_{cu}}{25}\right)^{1/3} \qquad \text{Eq. 3.3}$$

$$v_s = A_{sv} f_{yd} / b_v s_v \quad (MPa) \qquad \text{Eq. 3.4}$$

Where: $v$ = design shear stress ($N/mm^2$); $V$ = design shear force at ULS ($kN$); $b_v$ = web width ($mm$); $v_c$ = concrete contribution ($N/mm^2$); $v_s$ = steel contribution ($N/mm^2$); $A_s$ = longitudinal steel area ($mm^2$); $d$ = effective depth ($mm$); $f_{cu}$ = characteristic concrete strength ($N/mm^2$); $A_{sv}$ = link cross sectional area ($mm$); $f_{yd}$ = design link yield strength ($N/mm^2$); $s_v$ = link spacing ($mm$).

### 3.2.1. BS5400-4:1990. (CoP for design of concrete bridges)

The design of bridge piers follows the same general approach to shear design as BS8110-1. Slenderness is considered, before *PΔ* effects are applied to obtain the section's axial and moment capacity at ultimate limit state. The shear resistance of a column is given a factored value of an equivalent beam in shear. BS5400-4 requires minimum links in all sections, and where design links are required $0.4N/mm^2$ is added to the capacity requirement to account for the effects of repeated loading. The concrete contribution in BS5400-4 is defined in Eq. 3.5, where a slightly different size effect factor is used.

$$v_{c,8110} \equiv \xi_s v_{c\,5400} = \frac{0.27}{\gamma_m}\left(\frac{100A_s}{b_v d}\right)^{1/3}(f_{cu})^{1/3}\left(\frac{500}{d}\right)^{1/4} \qquad \left(\not> 0.75\sqrt{f_{cu}} \not> 4.75MPa\right) \qquad \text{Eq. 3.5}$$

## 3.3. Design Manual for Roads and Bridges (DMRB)

### 3.3.1. BD74/00 (Foundations) (2000); BD44/95 (Assessment of Concrete Highway Bridges and Structures) (1995)

BD74/00 is essentially an implementation document for the use of BS8004 when designing roads to the Highways Agency specifications. There are a number of alterations and annexes, including for the design of piles, which are not covered in specific detail in BS8004. The design approach for shear is taken directly from BS5400-4 and hence §3.2.1 is applicable.

Assessment codes for existing structures are, in general, less conservative than design codes. This is illustrated by considering shear enhancement clauses in BD44/95, where shear enhancement can be taken within a distance of $a_v<3d$ (Figure 3.1) compared to the $a_v<2d$ found in BS5400-4. The interesting point to BD44/95 is that the calculation for $v_c$ in fact provides a lower result than the design code, which is unusual (Eq. 3.6, Eq. 3.7). This is explained in BA44 (1996) by the fact that the value in BS5400-4 is the mean of the experimental data divided by $\gamma_m$ (Clarke, 1987), as opposed to the characteristic value which is used in BD44/95.

BD44/95:

$$v_c = \frac{0.24}{\gamma_m}\left(\frac{100A_s}{b_w d}\right)^{1/3}\left(f_{cu}\right)^{1/3} \qquad \text{Eq. 3.6}$$

BS5400-4:

$$v_c = \frac{0.27}{\gamma_m}\left(\frac{100A_s}{b_w d}\right)^{1/3}\left(f_{cu}\right)^{1/3} \qquad \text{Eq. 3.7}$$

## 3.4. American and Canadian Approaches

### 3.4.1. ACI 318, Structural Concrete (2005)

The American design code is also based on a modified truss analogy. The formulae for stirrup components are essentially the same as BS8110-1 and the concrete contribution (§2.4) is given by Eq. 3.8. The commentary notes that '*research results have shown that deep, lightly reinforced one-way slabs, particularly if constructed with high-strength concrete, may fail at shear loads less than $V_c$*' (ACI 318-R, 2005 cl.11.5.6.1), which is perhaps an indication of the limitations faced in shear design to existing codes. No additional clauses are presented for circular sections.

$$V_c = 0.17\left(1+\frac{N_u}{14A_g}\right)\sqrt{f'_c}\,b_w d \qquad \text{(kN) } \textit{(In SI Units)} \qquad \text{Eq. 3.8}$$

Where $N_u$ = Axial load; $A_g$ = gross concrete area ($mm^2$); $f'_c$ = concrete compressive strength ($N/mm^2$); $b_w$ = web width ($mm$); $d$ = effective depth ($mm$).

### 3.4.2. CSA S6-06. Highway Bridge Design Code (2006)

The Canadian Standards authority implements the MCFT approach (§2.8.3). This was originally presented as a series of tables (Collins et al., 1996) but now uses the simplified modified approach equations, making the design process easier to understand. The code also allows for a strut-and-tie model to be used, which is useful where longitudinal strains do not vary linearly over the depth of the member, or where shear flow is not constant over the member depth (CSA, 2006) which is particularly true in deep beam design. Where shear reinforcement is required (when applied shear is greater than the value given by Eq. 3.9) minimum steel requirements are given by Eq. 3.10 (to ensure ductility at high concrete strengths).

The total shear capacity is given by Eq. 3.12, where the components of resistance from *tension* in the concrete ($V_c$), stirrups ($V_s$) and prestressing ($V_p$) are combined. The effective shear depth, $d_v$, is taken as the larger of the values in Eq. 3.11, where $d$ is the distance from extreme compression fibre to centroid of tension reinforcement. The variables $\beta$ and $\theta$ are based on MCFT and are dependent on the longitudinal strain in the section, which is found for simplified cases by Eq. 3.17. For $f_c< 60MPa$ it may be assumed that $\beta = 0.18$ and $\theta = 42º$.

The equations for $V_c$ and $V_s$ remain recognisable to those used in other codes, but determining the variables is more complex. The approach provides references to relevant literature in the commentary (CSA S6-06-R, 2006), unlike the empirical approach found in British Codes. Throughout, the statement '*in lieu of more accurate calculations* [the variable] *shall be calculated as:*' is provided, giving the designer the opportunity to use the full MCFT method for a rigorous design.

$$V_f > \left(0.20\phi_c f_{cr} b_v d_v + 0.5\phi_p V_p\right) \qquad \text{Eq. 3.9}$$

$$d_v = 0.72h \not< 0.9d \qquad \text{Eq. 3.11}$$

$$A_v \not< 0.15 f_{cr}\left(b_v s / f_y\right) \qquad \text{Eq. 3.10}$$

Where: $\Phi_c$ = resistance factor for concrete (=0.75) and $\Phi_p$ = resistance factor for tendons (prestressing); $f_{cr}$ = cracking strength of concrete; $b_v$ = section diameter; $s$ = bar spacing; $d_v$ = effective shear depth; $h$ = member height; $b_v$ = web width.

$$V_r = V_c + V_s + V_p \qquad \text{Eq. 3.12}$$

Where: $V_r$ = section resistance; $V_c$ = resistance from concrete; $V_s$ = resistance from stirrups; $V_p$ = resistance from prestressing.

$$V_s = \frac{\phi_s f_y A_v d_v \left(\cot\theta + \cot\alpha\right)\sin\alpha}{s} \qquad \text{Eq. 3.13}$$

$$V_c = 2.5\beta\phi_c f_{cr} b_v d_v \qquad \text{Eq. 3.14}$$

Where $\alpha$ and $\theta$ as defined in Figure 2.10. $\Phi_s$ = resistance factor for bars (=0.90). $A_v$ = area of transverse reinforcement; and:

$$\beta = \left[\frac{0.4}{(1+1500\varepsilon_x)}\right]\left[\frac{1300}{(1000+s_{ze})}\right] \quad \text{Eq. 3.15}$$

$$\theta = (29+7000\varepsilon_x)(0.88+s_{ze}/2500) \quad \text{Eq. 3.16}$$

In general cases $s_{ze}$ = *300mm*, and the value for longitudinal strain is given by Eq. 3.17.

$$\varepsilon_x = \frac{M_f/d_v + V_f - V_p + 0.5N_f}{2(E_s A_s)} \quad \text{Eq. 3.17}$$

Where: $M_f$ = Moment; $V_f$ = Shear force and $N_f$ = Axial load at a section. $E_s$ = 200kN/mm$^2$; $A_s$ = area of flexural tension steel.

## 3.5. Basis for design

ACI-ASCE Committee 326 (1962) concluded that '*a fully rational design approach* [for shear] *does not seem possible at this time'* establishing empirically based methods for shear design as the norm for future ACI and British Standard approaches. Collins et al. (2008) highlighted the inconsistencies between current codified approaches by testing four slab strips. Here, predicted strengths using ACI 318, BS8110-1, BS EN 1992-1-1 and CSA S6-06 approaches are compared to experimental data and large variations are revealed. The maximum ratio of highest to lowest predicted failure load was 2.56, and both ACI 318 and BS EN 1992-1-1 approaches can be seriously unconservative, Figure 3.2 (where the total factor of safety is also included for a case when live load is 50% of the dead load). It is perhaps worrying that the BS8110-1 approach appears to be safer than the proposed BS EN 1992-1-1 model. Ideally a new code should introduce new, more accurate methods, from which a lower factor of safety may be taken, indicating an improved and more accurate design approach.

*Figure 3.2: Comparison of four design approaches for members without links (Collins, 2008).*

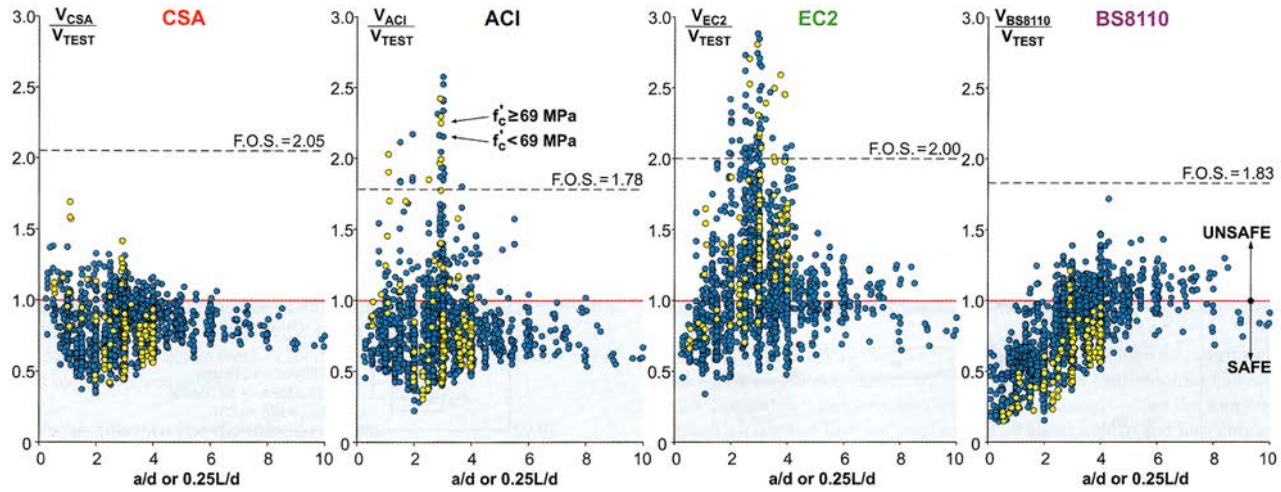


In comparison, flexural design using the various codes is essentially the same, and Collins et al. (2008) found just a 2% variation in predicted flexural strengths. Whereas flexural design has been established since the 1950s, shear design is more complex and by considering the older British codes, Collins et al. (2008) found that allowable shear forces have decreased by 55% over the last 50 years. In Canada, the collapse of the Laval Overpass in 2006 bought the deficiencies of shear design for concrete structures to the forefront of public attention. The subsequent public enquiry (Johnson, 2007) details both technical, constructional and maintenance problems which together contributed to this sudden collapse. At the time the Laval Overpass was designed, shear was not deemed to be critical. The Canadian code has subsequently been updated to use the MCFT approach (§3.4.2) and can now much better predict the behaviour of members in shear. An analysis of the Laval Overpass design using the MCFT approach did indeed show that shear would be a critical failure mode.

Leonhardt (1970) suggested that the reason for poor shear design is simply the huge number of variables involved when compared to flexural design; making many shear tests redundant as they cannot shed light on which variable is causing the effects seen. The MCFT approach of course is different in that it essentially considered complex membrane testing to verify a *theoretical* model, rather than an *empirical* one. Furthermore, previous design approaches have been based on a relatively limited data set, which before 1996 included very few shear tests on beams deeper than about 560mm, and yet the empirical formulae were extrapolated to relate to all cases.

Collins et al. (2008) also consider the relative safety factors for shear and flexure, and it is found that the BS8110-1 factor of safety against brittle shear failure is only 9% greater than that for a flexural failure mode which gives warning of impending collapse. In comparison, BS EN 1992-1-1 has a 30% increase in the factor of safety for shear, which appears to be more satisfactory. Furthermore, the concrete crushing limit in BS EN 1992-1-1 is based solely on concrete strength ($f'_c$) and tensile strains in the concrete are not considered. The CSA S6 (2006) approach is able to analyse the interaction between the compression strut and stirrup strains, which again seems to provide a more accurate approach. Perhaps the final issue for the basis of design using empirical data is the method in which members are tested. Often, testing for shear uses members that contain heavy longitudinal reinforcement to prevent premature flexural failure. The reality is that members with heavy longitudinal reinforcement will be subject to large moments, and in design it is preferable to have member behaviour that is governed by a ductile flexural failure rather than a brittle shear mode. Designing members for shear is critical, since a beam may potentially sit just below its failure load and exhibit no obvious signs that it is about to fail.

## 3.6. Conclusions

The current body of UK and North American guidance for the design of concrete in shear has been presented. Methods in use are limited to the approaches of BS8110-1 and BS5400-4, which essentially deal with shear in the same way, although different factors and limits are chosen to better represent the type of loading that the section is likely to experience. Shear strength is modelled as being dependent on a '*concrete contribution*' and a '*steel contribution*' (Figure 2.9) and this approach allows the designer to account for size effects (§2.6), something the Eurocode model (§4) is unable to do for reinforced sections. The American code is broadly similar to the BS5400-4 approach, and also sums the concrete and steel contributions. The Canadians use the most advanced method, and analysis using this approach (§6.9) is superb.

Concerns raised over shear capacity predictions in both the Eurocode and British Standard models for slabs are presently provoking debate. Responses in the lead up to 2010 may provide some hint at future revisions to the code, although it is unlikely that a compression field theory based approach will be adopted in the near future. The presence of axial load and its effect on section design is considered further in the following chapter, where comparisons are made between the BS5400-4 and the equivalent Eurocode approaches. The variable angle truss model is now considered in detail (§4) and literature surrounding circular sections is reviewed (§5) before new design equations for circular sections in shear are presented in §6.

# 4. Eurocode Approach

## 4.1. Introduction

This Chapter considers the Eurocode model for shear design. Equations for shear design are assessed and compared to those of §3, with the aim of informing a new approach for the design of circular sections (§6). The presence of axial load is considered and comparisons between the approaches of BS EN 1992-1-1 and BS5400-4 are made.

## 4.2. Basis of design

### 4.2.1. Stress-strain relationships and section design

The material models used in BS EN 1992-1-1 are presented in Figure 4.1(l). Within BS EN 1992-1-1 there are distinct stress-strain relationships for both the analysis and design of sections; here only the design approach is considered. Similarly to BS5400-4, BS EN 1992-1-1 also allows the use of a rectangular stress block for design, Figure 4.1(r). Concrete compressive and tensile design strengths are given by Eq. 4.1 and Eq. 4.2 respectively, with the designer able to choose between a bilinear or a parabola-rectangle relationship for concrete under compression. The variables $\lambda$ and $\eta$ have constant values (as defined in the National Annex) of *0.8* and *1.0*, and reinforcing steel is taken with $f_{yk}$= *500MPa*. When considering seismic design, alternative yield strengths may be specified to satisfy the ductility requirements of BS EN 1998-2, remembering that ductility is inversely proportional to yield stress (Narayanan, 2005).

### 4.2.2. Shear approach

BS EN 1992-1-1 uses a variable angle truss model, which differs from previous approaches by assuming that once cracked, only the links provide any shear resistance for the section. In simple terms, the design shear resistance of a section is given by a 'steel contribution' type equation ($V_{Rd,s}$), the value of which is limited by crushing considerations in inclined the concrete strut ($V_{Rd,max}$) (all equations are defined in §4.3). The advantage of the variable angle model is that it is more theoretically consistent, and does not rely on empirical analysis to determine a 'concrete contribution' in the cracked section. The BS EN 1992-1-1

approach suggests that sections generally fail with a strut angle of *cot(θ)=2.5*, although high applied loads may require the use of a steeper truss angle. For members without shear reinforcement the shear strength is primarily governed by concrete strength, longitudinal reinforcement and member depth. Unreinforced sections also remain susceptible to the size effect (§2.6).

*Figure 4.1: Stress-strain plot for concrete and steel reinforcement (l); Concrete stress block (r).*

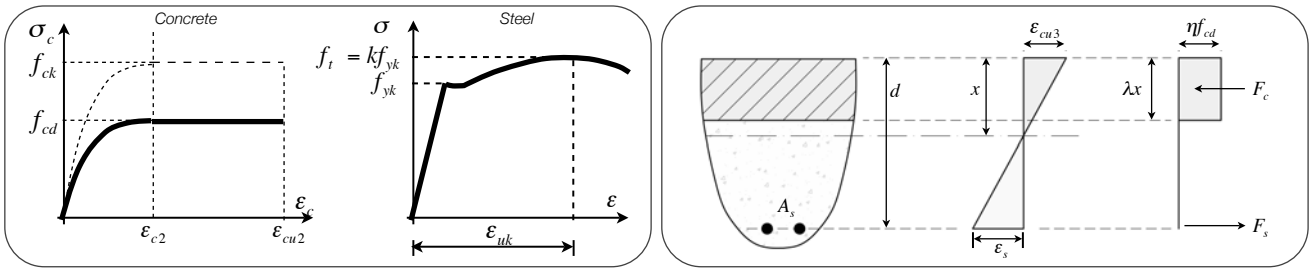


$$f_{cd} = \alpha_{cc} f_{ck} / \gamma_c \qquad \text{Eq. 4.1}$$

$\alpha_{cc}$ = coefficient for long term effects (usually 1.0); $f_{ck}$ = characteristic compressive strength; $\gamma_c$ = partial safety factor.

$$f_{ctd} = \alpha_{ct} f_{ctk,0.05} / \gamma_c \qquad \text{Eq. 4.2}$$

$\alpha_{ct}$ = 1.0; $f_{ctk,0.05} = 0.7 f_{ctm}$; $f_{ctm}$ = mean axial tensile strength of concrete.

The conceptual approach to shear is simple, but as has been seen, the reality of shear in concrete is anything but. In the simplification process, some variables are neglected and thus accuracy may be lost. Choosing the most important variables is difficult, as what is critical in one case may not be in another (Cladera, 2007; Regan, 1993), which may lead to unexpected non-conservative results. Analysis by Cladera (2007) shows that the truss approach for rectangular sections is, in general, over conservative for lightly reinforced sections, and non-conservative for heavily reinforced sections. The same effect is seen in the analysis of circular sections, where the BS EN 1992-1-1 equations can lead to both safe and unsafe results for sections with differing longitudinal reinforcement and concrete strengths (§6).

It is also worth noting that the shear design equations present in the final version of BS EN 1992-1-1 have changed significantly over the years of development. In the DD ENV (1991) release, a concrete contribution was included in the same way as found in BS8110-1, shown in Eq. 4.3. This formulation is unwieldy, and highlights the simplicity of the current BS EN 1992-1-1 method, but does include an axial load component and what appears to be a size effect factor. There is no indication as to where the various factors came from, but are most likely to be empirically derived.

$$V_{Rd} = V_{cd} + V_{wd} \text{ (Shear resistance = Concrete contribution + Stirrup Contribution)} \qquad \text{Eq. 4.3}$$

$$\text{Where: } V_{Cd} = \left(\tau_{Rd} k\left(1.2 + 40\rho_1\right) + 0.15\sigma_{cp}\right) b_w d; \quad V_{Wd} = \left(\frac{A_{sw} f_{ywd}}{s} 0.9d\right) \qquad \text{Eq. 4.4}$$

$$\text{And: } \tau_{Rd} = \frac{0.25 f_{ctk\,0.05}}{\gamma_c}; k = 1.6 - d; \rho_1 = \left(\frac{A_{sl}}{b_w d}\right) \not> 0.2; \sigma_{sp} = \frac{N_{Sd}}{A_c}$$

Interestingly, shear enhancement was applied at *a/d ≤ 2.5* rather than *2* as found in the current revision. The code then had two methods for shear design, the second being the variable angle truss. Confusingly, this second method did not include a concrete contribution in the equivalent to Eq. 4.3 and so is more similar to the current code revision. Furthermore, the strut angle $\theta$ was limited in the range *0.4 ≤ cot (θ) < 2.5*, giving a steeper (maximum 68º) possible strut angle while also allowing the designer to specify any other limits to $\theta$, '*provided they can be justified*'.

## 4.3. Design formulae for BS EN 1992-1-1:2004

Shear reinforcement is required when $V_{Ed} > V_{Rd,c}$ (Eq. 4.5); the resistance of the section is then given by Eq. 4.6. The BS EN 1992-1-1 truss model is presented in Figure 4.2, where the relationships are clearly defined. The design of shear reinforcement is determined by considering the design shear force which can be sustained by yielding the shear reinforcement ($V_{Rd,s}$), without crushing the compression struts ($V_{Rd,max}$). For both vertical and inclined stirrups, values for $V_{Rd,s}$ and $V_{Rd,max}$ are given in Table 4.1. The equation for concrete crushing, $V_{Rd,max}$ includes a coefficient $\alpha_{cw}$ to take account of the stresses in the compression chord. Should a section be failing in crushing, rather than by failure of the stirrups, the concrete strength reduction factor, $\nu$, is altered, with the recommended value given in Eq. 4.8. However, if the design shear stress in the shear reinforcement is less than 80% of $f_{yk}$ then increased values for ν are permissible. Values for $\alpha_{cw}$ are typically taken as 1, unless there is significant axial compression (§4.4).

$$V_{Ed} > V_{Rd,c} \quad \text{Eq. 4.5}$$

$$V_{Rd} = V_{Rd,s} + V_{ccd} + V_{td} \quad \text{Eq. 4.6}$$

$$1.0 \le \cot\theta \le 2.5 \quad \text{Eq. 4.7}$$

$$\nu = 0.6\left[1 - f_{ck}/250\right] \quad \text{Eq. 4.8}$$

Where: $V_{Ed}$ = the design shear force in the section; $V_{Rd,c}$ = design shear resistance of the section without shear reinforcement; $V_{Rd,s}$ = shear force sustained by yielding the shear reinforcement; $V_{ccd}$ = shear component of force in the compression area in the case of an inclined compression chord; $V_{td}$ = shear component of force in the tensile reinforcement in the case of an inclined tension chord.

*Figure 4.2: The truss model.*

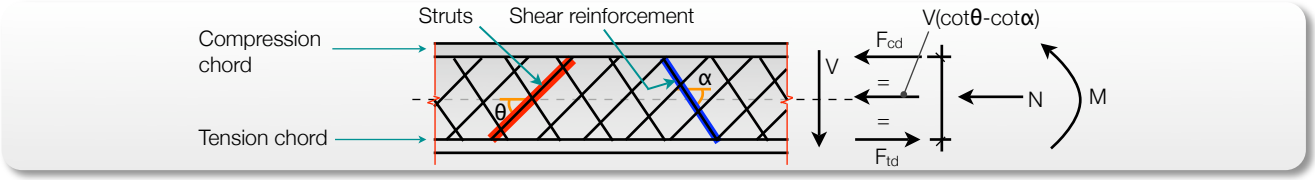


Where: $\alpha$ = Angle between shear reinforcement and the axis perpendicular to the shear force;
$\theta$ = Angle between the concrete compression strut and the beam axis perpendicular to the shear force.

*Table 4.1: BS EN 1992-1-1 Design Equations.*

| | $V_{Rd,s}$ | $V_{Rd,max}$ |
|---|---|---|
| Vertical stirrups | $V_{Rd,s} = \frac{A_{sw}}{s} z f_{ywd} \cot\theta$ Eq. 4.9 | $V_{Rd,max} = \frac{\alpha_{cw} b_w z \nu_1 f_{cd}}{\cot\theta + \tan\theta}$ Eq. 4.10 |
| Inclined stirrups | $V_{Rd,s} = \frac{A_{sw}}{s} z f_{ywd} (\cot\theta + \cot\alpha)\sin\alpha$ Eq. 4.11 | $V_{Rd,max} = \frac{\alpha_{cw} b_w z \nu_1 f_{cd} (\cot\theta + \cot\alpha)}{1 + \cot^2\theta}$ Eq. 4.12 |

Where: $A_{sw}$ = shear reinforcement cross sectional area; $s$ = stirrup spacing; $f_{ywd}$ = design yield strength of the shear reinforcement; $\alpha_{cw}$ = coefficient for the state of stress in the compression chord (§4.4); $\nu_1$ = strength reduction factor for concrete cracked in shear; $b_w$ = minimum width between tension and compression chords; $z$ = lever arm; $f_{cd}$ = design value of compressive strength; $\theta$, $\alpha$ = Figure 4.2.

When a section is subject to high fatigue loading (for example a bridge under cyclic traffic loads), BS EN 1992-1-1 includes a separate fatigue check, where the truss angle is limited as shown in Eq. 4.13 (*cl.3.8.2(3)*). The truss angle limit in general design of *cot(θ)= 2.5* (Eq. 4.7) is taken from the Danish Concrete code (DS 411), and was originally introduced after experimental results showed that wide cracks formed when *cot(θ)* was greater than *2.5*. Therefore the upper limit to *cot(θ)* of *2.5* is a cracking limit (but remains under the ULS check), and in members with small amounts of shear reinforcement does not necessarily imply that failure loads will be reached.

$$\tan\theta_{fat} = \sqrt{\tan\theta} \le 1.0 \quad \text{Eq. 4.13}$$

Where $\theta$ = angle of compression strut, Figure 4.2

The truss analogy, as a lower bound approach, must satisfy equilibrium at all locations. Therefore compression in the concrete strut must be considered in both horizontal and vertical components, resulting in an additional horizontal tension in both the top and bottom chords as shown in Figure 2.10. The additional force ($\Delta F_{td}$) is determined for a rectangular section as shown in Eq. 4.14. Its application to circular sections is analysed in depth in §6.4, as no provisions currently exist for sections with distributed longitudinal bars. For members without shear reinforcement, the Eurocode 'shift rule' can also be applied (see BS EN 1992-1-1 *cl.9.2.1.3(2)*), where the moment diagram is shifted by a distance $a_1$ (Eq. 4.15) from is original position.

$$\Delta F_{td} = \frac{1}{2} V \left( \frac{1}{\tan\theta} - \frac{1}{\tan\alpha} \right) \quad \text{Eq. 4.14}$$

$$a_1 = z(\cot\theta - \cot\alpha)/2 \quad \text{Eq. 4.15}$$

### 4.3.1. NDP

It is worth noting that BS EN 1992-1-1 has 121 nationally determined parameters, more than any other Eurocode, due primarily to the difficulties of harmonisation between EU states. In future development of the concrete code it may be sensible to put aside 'old' methods of shear design and concentrate on the modern approaches illustrated in §2. However, difficulties associated with implementing new design approaches may mean that the truss model is used for a long time to come.

## 4.4. Axial load

Axial load has been briefly discussed (§2.5) and in general moderate axial compression is deemed to increase the shear capacity of a section. As will be seen in §6.5, crushing of the inclined compression strut is unlikely to govern design. However, some concerns have been raised (Jackson, 2006) over the web crushing equation, Eq. 4.10, specifically in terms of prestressed concrete beams, although the same formula is used for all axially loaded reinforced concrete elements. In Figure 4.3 the shear capacities, as predicted by BS 5400-4 and BS EN 1992-1-1, are plotted against the ratio of $A_s f_y/bs$ for a section using *50N/mm²* concrete. It is clear that BS EN 1992-1-1 allows fewer links at low values of shear (since a flatter truss angle may be used, Eq. 4.9) and the crushing limit (Eq. 4.10) is greatly increased when compared to BS 5400-4. However, as noted by Jackson (2006) a greater amount of shear steel is required to take advantage of this increase in capacity in BS EN 1992-1-1.

The BS EN 1992-1-1 equations are plotted for stirrups with a truss angle of $\cot(\theta) = 2.5$ up to the crushing limit (Figure 4.3). The truss angle is then reduced incrementally to $\cot(\theta) = 1.0$ (45º) to obtain the maximum crushing capacity. The BS5400-4 equations are also shown, where the longitudinal steel ratio ($A_s/bd$) is taken as 1%. Figure 4.3 also shows the effect on the design equations when the stress in the stirrups is less than 80% of the yield stress and Eq. 4.8 is used, which gives a higher value for the concrete effectiveness factor (Eq. 4.8). Whilst Jackson (2006) describes the basis of the 80% rule for $\nu$ as obscure, the limit essentially assumes a concrete strength, $f_{ck}$, of 0N/mm².

*Figure 4.3: Shear capacity and link area comparison, BS EN 1992-1-1 and BS5400-4.*

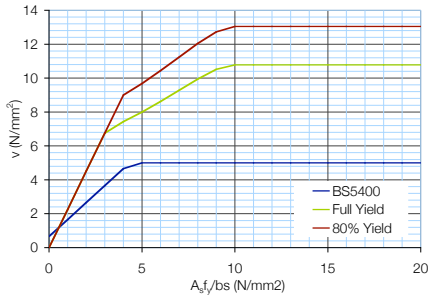


BS5400

$$v = \frac{A_s f_y}{bs} - 0.4 + v_c \qquad v_c = 0.27(1)^{1/3}\left(f_{cu}\right)^{1/3}$$

EN 1992-1

$$v = \frac{A_s}{sb}\left(0.9 f_y \cot\theta\right) \quad \text{(Stirrups)} \qquad < \quad v = \frac{0.9\alpha\nu f_c}{\cot\theta + \tan\theta} \quad \text{(Crushing)}$$

Yield, EC2

$$v = 0.6\left[1 - f_{ck}/250\right] \quad \text{(Full yield limit)} \qquad v = 0.6 \quad \text{(80% Yield limit)}$$

Under axial load, $V_{Rd,max}$ (Eq. 4.10) is enhanced by the factor $\alpha_{cw}$, which has a maximum value of 1.25. The enhancement comes from the fact that under axial compression the direction of the principal compression is closer to the horizontal (Jackson, 2006); in turn this means that the struts rotate less to obtain the optimum value for link design. However, BS EN 1992-1-1 does not take the effect of axial load into account when calculating the link capacity, Eq. 4.9. As has been seen in Figure 4.3 it is not until relatively high shear stresses that the crushing limit must be used, and in most design situations web crushing will not be a critical consideration. BS EN 1992-1-1 does not consider axial load entirely satisfactorily, since high compressions could potentially reduce the shear capacity of a section if an accurate definition for $z$ is taken (rather than assuming $0.9d$). This is illustrated in Figure 4.4, where significant axial load increases the depth of the compression zone, which in turn reduces the actual lever arm, $z$. If this reduction in the lever arm, $z$, is applied to Eq. 4.9 a reduced capacity is calculated, contrary to the expected increase in capacity under axial loads. This is illogical since the application of axial load prevents cracks from opening and increases the actions of aggregate interlock, both of which should increase shear capacity.

*Figure 4.4: Qualitative analysis of the application of axial load to a circular section.*

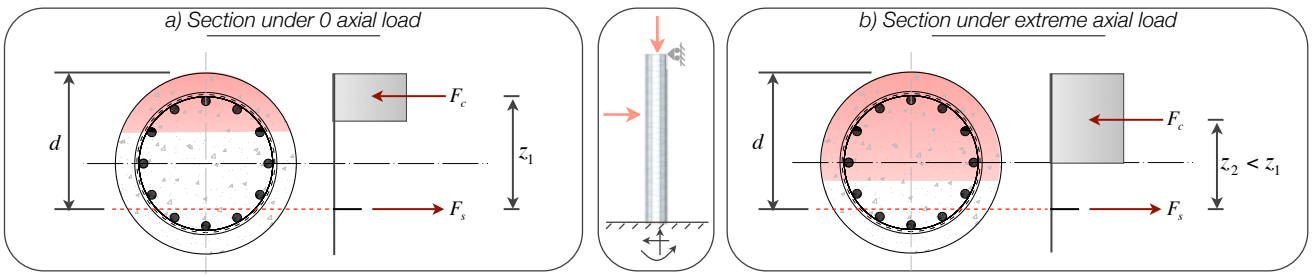


## 4.5. Concrete strength

BS EN 1992-1-1 allows the use of high strength concrete (up to C90/105), although the National Annex for the UK limits the shear strength of concrete strength classes higher than C50/60 to C50/60 (cube strength *60N/mm²*). A summary of currently available test data for circular sections (as analysed in §5 and §6) is shown in Table 4.2, where the maximum cube strength recorded is slightly less than the maximum allowable, and the average is approximately half the maximum. Where high strength

concrete is used, the ultimate compressive strain capacity is reduced (from $\varepsilon_{cu} = 0.0035$ at $f_{ck} < 50MPa$ to $\varepsilon_{cu} = 0.0028$ at $f_{ck} = 90MPa$). In part, this reduction accounts for the more brittle behaviour of high strength concrete, which tends to fail in a more explosive (and therefore less safe) manner.

The use of a higher strength concrete would be expected to have two effects, firstly to improve the peak shear capacity of the section and secondly to reduce its ductility. Higher strength concrete fails at lower values of strain, but provides higher peak strength, as seen in Figure 2.1. However, given that BS EN 1992-1-1 considers the concrete to be ineffective once cracked, and that shear capacity comes solely from the links, this increase in strength has little bearing on the stirrup requirements. An increase in concrete strength should theoretically increase the lever arm, $z$, if an accurate definition is used (such that the lever arm is the '*distance between the centroid of the more tensile chord and the more compressive chord*', (PD6687-2, p.12)) which would be beneficial, but in general this improvement will be slight. Therefore, when specifying high strength concrete it is essential to ensure that the concrete crushing limit is analysed for a maximum of C50/60 grade concrete and that reduced values for the ultimate compressive strain are used.

In seismic design, where ductility is a prime concern, BS EN 1998-2 recommends that the values of $V_{Rd,c}$, $V_{Rd,max}$ and $V_{Rd,s}$ all be divided by an additional partial safety factor, $\gamma_{Bd1}$, (which takes a recommended value of 1.25[1]) specifically noted as a factor 'against brittle failure'. However, this factor is presented as constant for all concrete strengths, which seems to imply that it is more conservative when low strength concrete is used, and less conservative for higher strength concrete. The effect of high shear steel percentages is not discussed, but by providing more effective confinement to the compression zone a more ductile response could reasonably be expected. In the design of FRP reinforced sections, where ductility is crucial (as the sections are over-reinforced), the compression zone is often helically wrapped with FRP to provide this additional ductility.

*Table 4.2: Range of concrete strengths of available test data for circular columns.*

| Experimental data set | Minimum concrete strength N/mm² | Maximum recorded concrete strength N/mm² | Average N/mm² | Approximate equivalent cylinder strength N/mm² |
|---|---|---|---|---|
| Capon and de Cossio (1966), §8.2 | 13.15 | 45.00 | 25.42 | 20 |
| Clarke and Birjandi (1993), §8.3 | 20.10 | 50.50 | 33.97 | 25 |
| Collins (2002), §8.4 | 19.30 | 40.40 | 30.86 | 25 |

## 4.6. Conclusions

The Eurocode approach to shear differs to the British Standards approach in that it assumes the shear capacity of a cracked section to be dependent on the stirrup contribution only. This is a more attractive theoretical model, and the variable angle model is better able to represent the response of concrete sections and no longer relies on empirically derived concrete contributions. The Eurocode model for stirrup design therefore no longer considers size effects, and is relatively insensitive to concrete strength. The stages of variable angle truss model behaviour are summarised in Figure 4.5 for a lightly reinforced section. Heavily shear reinforced sections may not reach the yielding stress of the steel, limiting the angle at failure to that which occurs at crushing of the concrete struts.

*Figure 4.5: Stages of behaviour in the truss model (after Walraven, 2008).*

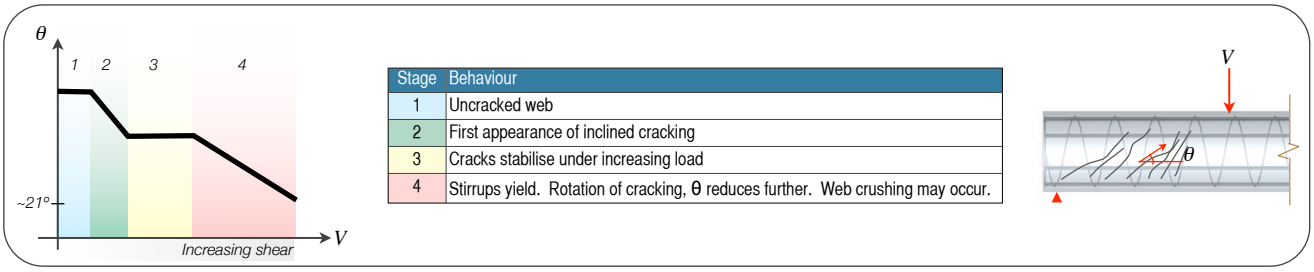


The influence of axial load has been investigated and expected increases in shear capacity when axial load is applied are not seen in BS EN 1992-1-1. Furthermore, accurate analysis of the lever arm, $z$, could potentially lead to a reduction in predicted shear capacity for axially loaded and reinforced sections. The following chapter introduces the design of circular sections, presenting both theoretical and experimental work. The geometry of closed and spirally bound sections is discussed, and existing design guidance for circular sections is analysed. The findings of §5 then go on to influence the new design equations for circular sections presented in §6.

[1] At the present time (February 2009) the National Annex for BS EN 1998-2 is unpublished. NDPs may be different to those stated in the text.

# 5. Circular sections

## 5.1. Introduction

The preceding chapters have considered a significant body of theoretical work, providing a sound basis from which to build this dissertation. Now that codified design methods have been fully considered, detailed analysis is given to the specific issues surrounding circular sections. This chapter considers work ranging from some of the earliest experimental data to more recent papers considering the Eurocodes. Given the nature of this work, additional papers have been utilised throughout the dissertation to support and inform analysis and discussion.

## 5.2. Shear behaviour

### 5.2.1. Early Work

Capon (1966) undertook some of the earliest shear tests on circular concrete columns following the earthquakes of Mexico City (1957) and Coatzacoalcos-Jaltipan (1959), where a large number of circular columns were found to have failed in shear (De Cossio, 1961). It is from this early stage that design for earthquakes has played a role in the collection of experimental test data. De Cossio (1961) also notes that many of the failures in the aforementioned earthquakes had been designed to the American ACI-318 code (then 1951 edition). Similar earthquakes in Chile in the same period, where the German *DIN* code was used, resulted in fewer shear failures, although no data is available to verify this. The first tests by Capon included 21 specimens ranging from 150mm to 250mm in diameter. Of the eleven columns that failed in shear, four of these were tested with axial load and two specimens had stirrups. The test results are compared by the author (Figure 5.1) to calculated shear capacities using the BS5400-4 method (§3.2.1, Table 5.2) with material partial safety factors set to 1.0, and taking definitions for breadth and effective depth from the American Concrete Institute code ACI 318 (1999) such that the breadth is the diameter of the section and the effective depth, *d*, is the distance from the extreme compression fibre to the centroid of the tension zone, Figure 5.1(r).

*Figure 5.1: Test results comparison (l); Section dimensions (r).*

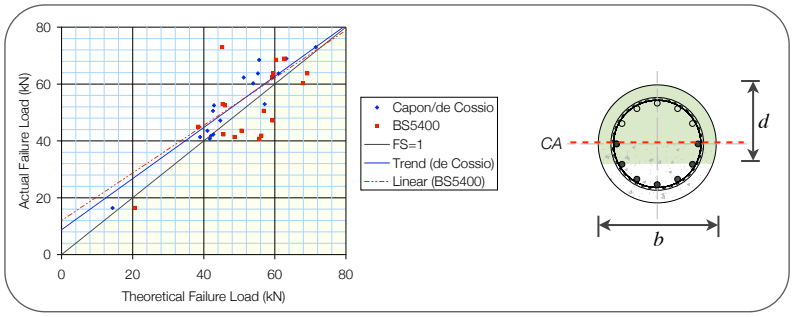


Capon's analysis used 13 separate column parameters to determine the most accurate method of modelling a circular section when using formulae designed for rectangular sections. This included four definitions for effective depth, three for measuring steel area, and six to determine the effective area of the column. It is unsurprising, therefore, that the fit shown in Capon's analysis (Figure 5.1(l)) is relatively accurate. However, there is considerable scatter in the results and Capon's equations appear to become unconservative beyond the range of the test data.

It was found that when using a BS5400-4 approach, 9 of the analysis results were non-conservative, illustrating the difficulties of predicting shear capacity for circular sections. Capon concedes that the limited number of tests undertaken make it difficult to drawn firm conclusions, however some general statements are made. It is found by comparing test results that the percentage of longitudinal steel has a greater influence on shear capacity than the ratio *Vd/M* (shear force divided by moment). Further, the greater the space between layers of steel, the lower the inclined cracking load. This is attributed to the fact that the longitudinal bars create an effect similar to horizontal stirrups, as cracking occurs in small stages between the bars to combine into a larger crack across the section. Only four tests included shear reinforcement, which is surprising as the paper set out to determine design guidance for circular columns. The testing of non-shear reinforced sections is repeated in much of the available literature.

Cracked sections were in some cases retested and Capon found that the ultimate capacity of the section was not adversely affected by having been previously cracked. It could be surmised from this that cracking of a section under ultimate loading will not affect the long term strength of the column. However, cracking leaves the section open to corrosion and degradation through water ingress which in turn will lead to reduced capacity through spalling of the concrete and rusting of the reinforcement. Capon (1966, p26) concludes that the '*prediction of bending capacity using the rectangular stress distribution leads to conservative results*'. The shear strength of the columns tested was deemed to be primarily dependent on the concrete strength and cross sectional area, with longitudinal steel percentages being less important.

### 5.2.2. British Cement Association tests

Recognised as the next major development, Clarke (1993), working with the British Cement Association (BCA) tested 50 specimens in shear and produced one of the largest experimental data sets available. The impetus for this work came from the British Piling industry where concern had been raised over the lack of design guidance for piles subject to high shear loads. Concrete strength, longitudinal and shear reinforcement percentages, axial load and section diameter were all varied to provide a wide ranging set of results. Three column diameters and three column lengths were assessed with longitudinal reinforcement percentages of between *0.9%* and *5.6%*. Where shear reinforcement was provided it was in the form of closed links except in six tests where spirals with a *150mm* pitch were used. Nominal concrete mix strengths ranged from *25N/mm²* to *50N/mm²*.

In Clarke's analysis, the effective depth, *d*, was taken as shown in Figure 5.1(r) and the sensible step of removing the column width, *b,* from the shear equations was taken to consider shear forces rather than stresses. This removes the difficulties of defining *b*, which if taken as the section diameter can lead to an effective shear area that is greater than the cross sectional area of the circle itself. The results of Clarke's analysis are presented throughout §6, where they are compared to the newly derived variable angle truss equations. Geometrical relationships for circular sections have been formed by many different researchers, the most useful of these are presented and compared in §5.3, before further analysis is undertaken.

## 5.3. Geometry

Circular geometry is assessed to produce the best design formulae for circular sections. Both Clarke (1993) and Capon (1966) calculated effective depths on a case-by-case basis, taking the distance from extreme compression fibre to the centroid of tension steel. However, Feltham (2004) notes that the orientation of the pile or column relative to the applied shearing force is usually unknown and it would therefore be better to have a general equation for effective depth that can disregard the plan layout of the longitudinal bars. It can be shown that a sensible estimation for the distance to the centroid of the tension bars below the centre of the section is given by $2r_s/\pi$, Figure 5.2. The effective depth is then defined by Eq. 5.1 and given the low error seen when using this formula (maximum 3.7%), it will be used in the remainder of the analysis found in this dissertation.

*Figure 5.2:Calculation of effective depth progression.*

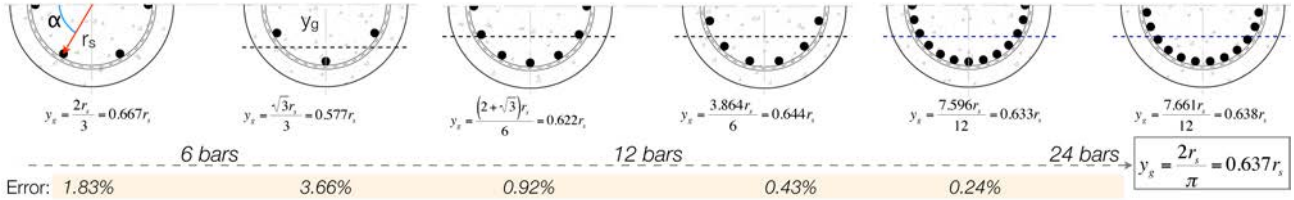


$$d = r(1+\sin\alpha) \qquad \text{Eq. 5.1}$$

Where $\sin\alpha = 2r_s/\pi r; 0 < \alpha < \pi/2$ Eq. 5.2

And: $r$ = centre to extreme fibre radius; $r_s$ = radius to centre of longitudinal steel.

For design codes which include a concrete contribution (Figure 2.9), this contribution is typically defined in terms of the effective shear area (*bd*, Eq. 3.6). In a circular section this definition has the potential to overestimate the shear area and Feltham (2004) presents a simple and accurate method to determine the actual shear area of the circle, as shown in Figure 5.3. The resulting equation (Eq. 5.4) may therefore replace the '*bd*' term in all BS5400-4 and BS8110-1 shear equations.

*Figure 5.3: Section definitions.*

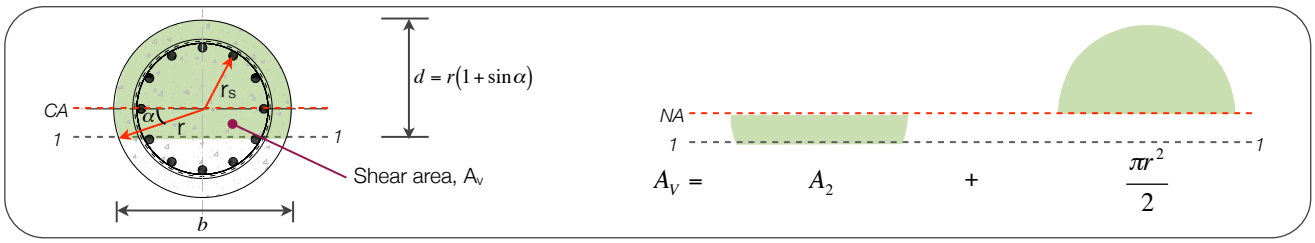


Area of section above the line 1-1 in Figure 5.3 is given by:

$$A_v = 0.5\pi r^2 + \left(0.5\pi r^2 - 0.5r^2\left(\theta_c - \sin\theta_c\right)\right) \text{ Where : } \theta_c = (\pi - 2\alpha) \qquad \text{Eq. 5.3}$$

Therefore the shear area, $A_v$ is given by:

$$A_v = r^2\left(\frac{\pi}{2} + \alpha + \sin\alpha\cos\alpha\right) \qquad \text{Eq. 5.4}$$

### 5.3.1. Link efficiency

Considering the section shown in Figure 5.3, it is evident that applied shear forces are resisted only by the vertical component of the force in the link, reducing their efficiency when compared to a rectangular section. Circular sections are reinforced with either spirals or closed links, and the efficiency of both is dependent primarily on the geometry of the section. The number of links which intersect a failure plane and thus contribute to the shear strength of a section is given by the depth of the member divided by the link spacing. In the case of vertical links, Feltham (2004) suggests that only the portion of link within the effective depth should be considered as contributing to the overall section resistance. Thus, the section capacity is determined by the sum of the vertical components of force in the stirrups within the active area for links, as shown in Figure 5.4. By integrating between the top and bottom of the effective depth zone, the shear force carried by the links is determined, Eq. 5.5. The integration (Feltham, 2004) has been reviewed and is presented below in an abridged form. The result for closed links is given by Eq. 5.8.

*Figure 5.4: Geometry for closed links.*

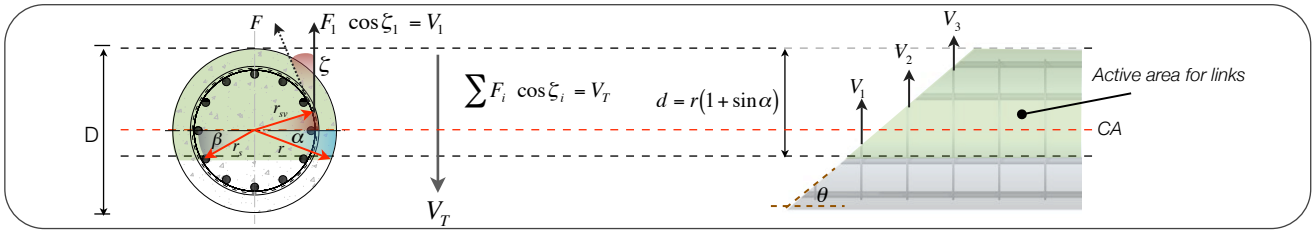


$$\frac{A_{steel} f_y}{s} \int \cos\zeta dx \text{ and } \sin\beta = \frac{2r_s}{\pi r_{sv}} \qquad \text{Eq. 5.5}$$

Using Eq. 5.1 then the following may be found (see Feltham, 2004) for the total force in the links.

$$\frac{A_{steel} f_y}{s} \int_{-\beta}^{\pi/2} \cos\zeta \left( r\cos\zeta \frac{(1+\sin\alpha)}{(1+\sin\beta)} d\zeta \right) \qquad \text{Eq. 5.6}$$

And since $\int \cos^2\zeta d\zeta = \zeta/2 + 0.25\sin(2\zeta)$. Then by solving Eq. 5.6 the force taken by the links is given by Eq. 5.7.

$$I = \frac{A_{steel} f_y}{s} r \frac{(1+\sin\alpha)}{(1+\sin\beta)} \left[ \frac{\zeta}{2} + \frac{1}{4}\sin(2\zeta) \right]_{-\beta}^{\pi/2} \Rightarrow \frac{A_{steel} f_y}{s} r \frac{(1+\sin\alpha)}{(1+\sin\beta)} \frac{1}{2} \left[ \frac{\pi}{2} + \beta + \frac{1}{2} 2\sin\beta\cos\beta \right] \qquad \text{Eq. 5.7}$$

$$\Rightarrow \frac{A_{steel} f_y}{2s} r \frac{(1+\sin\alpha)}{(1+\sin\beta)} \left( \frac{\pi}{2} + \beta + \sin\beta\cos\beta \right) \qquad \text{Eq. 5.8}$$

Which can also be rearranged as a stress, such that:

$$v = \frac{A_{steel} f_y}{4ds} \frac{(1+\sin\alpha)}{(1+\sin\beta)} \left( \frac{\pi}{2} + \beta + \sin\beta\cos\beta \right) \qquad \text{Eq. 5.9}$$

Where: d = effective depth as given by Eq. 5.1

### 5.3.2. Spiral links

The design of circular columns can use either discrete or continuous links. The practical design of small diameter columns may lead to a square cage inserted into circular formwork (and hence can be designed as a square section). Spirals can usually only practically be used for column diameters of greater than 300mm (Ambrose, 2007), and spiral reinforcement makes bar spacing critical and limits the possible steel percentages in the section. In very large diameter circular columns, it would be feasible to overcome this problem by using concentric rings of steel, but analysis of this is complex and is not considered here.

Clarke (1993) considered the design of spiral links by firstly analysing the BS8110 approach for inclined links. It is noted that the BS8110-1 approach is inconsistent since the capacity of bent-up bars is based on the geometry *d-d'* (Figure 3.1(r)), whilst vertical link design is based solely on the effective depth, *d*. The Eurocodes on the other hand consider vertical links as a special case of inclined links; this approach makes more sense conceptually. Clarke applies this principal to BS8110-1 by rearranging the formula for inclined links and assuming a concrete strut angle of *45º*. This results in Eq. 5.12, where the capacity of an inclined link is found as a simple geometric factor of a vertical link with the same cross sectional area.

Then, by taking the spiral as a special case of an inclined link, Clarke produced an efficiency factor for spiral links when compared to their equivalent vertical links. This factor arises from the fact that the legs of vertical shear links both cross the inclined shear plane at the same angle, whereas in spiral reinforcement the angle between the leg and the failure plane is different on either side of the centre line of the column, Figure 5.5. The two opposing legs in spirally bound sections will be at

angles α and (180-α) to each other, which, when combined with Eq. 5.12, results in an overall efficiency of *sin(α)*. This relationship is summarised in a table of efficiency factors for different values of spiral pitch (given as a proportion of *d*), Table 5.1.

Current BS8110 equation for bent up bars (cl.3.4.5.6):

$$V_b = A_{sb}\left(0.87 f_{yv}\right)\left(\cos\alpha + \sin\alpha \cot\beta\right)\left(d - d'\right)\left(s_b^{-1}\right) \qquad \text{Eq. 5.10}$$

Equivalent equation for vertical links

$$V_v = \frac{A_{gv}\left(0.87 f_{yv}\right)\left(d\right)}{s_v} \qquad \text{Eq. 5.11}$$

Rearranged for bent up bars:

$$V_b = V_v\left(\cos\alpha + \sin\alpha \cot\beta\right) \qquad \text{Eq. 5.12}$$

*Table 5.1: Pitch and efficiency of spiral shear links (Clarke, 1993)*

| Pitch | Efficiency | Pitch | Efficiency |
|---|---|---|---|
| **0.20** | 1.00 | **0.80** | 0.93 |
| **0.40** | 0.98 | **1.00** (i.e. *d*) | 0.89 |
| **0.60** | 0.96 | | |

Given the difference in angle on either side of the shear plane for each revolution of the spiral, it is logical to assume that one side of the spiral has a greater load capacity than the other. If these unequal forces are considered the section is not in equilibrium, but instead has a torsional moment acting along it. The truss analogy, being a lower bound solution, must satisfy equilibrium at all locations and so an unequal force distribution cannot be used. Feltham (2004) proposes that the lower of the two values be taken as acting on both sides of the section, thus providing a conservative approach. The shear force taken by spiral links is more complex than for a vertical link, since intersections with the failure plane must now consider three-dimensional variations in the link geometry, Figure 5.5. Feltham (2004) provides a detailed analysis of spirally reinforced sections to determine the vertical component of force, *F′*, in the spiral link, Eq. 5.13. This is given as a factor of the force, *F*, as found for a closed link reinforced circular section (Figure 5.4).

In order to assess a 'smeared section' where the spiral links are treated as a continuum, the link spacing must be given in terms of the angle ζ, Figure 5.6. The position of the link along axis of the column is given by Eq. 5.16 and its location over the height of the section by Eq. 5.15. The spacing of the links is related to the pitch as shown in Figure 5.6, and this can then be rearranged to define the spacing of the spirals, *s*, in terms of ζ, *β* and *α*, Figure 5.6, Figure 5.7 and Eq. 5.20. Full derivations are given by Feltham (2004).

*Figure 5.5: Spiral link geometry.*

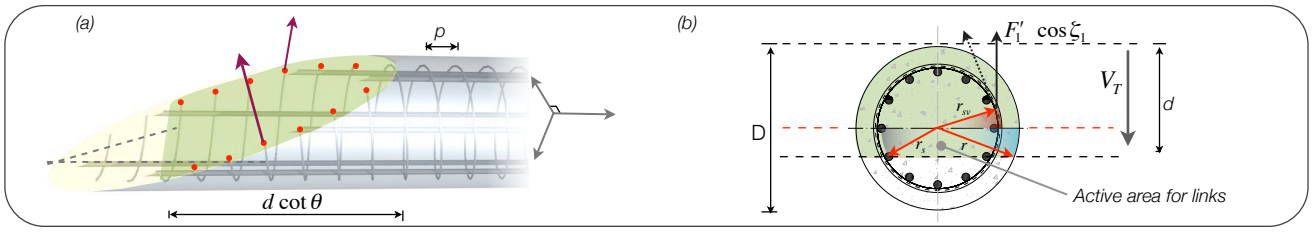


Total force carried by the links is given by: $\sum_{i=1}^{m} 2F_i' \cos\zeta_i$ . By substitution *F′* is equal to Eq. 5.14.

$$F' = F\left(1 + \left(\frac{p}{2\pi r_{sv}}\right)^2\right)^{-0.5} \qquad \text{Eq. 5.13}$$

$$F' = \left(1 + \left(\frac{p}{2\pi r_{sv}}\right)^2\right)^{-0.5} \sum_{i=1}^{m}\left(2F_i \cos\zeta_i\right) \qquad \text{Eq. 5.14}$$

*Figure 5.6: Angle derivations.*

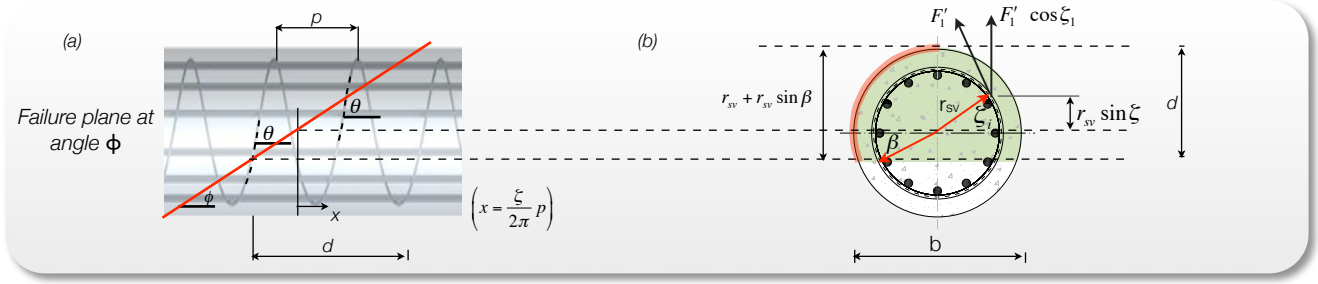

$$z = r_{sv}\sin\zeta \text{ and } x = \frac{\zeta}{2\pi}p$$ Eq. 5.15, Eq. 5.16

The angle between link and column axis is then given by θ, where:

$$\tan\theta = \left(\frac{dz}{dx}\right) = \left(\frac{d}{d\zeta}r_{sv}\sin\zeta\right)\frac{1}{\frac{\zeta}{2\pi}p\frac{d}{d\zeta}} = \frac{2\pi r_{sv}\cos\zeta}{p}$$ Eq. 5.17

Then, the crack inclination angle, ϕ, is given by: $\tan\phi = \frac{r_{sv} + r_{sv}\sin\beta}{d}$ Eq. 5.18

And applying Eq. 5.1: $\tan\phi = \frac{r_{sv}}{r}\left(\frac{1+\sin\beta}{1+\sin\alpha}\right)$ Eq. 5.19

*Figure 5.7: Pitch and spacing relationship.*

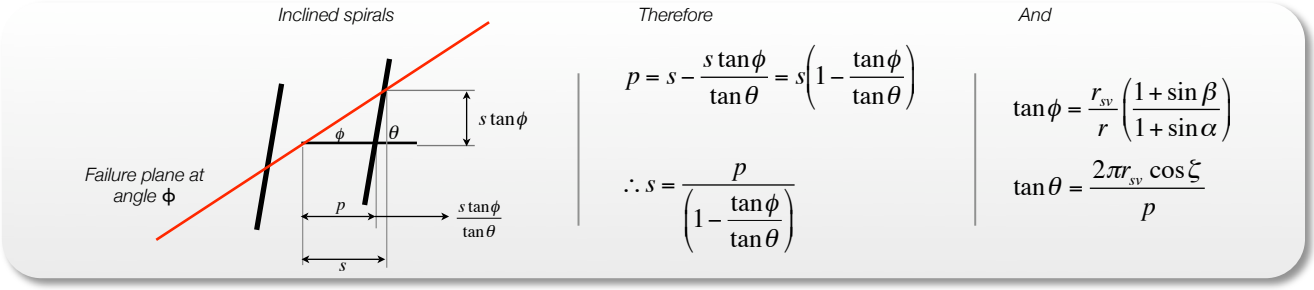


$$\Rightarrow s = \frac{p}{\left(1 - \left(\frac{1+\sin\beta}{1+\sin\alpha}\right)\frac{p}{2\pi r_{sv}\cos\zeta}\right)}$$ Eq. 5.20

The equations are solved as for flat links, with the force given by Eq. 5.14 integrated over all values of *cos(ζ)*, Eq. 5.21 (Feltham, 2004)

$$\left(1+\left(\frac{p}{2\pi r_{sv}}\right)^2\right)^{-0.5}\frac{f_y A_{sv} r}{p}\left[\left(\frac{\pi}{2}+\beta+\sin\beta\cos\beta\right)\frac{(1+\sin\alpha)}{(1+\sin\beta)} - \frac{p(1+\sin\beta)}{\pi r}\right]$$ Eq. 5.21

Which could be extended to a variable angle model (§6.3), given by Eq. 5.22.

$$\left(1+\left(\frac{p}{2\pi r_{sv}}\right)^2\right)^{-0.5}\frac{f_y A_{sv} r\cot\theta}{p}\left[\left(\frac{\pi}{2}+\beta+\sin\beta\cos\beta\right)\frac{(1+\sin\alpha)}{(1+\sin\beta)} - \frac{p(1+\sin\beta)}{\pi r}\right]$$ Eq. 5.22

The proposed equation (Eq. 5.21) is rather complex and unwieldy to use. Turmo et al. (2008) provide a further analysis which allows the designer to vary the depth over which the links are effective (where previously this had been assumed to be *d*). This method is analysed in greater detail in §6.3.4, and comparisons can be drawn between the factors used in Eq. 5.21 and Eq. 6.21.

In conclusion, Clarke (1993) notes that tests on concrete in shear tend to give proportionally large amounts of scatter. In work by Brown (2006) 1200 tests on rectangular sections were compiled, of which 47% had some shear reinforcement. The data showed considerable scatter and 7% of tests were deemed unsafe, leading to alterations to the ACI-318 code. In contrast, Clarke (1993) provides a test database of under 100 samples, greatly reducing accuracy and range of applicability for any empirical formulae derived.

Whilst the determination of empirical trends can be made difficult by the large number of tests required, Feltham concludes that the approach shown above is valid. In comparing theoretical and experimental results, it is shown that the effects of varying longitudinal reinforcement, concrete strength or shear reinforcement do not affect the ability to calculate shear capacity with good accuracy. The recommendations for the design of circular sections as put forward by Clarke are summarised as follows:

- Area of tension reinforcement should be taken as the area of steel below the mid-depth of the section;
- Effective depth, *d*, is taken from the extreme compression fibre to the centroid of the steel area;
- In determining concrete capacity, the term *bd* should be replaced with the true area to the effective depth of the section;
- When spirals are used, their efficiency is reduced as shown in Table 5.1.

### 5.3.3. Design approach comparisons

The approach proposed by Feltham (2004), as presented above, can be compared to the approaches of Clarke (1993) (referred to as the BCA approach) and to Highways Agency design documents BD42 (2000) and BD74 (2000) which in turn both make reference to the current code of practice for foundations (BS8004, 1986) (see §3 for further details). BD74/00 also includes, as an Appendix, a design approach for bending, axial and shear forces on circular piles. In this, three of Clarke's recommendations are included but no adjustment is made for the actual shear area of the section, $A_v$ (Eq. 5.4).

*Figure 5.8: Method comparison.*

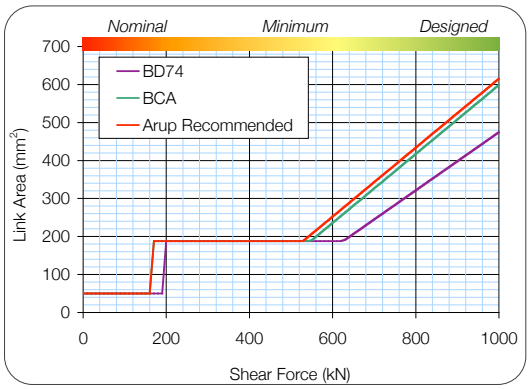


A comparison of the three approaches (Figure 5.8, Spreadsheet 5.1) is interesting and reveals some close similarities. The three approaches are compared by plotting applied shear force against link requirements for a nominal 900mm diameter section. It is clear that the BD74 method gives a smaller required design reinforcement area than either the Feltham (2004) or BCA methods, suggesting that BD74 has not properly accounted for the reduction in efficiency seen in circular sections. All three methods give the same nominal value of shear reinforcement, since they all use the same definition for minimum steel area.

### 5.3.4. Discrete and continuum models for shear

Design codes typically assume a 'smeared' distribution of steel through a section, whereas the reality is of course a discrete distribution. Kim (2005) assesses the effects of link distribution in a circular section by considering the number of links intersecting an inclined crack. A variable, *N*, is defined as the number of spaces between reinforcing hoops crossing a crack generated in shear. When link spacing is high, there will be fewer links crossing a shear crack (and therefore a lower value for *N*). Kim (2005) uses this value to define a correction factor for sections with widely spaced shear reinforcement. However, this approach has not been taken up in design codes, since minimum steel requirements tend to prevent widely spaced shear reinforcement from being used. The result of this is that the continuum truss model is, in most cases, an acceptable simplification for design purposes.

## 5.4. Seismic design

Much research has been undertaken into the seismic behaviour of circular sections, which are often perceived as being the best shape for seismic design due to their uniform directional strength. In seismic design, the provision of ductility can be an overriding concern. Shear, being a non-ductile mode of failure, is therefore critical in many cases. Priestley et al. (1994) provide an expression for the shear capacity of circular sections which broadly follows those seen previously. Shear carried by the transverse reinforcement in a section is considered by resolving parallel to applied shear forces, Eq. 5.23, for a variable angle truss model, and the links are assumed to be effective over their entire height (*D'*), which is potentially non-conservative.

$$V_s = \frac{\pi\left(2A_{sh}f_{yh}\right)D'}{4s}\cot\theta \qquad (kN)$$ Eq. 5.23

Where: $A_{sh}$ = area of the hoop; $D'$ = diameter of section confined between the circular links; $s$ = pitch of bars

### 5.4.1. Formula development

Eq. 5.23 assumes that the stirrups are effective over their full height. Kowalsky (2000) notes that within the compression zone, cracks must be closed and so there cannot be any shear transfer by strain in the reinforcement in this zone. It is then sensible to say that stirrups provide shear resistance only in the tension zone and therefore the equations should be effective over a reduced area, shown as *(D-c-cover)* in Figure 5.9. Kowalsky et al. (1995) considered the effective area of a circular link simply as being the component of link area in the direction of the applied shear. The effective area (Figure 5.9) is given by Eq. 5.24 which can then be integrated across the section to obtain Eq. 5.25, where the '*effectiveness factor*' is approximated to $\pi/2$. Turmo et al. (2008) consider a more general factor (§6 and Table 6.2) which varies depending on the section geometry.

$$A_{eff} = A_{sp}\cos\gamma \qquad \text{And so:} \qquad A_{eff} = 2A_{sp}\frac{\sqrt{r^2 - x^2}}{r}$$ Eq. 5.24

Where $A_{eff}$ = effective spiral area in direction of applied shear; $A_{sp}$ = real spiral area; $\gamma$ = angle between tangent to spiral and direction of applied shear; $r$ = confined core radius.

$$\text{And since } n = \frac{D-c-\text{cov}}{(\tan\theta)s} \text{ then } V_{sg} = \frac{\int_{x=-(r-c)}^{r} 2A_{sp}f_y \sqrt{r^2-x^2}\,/\,r\,dx}{D-c-\text{cov}} \frac{D-c-\text{cov}}{s}\cot\theta$$

$$\Rightarrow V_{sg} = \frac{\pi}{2} A_{sp} f_y \frac{D-c-\text{cov}}{s}\cot\theta \qquad \text{Eq. 5.25}$$

*Figure 5.9: Section layout for Eq. 5.25 adapted from Kowalsky (2000) and Kowalsky et al. (1995).*

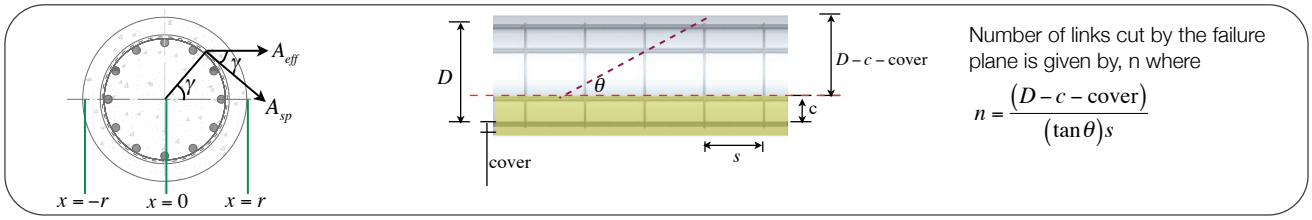


## 5.5. Codified design

Codified design provisions for circular sections are summarised in Table 5.2, where analysis from §3, §4 and §5 is collated. In BS8110, irregular sections are considered just once, when it is noted that: (*cl.3.8.1) 'While the provisions relate primarily to rectangular cross sections, the principles involved may be applied to other shapes where appropriate.*' It is therefore up to the designer to adapt the provisions of the code for circular sections, and to decide if the section is 'appropriate' as no guidance is given on this general statement.

In BS EN 1992-1-1, no mention is made of circular sections, but BS EN 1998-2 appears to have adopted Feltham's definition for effective depth in circular sections (*cl.5.6.3.3(2)*). For consistency, it is therefore recommended that BS EN 1992-1-1 should reference BS EN 1998-2. ACI 318 provides a simple definition for the effective depth of a circular section as discussed in §5.2, but this is the limit of its analysis. The Canadian S6-06 does not explicitly mention circular sections, but the MCFT approach may be applied to any section geometry through computer analysis, hence the analysis method (§2.8.3) and design equations (§3.4.2) can be applied to circular sections.

## 5.6. Conclusions

The analysis undertaken thus far is sufficient to show that there is a requirement for the design of members in shear to be rationalised. Work by Collins and others, moving towards a compression field theory for concrete appears to be a fruitful approach. However, BS EN 1992-1-1 uses only the truss analogy and so any design guidance must follow this model. Recent research has begun to bring this together, with the work by Turmo et al. (2008) being particularly fruitful for comparison and verification of proposed design approaches. The geometric ratios from Clarke (1993), Feltham (2004) and Kowalsky (2000) will help to shape the design equations of §6.

The truss analogy for rectangular sections is a powerful design method and is relatively simple to envisage. Defining a circular truss is more difficult, Figure 5.10. Here, the circular truss has been given elliptical top and bottom chords and ellipsoidal web members. Their behaviour under applied loads is not at all clear, and the influence of longitudinal steel may be more significant in circular sections that in rectangular sections. The provision of a circular truss model (Figure 6.44) is a key outcome of §6.

*Figure 5.10: Simplified comparison of rectangular (l) and circular (r) trusses.*

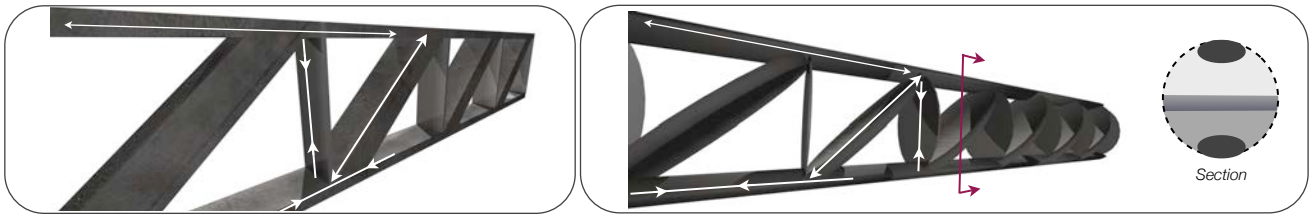


The lack of relevant test data is a significant hindrance to the development of a new design method and since the majority of new tests are being carried out from a seismic engineering perspective the database of shear tests for regular concrete sections is unlikely to be matched. With codified design methods fully established, and key papers surrounding circular section design introduced, new design guidance for circular sections is now considered. §6 presents variable angle truss equations for circular sections based on the Eurocode model. The additional tensile force and crushing are also considered, before an upper bound plasticity approach is presented, and the economics of design are analysed.

*Table 5.2: A summary of approaches to shear design for circular sections.*

| Variable | BS8110 | BS5400 | BD74/00<br>BD42/00 | Clarke | Feltham | ACI 318 | S6-06 |
|---|---|---|---|---|---|---|---|
| *b* | Diameter | Diameter | Diameter | Diameter | Diameter | Diameter | Diameter |
| *d* | "Effective depth to tension reinforcement" | "Effective depth to tension reinforcement" | "Distance from the extreme fibre with maximum compression to the centroid of the reinforcement in the half of the pile opposite the extreme compression fibre." | Distance to the centroid of the steel in the tension zone, assuming neutral axis at centre of the section | $d = r(1+\sin\alpha)$ | Distance from extreme compression fiber to centroid of longitudinal tension reinforcement.<br>Alternatively, effective depth = 0.8 x diameter | Effective shear depth, $d_v = 0.9d$.<br>Effective depth, $d$ = distance from extreme compression fibre to centroid of tension reinforcement |
| *Cross sectional area* | $bd$ | $bd$ | $bd$ | Area in the effective depth zone | $A_v = r^2\left(\frac{\pi}{2}+\alpha+\sin\alpha\cos\alpha\right)$ | $bd$ | - |
| *Area of tension steel* | - | - | - | Area of steel below mid-depth | - | - | - |
| $v_c$ | $v_c = 0.79\left(\frac{100A_s}{b_v d}\right)^{1/3}\left(\frac{400}{d}\right)^{1/4}\left(\frac{f_{cu}}{25}\right)^{1/3}\frac{1}{\gamma_m}$ | $\xi_c v_c = \frac{0.27}{\gamma_m}\left(\frac{100A_s}{b_w d}\right)^{1/3}\left(\frac{500}{d}\right)^{1/4}\left(f_{cu}\right)^{1/3}$ | *BS5400* | *BS5400* | *BS8110* | $V_c = 2\sqrt{f'_c}\, b_w d$<br>Where f'c is the concrete compressive strength in psi | $V_c = 2.5\beta\phi_c f_{cr} b_v d_v$ |
| $A_s$ | $v < 0.5v_c$ : - | $v \le \xi_s v_c$ : $A_{sv} \ge \frac{0.4bs_v}{0.87f_{yv}}$ | $v \le \frac{\xi_s v_c^*}{2}$ : - | $A_{sv} = \frac{V_{sv}s_v}{f_{yv}d}$<br>Where $V_{sv}$ is the shear force contribution of the links | Vertical links:<br>$A_{sv} \ge \frac{2rs_v(v-v_c)}{0.95f_{yv}}$<br>Spiral links<br>$A_{sv} \ge \frac{rp(v-v_c)}{0.95f_{yv}(1-0.225p/r)}$<br>Where p is the pitch of the link. | $V_u < \frac{\phi V_c}{2}$ : - | $A_{min}$ : $A_v \not< 0.15f_{cr}(b_v s/f_y)$ |
| | $0.5v_c < v < (v_c+0.4)$ : $A_{gv} \ge \frac{0.4b_v s_v}{0.87f_{yv}}$ | | $\frac{\xi_s v_c}{2} \le v \le \xi_s v_c^*$ : $A_{gv} \ge \frac{0.4b_v s_v}{0.87f_{yv}}$ | | | $V_u > \frac{\phi V_c}{2}$ : $A_v = 0.75\sqrt{f'_c}\frac{b_w s}{f_y}$ | |
| | $(v_c+0.4) < v < 0.8\sqrt{f_{cu}}$ : $A_{gv} \ge \frac{b_v s_v(v-v_c)}{0.87f_{yv}}$ | $v > \xi_s v_c$ : $A_{sv} \ge \frac{bs_v(v+0.4-\xi_c v_c)}{0.87f_{yv}}$ | $v > \xi_s v_c^*$ : $A_{sv} \ge \frac{s_v b(v-\xi_s v_c)}{f_{yv}/\gamma_{ms}}$ | | | $V_u > \phi V_c$ : $\frac{A_v}{s} = \frac{V_u - \phi V_c}{\phi f_y d}$ | |
| *Shear enhancement* | Enhancement when $a_v < 2d$.<br>Factor $v_c$ by $\frac{2dv_c}{a_v}$.<br>Limit to $0.8\sqrt{f_{cu}}$ or $5N/mm^2$ | Enhancement when $a_v < 2d$.<br>Factor $\xi_s v_c$ by $\frac{2dv_c}{a_v}$.<br>Limit to $0.75\sqrt{f_{cu}}$ or $4.75N/mm^2$ | BS5400 | Enhancement when $a_v < 3d$.<br>Factor $v_c$ by $\frac{3d}{a_v}$ | Enhancement when $a_v < 3d$.<br>Factor $v_c$ by $\frac{3d}{a_v}$ | For section taken at less than *d* from the support, they may be designed to the shear at *d* from the support. | For section taken at less than *d* from the support, they may be designed to the shear at *d* from the support. |
| *v* | $v = \frac{V}{bd}$<br>$v < 0.8\sqrt{f_{cu}}$ or $5N/mm^2$ | $v = \frac{V}{bd}$<br>$v < 0.75\sqrt{f_{cu}}$ or $4.75N/mm^2$ | $v = \frac{V}{bd}$<br>$v < 0.75\sqrt{f_{cu}}$ or $4.75N/mm^2$ | $\frac{V}{A_{eff}}$ | $v = \frac{V}{A_v}$ | Consideration in terms of shear forces rather than stresses | - |
| *Shear and axial load* | $v'_c = v_c + \frac{0.6NVh}{A_c M}$<br>Where N is axial load, M moment, h taken as diameter, $A_c$ is gross area. | Factor $\xi_s v_c$ by $\left(1+\frac{0.05N}{A_c}\right)$ | Where $v_c^*$ is factored by $\left(1+\frac{0.05N}{A_c}\right)$ | - | - | Factor $V_c$ by $\left(1+\frac{N_u}{2000A_g}\right)$<br>Where $N_u/A_g$ is in psi | - |
| *Additional load from truss mechanism* | - | $A_{sa} \ge \frac{V}{2(0.87f_y)}$<br>Where $A_{sa}$ is the area of anchored additional longitudinal reinforcement | $A_{sa} \ge \frac{V}{2(0.87f_y)}$ | - | - | - | - |
| *Biaxial shear* | - | $\frac{V_x}{V_{ux}} + \frac{V_y}{V_{uy}} \le 1$ | - | - | - | - | - |

# 6. Design approach

## 6.1. Introduction

After a presentation of the available test data for circular reinforced sections failing in shear, design procedures are considered with the following objectives:

- An extension of the variable angle truss model to cover circular sections, with equations derived for BS EN 1992;
- A system to deal with concrete crushing in a circular section;
- Development of an upper bound plasticity based approach;
- The use of BS EN 1992-1-1 truss angle limits of $1 \leq \cot\theta \leq 2.5$ in the design of circular sections;
- Analysis of unreinforced circular sections and their efficiency.

The work of Feltham (§5.3) is considered and design formulae for a fixed angle truss are extended to the variable angle truss model before being analysed against Clarke's (1993) experimental data. Work by Turmo et al. (2008) is then examined, and equilibrium is considered in terms of the additional tensile force, $\Delta F_{td}$ (§4.3), before web crushing in circular sections is analysed. Analysis is undertaken for a range of strut angles ($\theta$), but it should be remembered that the designer is in fact free to choose any value for $\theta$, within the limits illustrated in §4. Typically, $\cot(\theta)=2.5$ provides the most economical design. A new design approach for upper bound plasticity in circular sections is explored, before an evaluation of non-shear reinforced section design procedures in both BS EN 1992-1-1 and BS5400-4. The economics of design to BS EN 1992-1-1 are investigated, and comparisons to BS5400-4 are made. Design of circular sections using MCFT (§2.8.3) is then undertaken, and comparisons are made to the proposed Eurocode approach.

## 6.2. Test database

Verification of both existing and proposed design formulae will be carried out primarily using static load tests from Clarke (1993). A database of approximately 129 statically loaded tests compiled during the writing of this dissertation (see Appendices, §8) is provided on the accompanying CD, but as Clarke provides the most complete and consistent set, this is used exclusively. The PEER[2] online database provides test data for dynamic load tests, useful for potential future work in BS EN 1998-2.

### 6.2.1. Analysis

Basic statistical analysis of the data was carried out to determine its variability. Figure 6.1(a) shows that the majority of the columns tested are *300mm* in diameter. Clarke (1993) tested *300mm* diameter columns with up to *5.6%* longitudinal steel reinforcement ratio, as seen in Figure 6.1(b). Figure 6.1(c) shows that 25% of the specimens in the database contain no shear links, this being typical of the tests carried out by Capon (1966). Finally, just over 70% of the samples were tested without axial load. Application of axial load and shear is relatively difficult to carry out and complicates the correlation between loading and member behaviour. By initially using sections predominantly loaded in shear, cases with axial load can be considered separately in order to assess the effects of axial load on shear capacity (§4.4). The assessment of shear strength also relies on the concrete strength ($f_{cu}$) and Figure 6.1(e) shows the variation in cube strength for the available data. Both Capon and Clarke provide concrete cube data, whilst only Capon provides the stirrup yield strength, Figure 6.1(f).

*Figure 6.1: Statistical variations in obtained test data (continued on following page).*

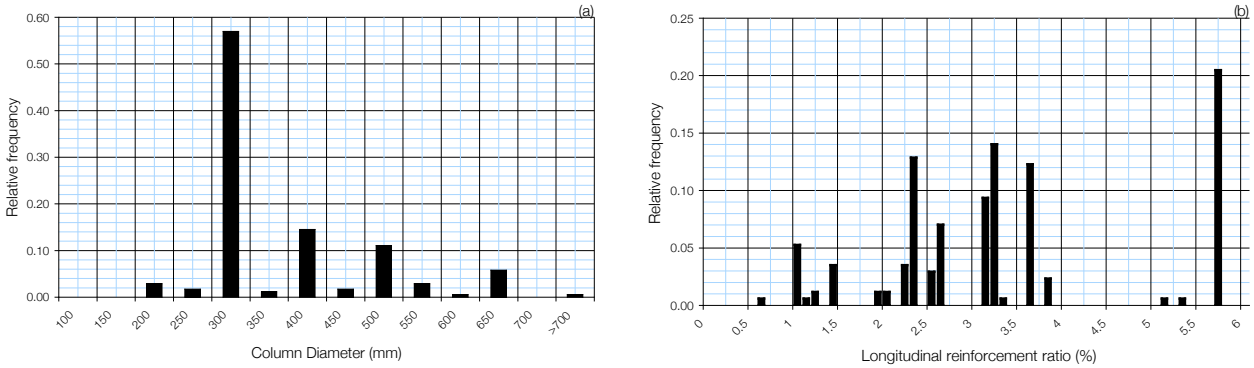


[2] *Pacific Earthquake Engineering Research Centre, University of Washington*

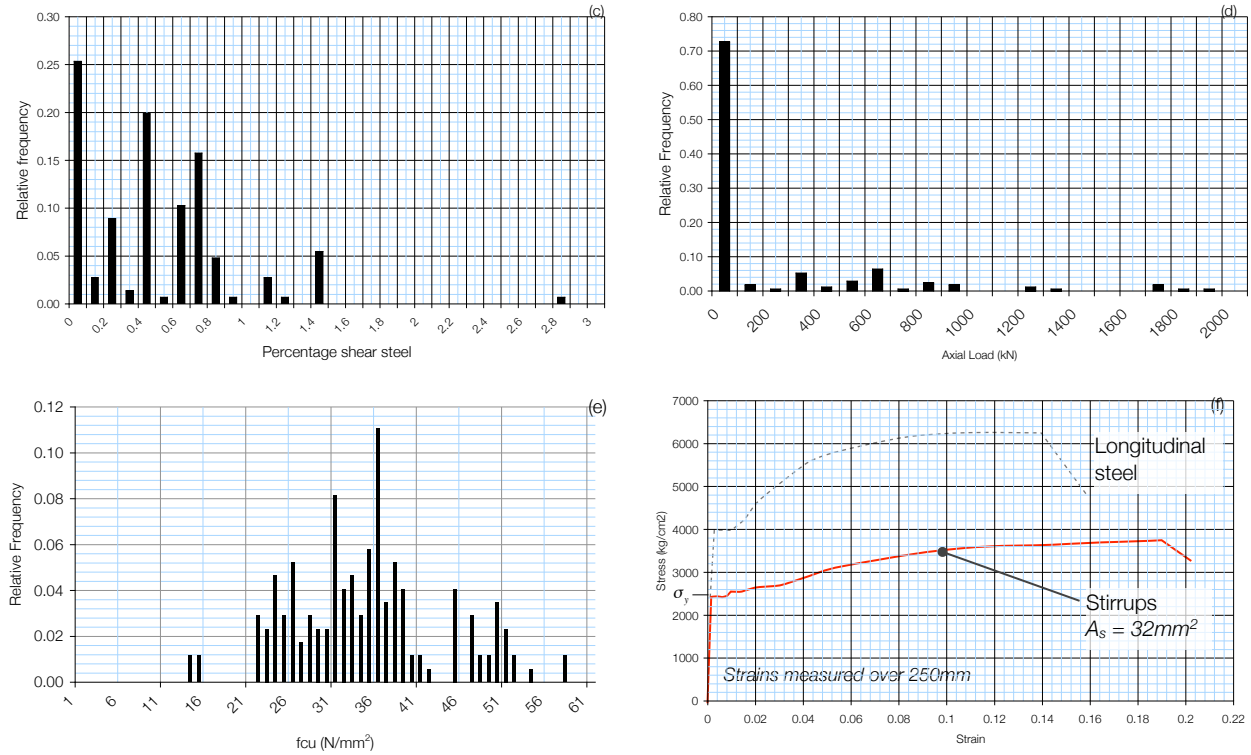


The principal relationships derived thus far are summarised in Figure 6.2. Values for $f_{cu}$ are given equivalent cylinder strengths (for analysis to BS EN 1992-1-1) by considering *Table 3.1* of BS EN 1992-1-1. Partial safety factors are given in *Table 2.1N* (BS EN 1992-1-1). The analysis by Feltham (2004), §5.3, is extended to a variable angle truss model for BS EN 1992-1-1 in §6.3.

*Figure 6.2: Section definitions.*

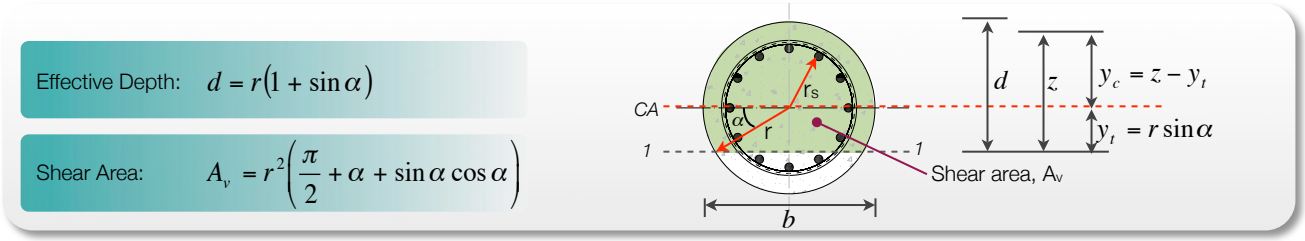


## 6.3. Variable angle truss

The equations of BS EN 1992-1-1 rely on the use of a variable angle truss. The most common use of circular sections is with vertical links and so it is the concrete strut angle which will usually be varied. Previous work by Feltham (2004) and Clarke (1993), §5.3.1, considered only a 45°-truss angle. Feltham's analysis is extended for a variable angle model below (Eq. 6.1 through Eq. 6.10), and all variables are defined in Figure 6.3. Analysis is undertaken by considering that as the truss angle ($\theta$) is reduced, the failure plane intersects more links and thus shear capacity is increased. §6.3.1 presents an analysis of these new variable angle equations. Sections with spiral links are considered separately in §6.3.4, and the procedure described below can similarly be applied to the spiral section analysis presented in §5.3.2. Similarities between the work of Feltham (2004) and Turmo et al. (2008) for spirally bound sections become apparent when Eq. 5.22 is compared to Eq. 6.22.

*Figure 6.3: General approach.*

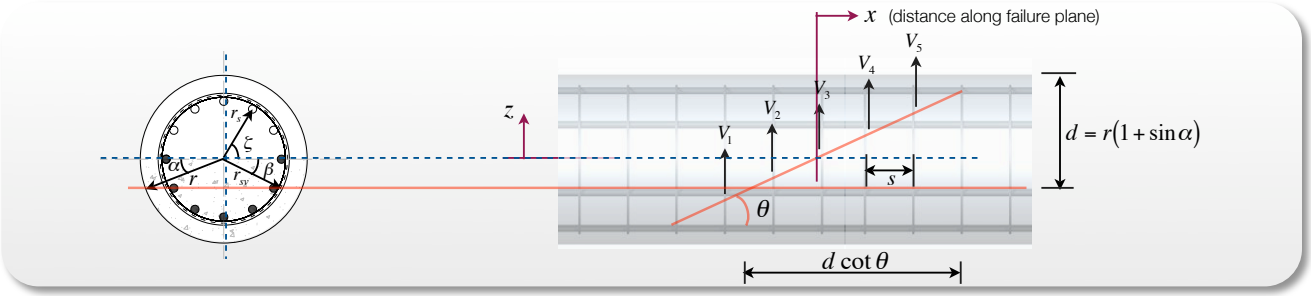

The number of links crossing the failure plane is given by Eq. 6.1 and the force in the links is given by Eq. 6.2. Force carried in the links is expressed by integrating along the length of the failure plane ($d\cot\theta$), Eq. 6.3. The relationship between $\xi$ and $x$ is given by Eq. 6.4 (see Figure 6.3) which is rearranged in Eq. 6.5. The differential ($dx/d\zeta$) may then be used in Eq. 6.7.

$$\frac{(d\cot\theta)}{s} \qquad \text{Eq. 6.1}$$

$$\frac{f_y A_s}{s}\frac{(d\cot\theta)}{(d\cot\theta)} \qquad \text{Eq. 6.2}$$

$$\frac{f_y A_s}{s}\int \cos\zeta dx \qquad \text{Eq. 6.3}$$

$$r_{sv}\sin\zeta = x\frac{r_{sv}(1+\sin\beta)}{d\cot\theta} \qquad \text{Eq. 6.4}$$

$$x = \frac{r_{sv}\sin\zeta\left(r(1+\sin\alpha)\cot\theta\right)}{r_{sv}(1+\sin\beta)} \qquad \text{Eq. 6.5}$$

$$\Rightarrow \frac{dx}{d\zeta} = \frac{r\cos\zeta}{\tan\theta}\left(\frac{1+\sin\alpha}{1+\sin\beta}\right) \qquad \text{Eq. 6.6}$$

$$\therefore dx = d\zeta\left(\frac{r\cos\zeta}{\tan\theta}\left(\frac{1+\sin\alpha}{1+\sin\beta}\right)\right)$$

The total force carried in the links is then found by the integral:

$$\frac{f_y A_s}{s}\int \cos\zeta dx \Rightarrow \frac{f_y A_s}{s}\int_{-\beta}^{\pi/2}\cos\zeta d\zeta\left(\frac{r\cos\zeta}{\tan\theta}\left(\frac{1+\sin\alpha}{1+\sin\beta}\right)\right) \qquad \text{Eq. 6.7}$$

$$\Rightarrow \frac{f_y A_s}{s}\left(\frac{r}{\tan\theta}\right)\left(\frac{1+\sin\alpha}{1+\sin\beta}\right)\int_{-\beta}^{\pi/2}\cos^2\zeta d\zeta \quad = \frac{f_y A_s}{s}\left(\frac{r}{\tan\theta}\right)\left(\frac{1+\sin\alpha}{1+\sin\beta}\right)\left[\frac{1}{2}(\zeta+\cos\zeta\sin\zeta)\right]_{-\beta}^{\pi/2} \qquad \text{Eq. 6.8}$$

Which is solved to give: $$\frac{f_y A_s r\cot\theta}{2s}\left(\frac{1+\sin\alpha}{1+\sin\beta}\right)\left(\frac{\pi}{2}+\beta+\sin\beta\cos\beta\right) \qquad \text{Eq. 6.9}$$

Total shear capacity is given either by links yielding or concrete crushing. Equate Eq. 6.8 to the shear force on the section to obtain:

$$\frac{f_y A_s r\cot\theta}{2s}\left(\frac{1+\sin\alpha}{1+\sin\beta}\right)\left(\frac{\pi}{2}+\beta+\sin\beta\cos\beta\right) \qquad \text{Eq. 6.10}$$

Where $f_y$ = link yield strength ($N/mm^2$); $A_s$ = area of links (both legs, $mm^2$); $s$ = spacing ($mm$); $\theta$, $\alpha$, and $\beta$ are defined in Figure 6.3

### 6.3.1. Analysis

Eq. 6.10 is the defining equation for the force carried in the links as the truss angle, $\theta$, is varied. As $cot(\theta)$ is varied in the range $1< cot(\theta)\leq 2.5$, more links are utilised, providing greater capacity. Data from Clarke (1993) is now analysed for the new variable angle model, and, in line with the Eurocode approach, it is assumed that the shear reinforcement provides all the shear capacity. The design yield strength of the links used in the original analysis has been confirmed as *250MPa* (J. Clarke, *pers. comm.*, 9th March 2009). The actual yield strength of the links is quite likely to have been greater than *250MPa*, but unfortunately no coupon tests were undertaken to verify this (see §6.3.2 for discussion). Figure 6.4 shows that the recommended value for the truss angle of $cot(\theta)=2.5$ provides the best results, but remains considerably more conservative than the previous BS5400-4 approach. At steeper truss angles the method is considerably conservative, as summarised in Table 6.1, where variability of the results is also highlighted. Analysis is initially carried out using partial safety factors set to 1.0, Figure 6.4(l); applying the material factor of $\gamma_s = 1.15$ simply reduces the capacity predictions. Full data is provided in Spreadsheet 6.1.

*Figure 6.4: Capacity for Eq. 6.10, $f_{yk}$ = 250N/mm² (l); Comparison to BS5400 '$V_s$' term (r).*

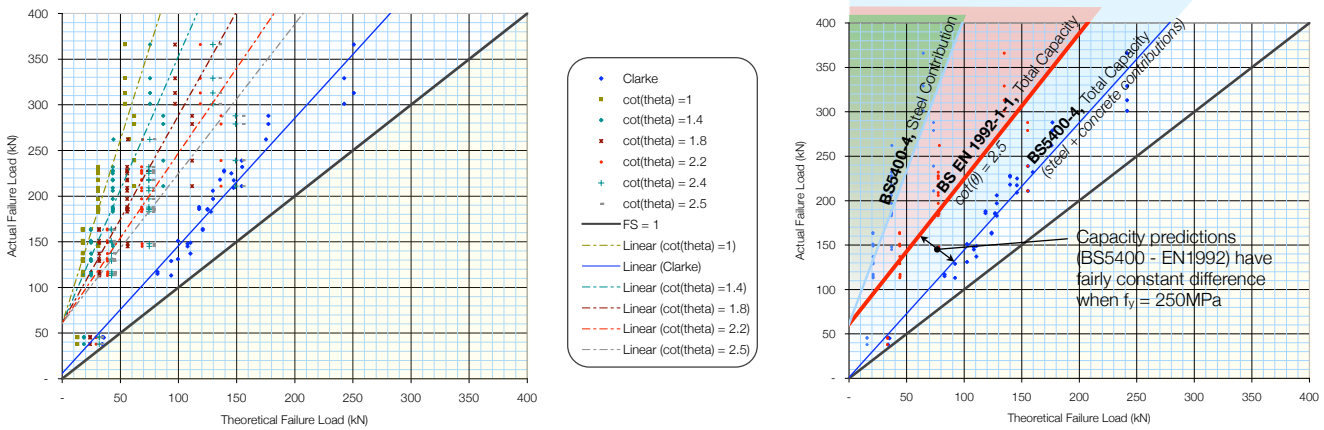


*Note: variations in shear span limits are presented in Spreadsheet 6.2.*

The analysis includes shear enhancement to BS EN 1992-1-1 (*cl. 6.2.3(8)*), although this is only applied at shear spans of less than *2d*. In the analysis by Clarke (also shown on Figure 6.4), enhancement was applied when sections were loaded at $a_v<3d$ from the supports (taken from BD44/95). The BS EN 1992-1-1 approach is adjusted for this limit in Spreadsheet 6.2, although relatively little benefit is obtained due to the test setup. The BS EN 1992-1-1 approach to the design of shear-reinforced sections highlights a number of problems. Firstly, as the capacity of the section is determined irrespective of any concrete capacity, step changes are seen in Figure 6.4, since the same section diameter, with the same shear stirrups must be predicted to fail at the same load, irrespective of concrete strength and longitudinal steel percentages. This is generalised in Figure 6.6

*Table 6.1: Effect of varying truss angle on $\varpi$ and standard deviation.*

| $\gamma_s = 1.00$ | | | | | |
|---|---|---|---|---|---|
| cot θ | $\varpi = V_a / V_{th}$ | SD | cot θ | $\varpi$ | SD |
| 1 | 5.84 | 1.92 | 2.2 | 2.65 | 0.87 |
| 1.4 | 4.17 | 1.37 | 2.4 | 2.43 | 0.80 |
| 1.8 | 3.24 | 1.07 | 2.5 | 2.34 | 0.77 |

*Figure 6.5: BS5400, BS EN 1992-1-1 comparison*

$$V_{5400} = V_c + V_s$$

$$V_{EC2} = 2.5V_{s,5400} \quad (\cot\theta = 2.5)$$

$f_y = 250MPa$

$V_{s,5400} = 0.3V_{5400}$

$\Rightarrow V_{EC2} = 2.5 \times 0.30V_{s,5400}$

$\Rightarrow V_{EC2} = 0.75V_{5400}$

$f_y = 500MPa$

$V_{s,5400} = 0.45V_{5400}$

$\Rightarrow V_{EC2} = 2.5 \times 0.45V_{s,5400}$

$\Rightarrow V_{EC2} = 1.125V_{5400}$

*Where 'EC2' refers to BS EN 1992-1-1 only*

*Figure 6.6: General effect of varying θ.*

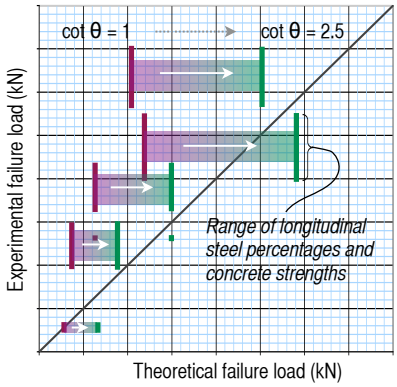


The analysis presented in §6.3.1 appears to be more conservative than Clarke's analysis to BS5400-4. Taking *cot(θ)=2.5* in the Eurocode model would be expected to provide a capacity prediction approximately *2.5* times that predicted by the steel term of an equivalent BS5400-4 approach. Analysis of the Clarke data (Spreadsheet 6.1) reveals that $V_s$ accounts, on average, for just *30%* of the total shear capacity when $f_{yk} = 250MPa$ (for sections failing in shear, with closed links). Knowing this, EN1992-1-1 is expected to predict a smaller overall capacity, at *75%* of the total BS5400-4 prediction (Figure 6.5). In comparison, by assuming $f_{yk} = 500MPa$ and carrying out the same analysis to BS5400, $V_s$ now accounts for *45%* of the total BS5400 prediction (which is now slightly less conservative, Figure 6.7(l)). The EN1992-1-1 prediction will then be *1.125* times that of BS5400, which is perhaps more what one would expect. It is clear that the stirrup yield strength is a crucial consideration when analysis is undertaken to BS EN 1992-1-1, and §6.3.2 considers the impact that doubling $f_{yk}$ has in both BS5400 and BS EN 1992-1-1.

### 6.3.2. The effect of yield stress in BS5400-4 and BS EN 1992-1-1.

The analysis presented above has shown that the proposed equations are conservative when compared to the analytical results presented by Clarke (1993). The Eurocode model, when a truss angle of 21° is taken, is generally expected to be slightly less conservative than the BS5400-4 model, which does not correlate to the results shown in Figure 6.4. The influence of yield strength in both the BS5400-4 and BS EN 1992-1-1 approaches is analysed in Figure 6.7 (without material partial safety factors). Work undertaken at around the same time as Clarke's experimental analysis tested similar bar diameters (*6-8mm*), and found yield strengths to be in the range *400-500MPa* (Ibell, 1992), as compared to the *250MPa* assumed in §6.3.1. These two limits (*250MPa* and *500MPa*) are assessed for both approaches, and it is seen that the BS5400-4 method as used by Clarke (Figure 6.7(l)) is relatively insensitive to a doubling of the yield strength. The BS EN 1992-1-1 model (shown for *cotθ=2.5*), which is dependent solely on the steel contribution, is considerably more sensitive, highlighting the need for an accurate value for $f_{yk}$.

*Figure 6.7: Effect of $f_{yk}$ on analysis results. Clarke method (l); BS EN 1992-1-1 variable angle truss (r).*

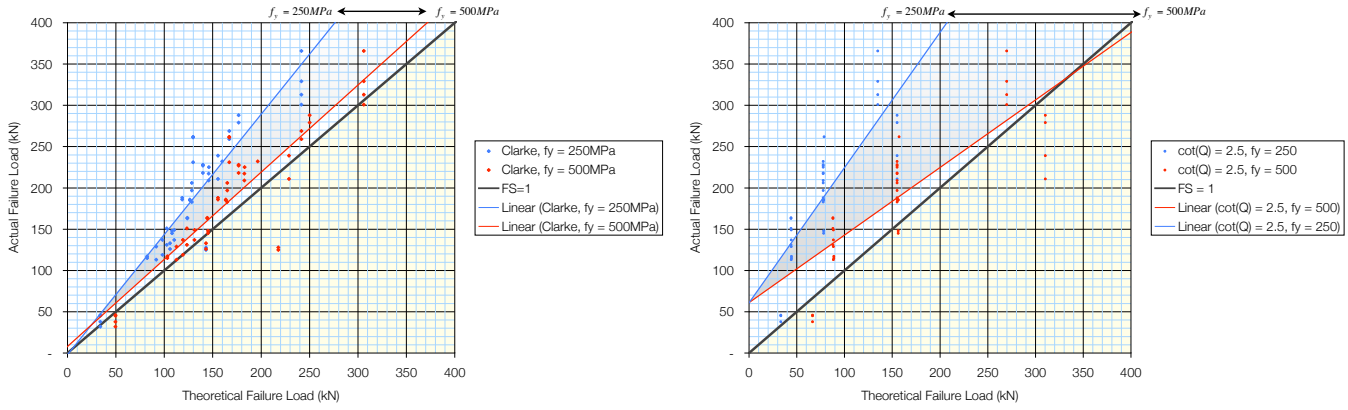

The analysis presented in Figure 6.7 must be treated with caution as it cannot *prove* the actual yield strength of the links used was greater than *250MPa*, it merely provides evidence to support this assumption. A value of *500MPa* is perhaps slightly too high, and produces non-conservative results when partial safety factors are set to 1.0 (Figure 6.7(r)). A value of approximately *400MPa* provides the best correlation to the test data from Clarke (1993). This analysis is presented in Spreadsheet 6.3.

The extension to the Feltham (2004) approach presented above provides a relatively poor correlation to available test data when $f_{yk}$ = *250MPa*, and is further hampered by overly complex equations which rely on a large number of variables. Results for non-shear reinforced sections are presented separately in §6.7. A second analysis for shear-reinforced sections is now considered in §6.3.3, working towards simplified design equations for both closed and spirally bound sections.

### 6.3.3. Eurocode design model approach

The basic Eurocode equation for design of members in shear with vertical links is shown in Eq. 6.11. A sensible approach for circular sections is to use a simple modification factor, Eq. 6.12. In §5.4 it was seen that Priestley et al. (1994) assumed the links to be effective over the full depth of the column, and Eq. 5.23 includes an efficiency factor of $\pi/4$ (*0.785*), while Kowalsky (2000) and Feltham (2004) both assume that only a portion of the links are effective. Recent work by Turmo et al. (2008) has considered the Eurocode approach for both solid and hollow circular sections, and by redeveloping the equations of Kowalsky (2000) a more general approach was developed by assuming the stirrups to be effective over a variable height, *z*. This is dependent solely on the geometry of the section (Figure 6.8), and allowed the efficiency factor presented in Eq. 6.14 to be developed. The factor is dependent on the ratios of $z/r_s$ and $z_0/r_s$ (Figure 6.8) but is *independent* of the chosen truss angle, $\theta$, allowing the more general formula, Eq. 6.16, to be used. Analysis using this approach is presented in Spreadsheet 6.4.

$$V_{Rd,s} = \frac{A_{sw}}{s} z f_{ywd} \cot\theta \qquad \text{Eq. 6.11}$$

$$V_{Rd,s} = \lambda_1 \frac{A_{sw}}{s} z f_{ywd} \cot\theta \qquad \text{Eq. 6.12}$$

Where: $\lambda_1$ = factor for circular sections

*Figure 6.8: Section definitions (Turmo et al., 2008).*

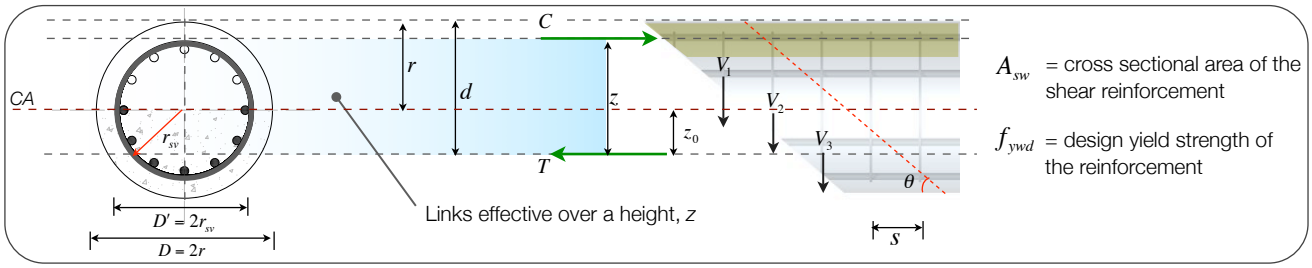


Feltham modification factor:

$$\lambda_1 = \frac{r\cot\theta}{2}\left(\frac{1+\sin\alpha}{1+\sin\beta}\right)\left(\frac{\pi}{2}+\beta+\sin\beta\cos\beta\right) \qquad \text{Eq. 6.13}$$

Turmo et al. modification factor:

$$\lambda_1 = \int_0^{z\cot\theta} \frac{\sqrt{r_{sv}^{\,2} - \left(z_0 - x\tan\theta\right)^2}}{r_{sv} z\cot\theta}\,dx \qquad \text{Eq. 6.14}$$

Where: $r_{sv}$ = radius of stirrups; $z_0$ = depth from centroid of section to centroid of tension steel. Measured from the base of the section, $z_0$ is approximated by Eq. 6.15. Where *r* is the section radius and ($\sin\alpha$) is given by Eq. 5.2.

$$z_0 = d - r = r\left(1+\sin\alpha\right) - r = r\sin\alpha \qquad \text{Eq. 6.15}$$

Generalised form of Eq. 6.14:

$$\lambda_1 = \int_0^1 \sqrt{1 - \left(\left(z_0 - zX\right)/r_s\right)^2}\,dX \qquad \text{Eq. 6.16}$$

$$\frac{z_0}{2r_{sv}} \not< \frac{z - r_{sv}}{2r_{sv}} \qquad \text{Eq. 6.17}$$

Eq. 6.16 is solved for different ratios of effective depth to column diameter in Table 6.2, ignoring impossible values and imposing the limits of Eq. 6.17. Turmo et al.'s method is essentially the same as previous approaches, and if the stirrups are made fully effective (by introducing the limits of Eq. 6.18) then Eq. 6.16 gives the same result as found in Priestley et al. (1994), making the 'effectiveness factor' equal to $\pi/4$, Eq. 6.19. The numerical integration of Eq. 6.16 is found in Spreadsheet 6.5.

$$z = 2r_{sv} \text{ and } z_0 = r_{sv} \qquad \text{Eq. 6.18}$$

$$\Rightarrow \lambda = \pi/4 \qquad \text{Eq. 6.19}$$

*Table 6.2: Effectiveness factor. (Turmo et al., 2008).*

| $z_0/2r_{sv}$ \ $z/2r_{sv}$ | 0.1 | 0.2 | 0.3 | 0.4 | 0.5 | 0.6 | 0.7 | 0.8 | 0.9 | 1.0 |
|---|---|---|---|---|---|---|---|---|---|---|
| **0.05** | 0.998 | 0.988 | 0.964 | 0.922 | 0.858 | - | - | - | - | - |
| **0.10** | 0.993 | 0.993 | 0.980 | 0.951 | 0.902 | 0.820 | - | - | - | - |
| **0.15** | 0.978 | 0.988 | 0.985 | 0.967 | 0.933 | 0.876 | - | - | - | - |
| **0.20** | 0.952 | 0.973 | 0.980 | 0.973 | 0.951 | 0.911 | 0.839 | - | - | - |
| **0.25** | 0.914 | 0.946 | 0.964 | 0.967 | 0.957 | 0.930 | 0.882 | - | - | - |
| **0.30** | 0.863 | 0.908 | 0.936 | 0.951 | 0.951 | 0.936 | 0.905 | 0.842 | - | - |
| **0.35** | 0.797 | 0.856 | 0.896 | 0.922 | 0.933 | 0.930 | 0.911 | 0.871 | - | - |
| **0.40** | 0.709 | 0.786 | 0.842 | 0.880 | 0.902 | 0.911 | 0.904 | 0.880 | 0.827 | - |
| **0.45** | 0.592 | 0.694 | 0.768 | 0.820 | 0.856 | 0.876 | 0.882 | 0.871 | 0.840 | - |
| **0.50** | 0.409 | 0.559 | 0.661 | 0.773 | 0.785 | 0.820 | 0.839 | 0.842 | 0.827 | 0.785 |

*Figure 6.9: Closed form solution for Eq. 6.16.*

$$\lambda_1 = \left[\frac{AB - C}{D}\right]_{X=0}^{X=1}$$

Where:

$$A = \left(zX - z_0\right) \qquad C = r_s \sin^{-1}\left(\frac{z_0 - zX}{r_s}\right)$$

$$B = \sqrt{\frac{r_s^{\,2} - \left(z_0 - zX\right)^2}{r_s^{\,2}}} \qquad D = 2z$$

*(Solved using Wolfram Mathematica® computational integration)*
*See Spreadsheet 6.5 for full analysis and notes.*

Effectiveness factors for different section geometries are analysed in Table 6.2 (above). A closed form solution for Eq. 6.16 has also been determined and is shown in Figure 6.9. This may be used instead of numerical integration, but is quite unwieldy. Turmo et al. (2008) provide a further simplification to this method by ignoring variations in effective depth along the length of the member. If it is assumed that the lever arm is constant at *0.8D* (where D is the column diameter), and the minimum value for $r_{sv}$ is taken as *0.45D* then Eq. 6.16 gives an effectiveness factor of *0.85*. Taking a lever arm of *0.8D* is consistent with an ACI 318 approach, although less accurate than that proposed by Feltham (2004). The approach culminates in Eq. 6.20, which is evaluated against experimental data from Clarke (1993) in Figure 6.10. Eq. 6.20 is now analysed for two definitions of *z*, (Table 6.3, Figure 6.10). Case 1 follows current BS EN 1992-1-1 rules for *z* and Case 2 follows ACI 318 (1999) guidelines.

$$V_{Rd,s} = 0.85\frac{A_{sw} f_{ywd}}{s} z \cot\theta \qquad \text{Eq. 6.20}$$

*Table 6.3: Design cases for Eq. 6.20.*

| Case 1 | | Case 2 | |
|---|---|---|---|
| $z = 0.9d$ | $d = r(1+\sin\alpha)$ | $z = 0.8D$ | $D$ = column diameter |

Figure 6.10 shows that simple modification factors can be used to model the behaviour of circular sections, although the results are conservative when $f_{yk}$ = *250MPa*. The recommended truss angle of *cot(θ)=2.5* provides the best fit, and Figure 6.10(r) provides the best results, although both analyses are considered slightly over-conservative. Note also that the maximum failure load in the analyses presented below is 366kN, making any extrapolation beyond these values less conclusive. Both methods have no unsafe results, but this does not in itself suggest a satisfactory design method has been achieved. In a similar manner to §6.3.1, the effect of an increase in link yield strength is shown in Figure 6.11 for Case 1 (*z = 0.9d*). The analysis using $f_{yk}$ = *500MPa* correlates better with experimental data, providing additional evidence that the yield strength of the links was greater than the *250MPa* as assumed in the original analysis by Clarke.

*Figure 6.10: Analysis of Eq. 6.20. $f_{yk}$ = 250N/mm² Case 1(l) and Case 2 (r).*

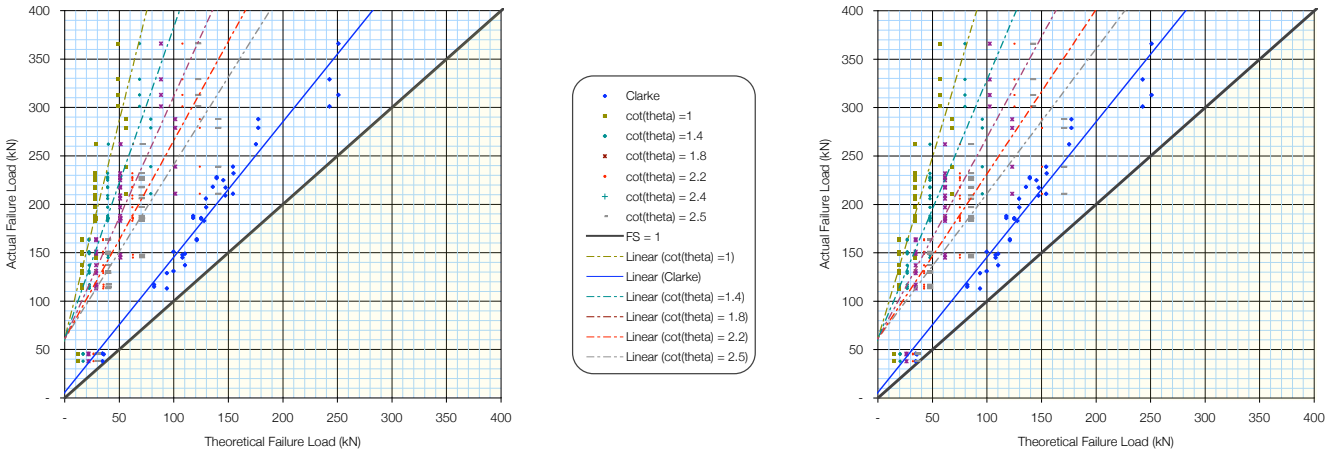

*Figure 6.11: Second analysis of Case 1; $f_{yk}$ = 500N/mm$^2$ (l) and $f_{ywd}$ = 434N/mm$^2$ (r) ($\gamma_s$ = 1.15).*

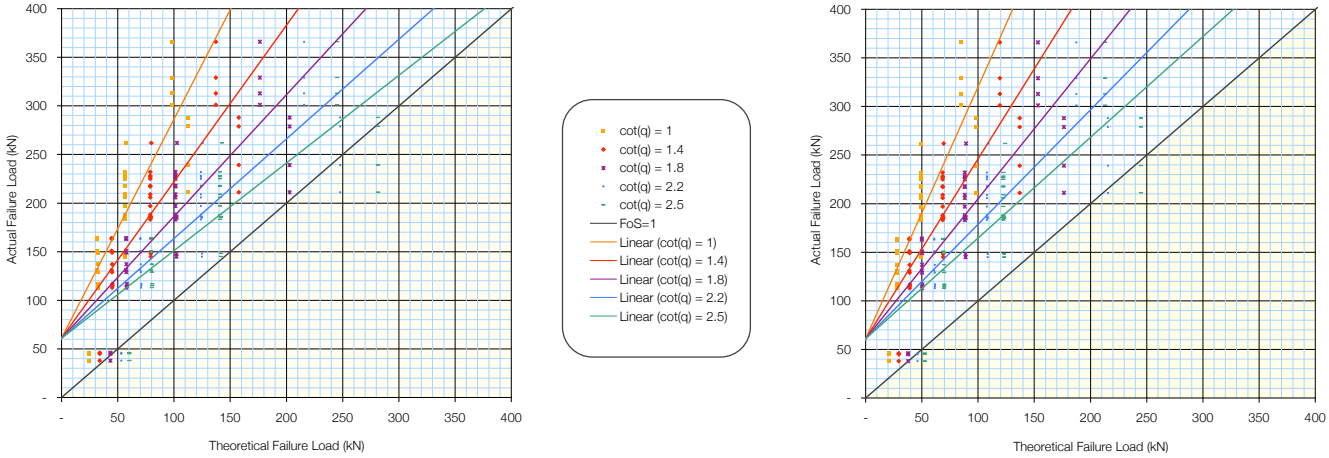


The analysis presented in §6.3 has determined two suitable methods for the design of circular members in shear. Feltham's definition for effective depth is to be combined with the equations from Turmo et al. (2008), which allow the height over which the links are effective (*z*) to be varied depending on section geometry. A design approach for BS EN 1992-1-1 is greatly simplified by taking $\lambda_1$ equal to 0.85, although again this may not be applicable in all cases. Both approaches are conservative, and analysis has been hampered by concerns over the true yield strength of the links used by Clarke. Further experimental testing is recommended, as this analysis has shown that the BS EN 1992-1-1 model is sensitive to the yield strength of the links. The above has solely considered the simpler analysis of closed links, and spirally bound sections are now considered (§6.3.4), although analysis is hampered by a lack of available test data.

### 6.3.4. Spiral links

Clarke (1993) determined that the efficiency of spiral links varies as shown in Table 5.1. Turmo et al. (2008) used the same approach as Feltham (2004) to introduce the efficiency factor shown in Eq. 6.21, which accounts for spiral section geometry better than the approach found in Clarke (1993). When the pitch is set to zero, Eq. 6.21 is equal to 1.00 and so the modified equation (Eq. 6.22) is valid for both spirally and vertically reinforced sections. Test data for members with spiral links is limited, but Eq. 6.22 is verified against Clarke's (1993) data in Figure 6.12 ($f_{yk}$ = *250MPa*). Trend lines are not drawn, since all sections were *300mm* in diameter, with the same pitch and shear span. Longitudinal steel was varied between *2.3%* and *5.6%*, and $f_{cu}$ between *22N/mm$^2$* and *49N/mm$^2$*. As has been discussed, the Eurocode approach is insensitive to these variations. Clarke's analysis is also shown, where it appears that better correlation with the test data is predicted by using a concrete contribution.

$$\lambda_2 = \left(\left(p/2\pi r_{sv}\right)^2 + 1\right)^{-0.5} \qquad \text{Eq. 6.21}$$

$$V_{Rd\,s} = \lambda_1 \lambda_2 \frac{A_s f_y}{s} z \cot\theta \qquad \text{(Where, in general: } \lambda_1 = 0.85\text{)} \qquad \text{Eq. 6.22}$$

*Figure 6.12: Members with spiral links ($f_{yk}$ = 250MPa)*

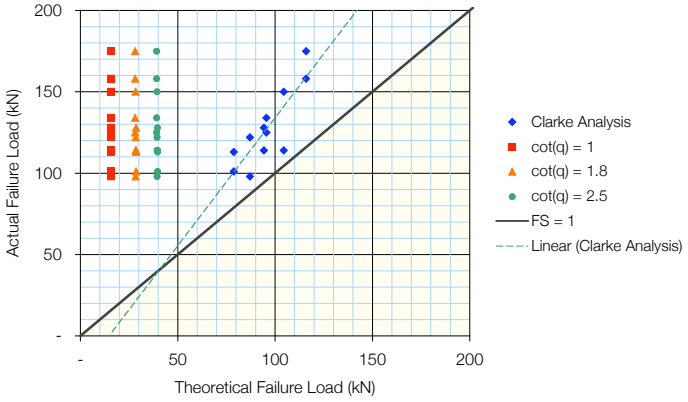


Whilst predictions for spirally bound sections are conservative (Figure 6.12), this is a limited data set and so verification of the proposed equation for spiral links is not provided. Sections with high concrete strengths and longitudinal steel percentages see capacity predictions up to 8 times less than experimental data. This is unsatisfactory, and further experimental data is required to properly assess the proposed Eurocode model for spirally bound sections.

With the above analyses in mind, the additional tensile force in the longitudinal reinforcement (BS EN 1992-1-1 *cl.6.2.3(7)*), which comes about from equilibrium of the truss model is now considered. Following this, crushing limits are assessed, before an upper bound plasticity approach (§6.6), unreinforced section design (§6.7), economic considerations (§6.8) and an entirely new approach to design are investigated (§6.9).

## 6.4. Additional tensile force, $\Delta F_{td}$

The concrete struts of the truss model are in uniaxial compression. Therefore, an additional tensile force (Eq. 4.14) must be applied to the longitudinal steel to satisfy equilibrium, Figure 6.13(l). This force is applied at the centroidal axis of the section, and is then divided between the tension and compression chords. Therefore, in a symmetrical section with discrete tension and compression chords, both chords feel an additional tension of half the total value. The model for a circular section (Figure 6.14) is determined by considering the tension chord to be located at a depth *d* from the extreme compression fibre, separated from the compression chord by a lever arm, *z*, which is taken as *0.9d*. The two chords are therefore not symmetrical about the centroidal axis, and the additional force is distributed between them as shown in Eq. 6.23 and Eq. 6.24. Where axial load is applied, it may also be divided between the chords in this manner, although a new value for *z* should be determined and this is not considered here. Once the chord forces have been determined, horizontal and moment equilibrium (Eq. 6.25) is checked.

*Figure 6.13: ΔF in regular sections (l); Circular sections (c); The effect at supports (r).*

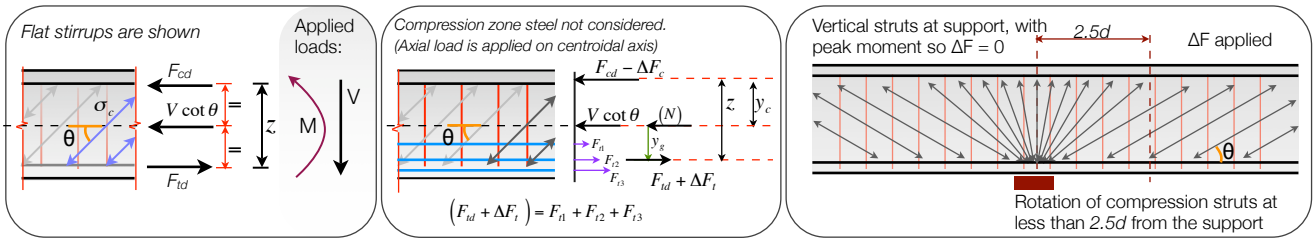


$$\Delta F_c = \frac{y_t}{z}\left(V\cot\theta\right) \qquad \text{Eq. 6.23}$$

$$\Delta F_t = \frac{y_c}{z}\left(V\cot\theta\right) \qquad \text{Eq. 6.24}$$

$$M = \left(F_{td}+\Delta F_t\right)z - \left(V\cot\theta\right)y_c \qquad \text{Eq. 6.25}$$

$$F_{td}+\Delta F_t = \sum F_{ti} \qquad \text{Eq. 6.26}$$

The bar forces ($F_{ti}$) in the real circular section are then determined by distributing the total force in the imaginary tension chord between the real bars in proportion to their distance from the compression chord, Figure 6.14(r). Some iteration may be required and this is undertaken in Spreadsheet 6.19, where analysis of the bar forces and equilibrium is considered in more detail. The end result should be that the sum of the forces in the real bars is equal to the total force in the imaginary tension chord, Eq. 6.26, and that these bar forces also satisfy moment equilibrium. BS EN 1992-1-1 *(cl.6.2.3(7))* limits the value of *ΔF* to ensure that it is correctly determined close to supports, where the concrete struts rotate and carry load directly to the support. Over the support, the struts are vertical and so longitudinal bar forces are found by considering *M/z* only. At *>2.5d* from the support the struts are again inclined at an angle *θ*, so *ΔF* is found as normal, Figure 6.13(r).

*Figure 6.14: General model for circular sections (l); Tension bar forces (r).*

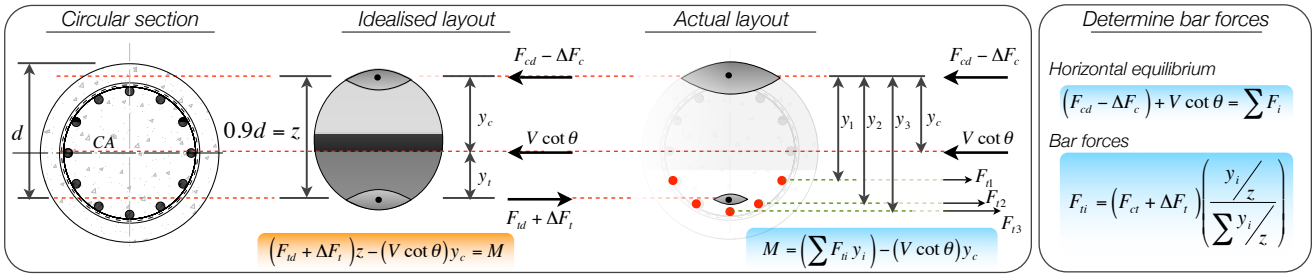


*Figure 6.15: Strain considerations.*

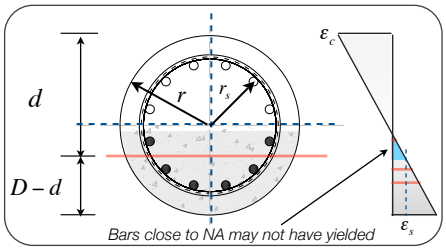


*Full analysis of the additional tensile force is found in Spreadsheet 6.19.*

### 6.4.1. Conclusions

By distributing *ΔF* between the longitudinal bars, each bar area would theoretically be increased by a different amount. A sensible simplification, given that load may be applied from any direction, is to consider only the largest required increase and apply this to all the bars in the section. Non-uniform longitudinal bar sizes are likely to lead to construction problems and should be avoided wherever possible. The designer should also check the level of strain in the bars; if they have not yielded then the strain distribution should be determined to find the force that is carried in the bar (Figure 6.15). The calculation of *ΔF* in a circular section is more complex than for a rectangle section, and care must be taken to ensure equilibrium is satisfied.

Analysis is further complicated by small errors which arise from the simplifying assumptions made for values of *z* and *d*. There may also be more than one possible solution to the longitudinal bar forces, which can complicate any required iterations. The use of Spreadsheet 6.19 is recommended, where the effect of taking moments about either the centroidal axis or the compression chord is analysed. It is found that it is often simpler to take moments about the compression chord.

In the BS EN 1992-1-1 model, it is assumed that $\Delta F$ is divided equally between the tension and compression chords. A comparison between this model and the proposed approach (§6.4) is presented below. A section with *12* longitudinal bars, *20mm* cover, *8mm* links and a *diameter:section length* aspect ratio of *1:10* is arbitrarily loaded at *2.5d* from its support for diameters ranging from *200-4000mm*. At small diameters the error in assuming $\Delta F_{td}=0.5V\cot(\theta)$ is significant, and even larger diameter sections do not divide $\Delta F$ equally. Therefore, in a section with distributed longitudinal steel, the simple assumption that $\Delta F_{td}=0.5V\cot(\theta)$ is potentially non-conservative for the tension chord, and over conservative for the compression chord.

*Figure 6.16: Simple model for ΔF (l); Error when compared to §6.4 (r).*

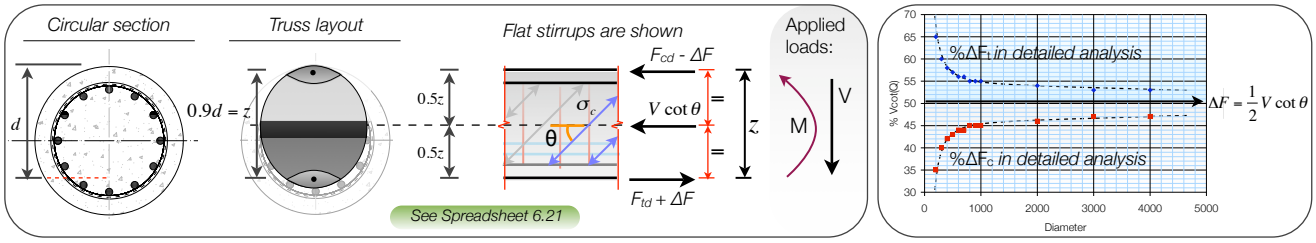


With two models for $\Delta F$ established and contrasted, forces in the concrete can now be considered. The shear capacity provided by stirrups, $V_{Rd,s}$, is limited by crushing of the concrete struts as described in §4.3. To satisfy the requirement of an equilibrium truss model, new formulae for crushing in circular sections are presented and analysed in §6.5.

## 6.5. Crushing

Although it is rare for a strong web-section to be limited by concrete crushing, in order to provide an equilibrium model consideration must be given to the stresses in the concrete struts. The method proposed by Turmo et al. (2008) did not consider concrete crushing as it is typically only found web-dominated sections. Crushing in a rectangular section is simple to apply, while in a circular section the elliptical inclined members are more difficult to analyse (Figure 5.10). Potential methods are shown in Figure 6.17(a,b), where the section beneath the compression chord is divided into discrete 'beams', each with a different effective depth to the longitudinal steel. The main problem in using this approach is seen when the central slice is considered. The transverse steel at the base of this slice is almost horizontal and so to provide any kind of vertical capacity would have to be highly stressed. Determining the layout of the fans would be arbitrary, with no certainty that the critical layout had been chosen. In addition, the rectangular layout creates two edge strips with more steel than the others, Figure 6.17(a).

*Figure 6.17: Concrete crushing models.*

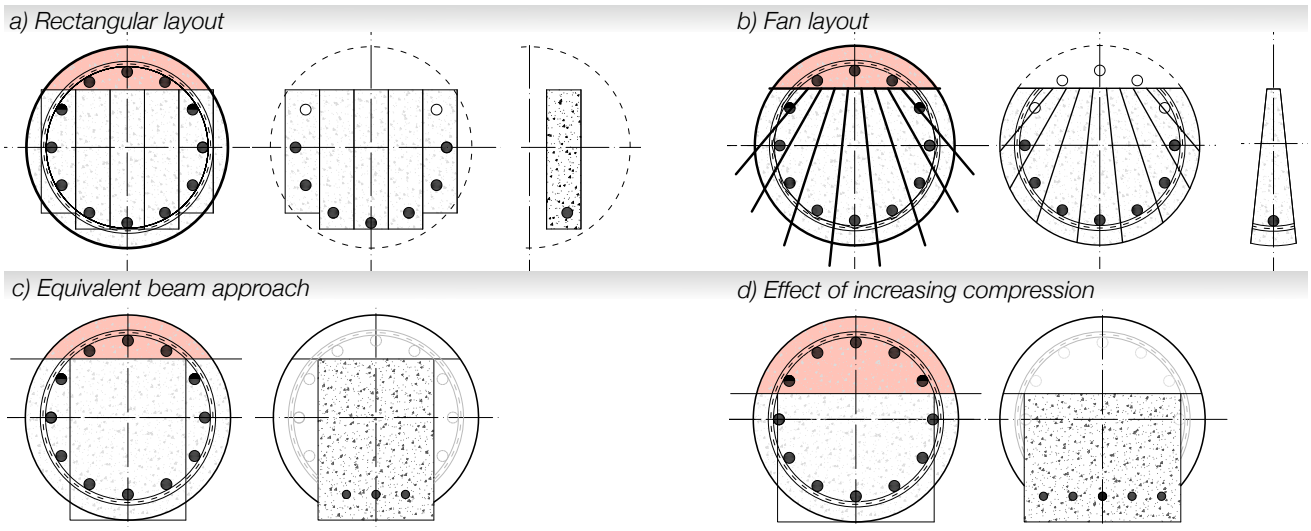


A more attractive alternative is to look at an equivalent rectangular section (Figure 6.17(c)). The width of the section is determined by the distance between the legs of the links at the base of the compression chord, and the equivalent section depth is extended to the base of the circular section. Longitudinal steel is located as shown in Figure 6.17(c) and the section

may then be analysed to BS EN 1992-1-1 as a regular section. However, this approach also presents some difficulties. Firstly, as axial compression increases, the width of the compression chord also increases, Figure 6.17(d). This can potentially lead to overestimation of the area of the new section, and therefore the limits shown in Eq. 6.34 and described below must be applied.

Section geometry is defined in Figure 6.18(l). The depth of the compression zone is found by considering the applied loads, with the effective depth defined by Eq. 5.1 (or by another method if axial load is applied) and the lever arm, *z*, is taken as *0.9d*. The required area of the compression chord is then given by Eq. 6.27 where $\eta$ is reduced by 10% since the width of the compression zone decreases in the direction of the extreme compression fibre (BS EN 1992-1-1 *cl.3.1.7(3)*). Concrete cube (as opposed cylinder) strengths are generally given in the available test results, meaning a reduction of *0.67* is applied. Whilst it would be conservative to ignore applied shear forces since they reduce the force in the compression chord, Eq. 6.28 is correct for equilibrium of the truss (see §6.4 and Figure 6.14). The area of the compression chord is found by considering the geometry of the circular section, Eq. 6.29, allowing the value of $\omega$ (Figure 6.18) to be found iteratively by equating the two values for $A_c$ as shown in Eq. 6.30. This is achieved for data from Clarke (1993) in Spreadsheet 6.6, using an Excel 'goal seek' function.

$$A_c = \frac{F_c}{0.9\eta f_{cd}} \text{ mm}^2 \qquad \text{Eq. 6.27}$$

Where $\eta = 0.67$ for cube tests

$$F_c = \frac{M}{z} - \left(\frac{y_t}{z}\right) V \cot\theta + \frac{N}{2} \qquad \text{Eq. 6.28}$$

*M* given by Eq. 6.35; V = applied shear force; N = axial load.

$$A_c = \frac{1}{2} r^2 (\omega - \sin\omega) \qquad \text{Eq. 6.29}$$

Where $\cos\left(\frac{\omega}{2}\right) = \left(\frac{r-c}{r}\right)$ (all angles in radians)

$$\frac{F_c}{0.603 f_{cu}} \equiv \frac{1}{2} r^2 (\omega - \sin\omega) \qquad \therefore (\omega - \sin\omega) = \frac{2A_c}{r^2} \qquad \text{Eq. 6.30}$$

$$c = r\left(1 - \cos\left(\frac{\omega}{2}\right)\right) \qquad \text{Eq. 6.31}$$

$$H = D - c \qquad \text{Eq. 6.32}$$

$$B = \frac{\pi r^2 - \frac{1}{2} r^2 (\omega - \sin\omega)}{D - c} \qquad \text{Eq. 6.33}$$

$$\pi r^2 - A_c \geq BH$$

Where $A_c$ is given by Eq. 6.27. Eq. 6.34

The depth of the compression zone, *c*, is then given by Eq. 6.31 and finally the two dimensions of the equivalent rectangle, *B* and *H*, are found as shown in Eq. 6.32 and Eq. 6.33. A final check on the section must ensure that the area of the equivalent rectangular section does not exceed the area of the circular section minus the area of the compression chord, Eq. 6.34.

*Figure 6.18: Definitions for equivalent rectangular beam (l); Column loading arrangement for analysis (r).*

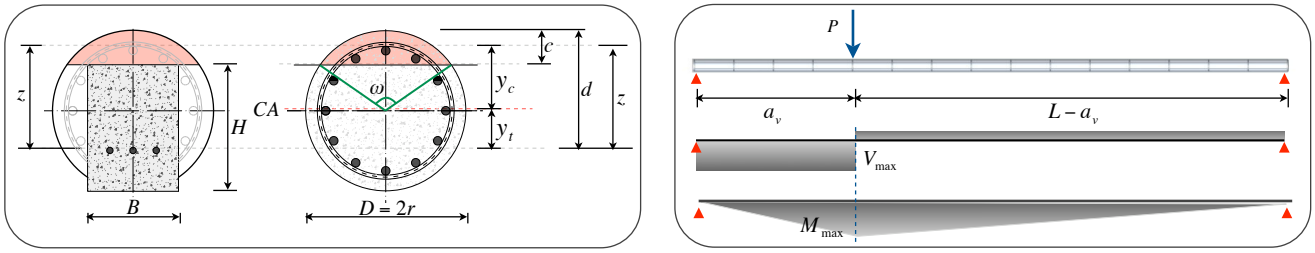


The value of $V_{Rd,max}$ is then found, taking the value of *z* found for the circular section as described above. Verification of the above formula is difficult as there is no available test data in which a crushing failure is actually recorded. Therefore any comparison with the available database should show failure load predictions above the actual failure load. To verify this, the test data from Clarke (1993) is analysed by considering the actual failure load and calculating the corresponding moment and shear force in the column, (Eq. 6.35). Clarke's experimental test layout is illustrated in Figure 6.18(r). $V_{Rd,max}$ is found as shown in Eq. 6.37 and is compared to the actual failure loads in Figure 6.19(l), where a truss angle of $cot(\theta) = 1.0$ is taken. The full range of truss angles is shown in Figure 6.19(r); there is just one value where a truss angle of $cot(\theta) = 2.5$ gives almost an exact prediction of the failure load ($V_a/V_{th} = 98\%$). As expected this occurs in a section with heavy reinforcement and low concrete strength. However, in general it can be seen that the members fail long before the concrete crushing limit ($V_{Rd,max}$) is reached.

$$M_{max} = \frac{P_a (a_v)(L - a_v)}{L} \qquad \text{Eq. 6.35}$$

$P_a$ = actual failure load; $a_v$ = shear span; *L* = column length.

$$V_{max} = \frac{P(L - a_v)}{L} \qquad \text{Eq. 6.36}$$

$$V_{Rd,\max} = \frac{\alpha_{cw} b_w z v_1 f_{cd}}{(\cot\theta + \tan\theta)} \qquad \text{Eq. 6.37}$$

Where (for zero axial load): $\alpha_{cw}$ = 1.0; $b_w$ = B (Eq. 6.33); $z$ = 0.9d; $v_1$ = 0.6; $f_{cd}$ = design concrete strength; $\theta$ = concrete strut angle
Alternatively, analysis of available data shows that $b_w$ may conservatively be taken as 80% of the section diameter (Spreadsheet 6.6).

*Figure 6.19: Analysis of crushing load for cot(θ) = 1.0 (l); Analysis for truss angles 1.0 ≤ cot(θ) ≤ 2.5 (r).*

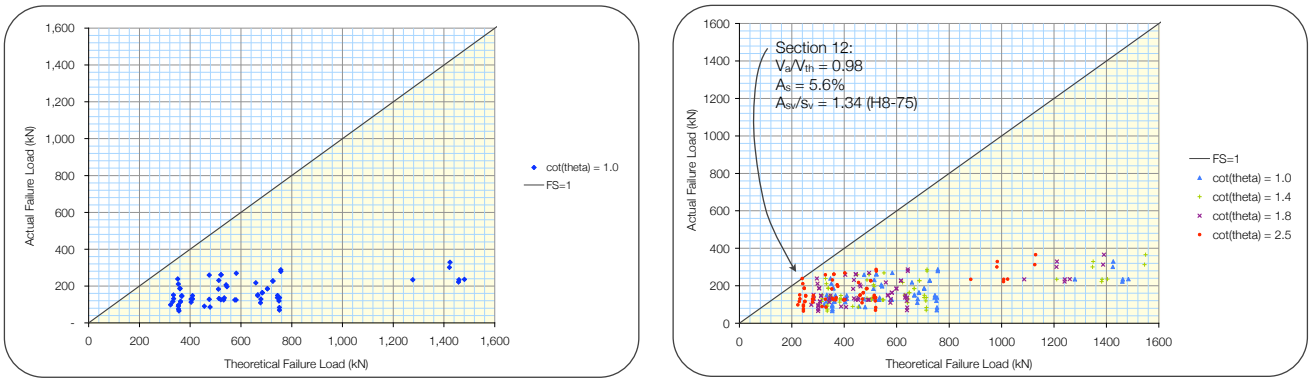


This analysis must be treated with caution since it does not prove that the formula presented above (Eq. 6.35) can in fact be used for the crushing analysis of circular sections, simply because there is no experimental data with which it can be properly verified, as discussed above. It should also be considered that early tests on prestressed I-beams by Hanson (1964) showed that under concentrated loading it was possible to achieve web crushing, stirrup failure and shear-compression failures; however when tested under uniform loads web crushing was not observed. Achieving a web-crushing failure in strong-web circular sections is therefore unlikely, although sections with heavy reinforcement may fail in crushing as discussed in §6.5.1. Further analysis of crushing in both rectangular and circular (including spirally-bound) sections is presented in Spreadsheet 6.6.

### 6.5.1. Forcing a crushing failure

By heavily shear reinforcing a circular section it is theoretically possible to force a crushing failure. Figure 6.20(l) shows that while crushing may govern in small diameter sections, it is less likely when larger diameters are used. This analysis is also presented in Spreadsheet 6.18, where different diameters and truss angles are investigated. Consider that $V_{Rd,max}$ = *1.8MN* for a *500mm* diameter section ($f_{ck}$=*40MPa; cot(θ)=1*). To force a crushing failure would therefore require $A_{sv}/s_v$ = *10.1*, which is approximately equal to *20mm* links at *50mm* centres ($f_{yk}$=*500MPa*, $A_{sv}/s_v$ = *12.6*). This is unlikely to occur in a realistic design situation. Taking *cot(θ)=2.5* provides a smaller value for $V_{Rd,max}$ and thus requires proportionally less steel to force a crushing failure. Larger diameter sections have sufficient capacity to make it essentially impossible to reinforce the section heavily enough to ensure crushing failure for any value of $\theta$. Therefore, it is only in certain cases that crushing limits will be a governing factor in design.

*Figure 6.20: Crushing failures for cot(θ) = 1 (l); Analysis of z = 0.9d (r).*

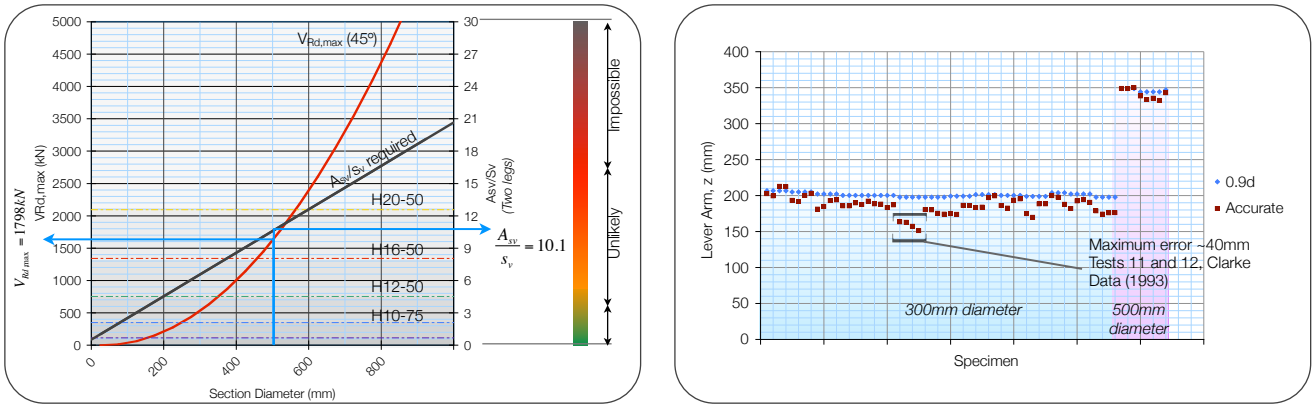


### 6.5.2. Analysis of z = 0.9d

The assumption that $z$ = *0.9d* in a circular section is briefly considered. Eq. 6.38 gives a more accurate definition of the lever arm for sections without axial load (the majority in Clarke database) taken between the centroid of tension steel and the centroid of the compression concrete (centroid of a segment of a circle). The depth of the compression zone and the angle $\omega$ (Figure 6.18) are found as described in §6.5. Figure 6.20(r) shows that the formula *0.9d* consistently overestimates the lever arm, which is not ideal as this potentially provides unconservative values for $V_{Rd,max}$. The largest error, of approximately 20% of the effective

depth, is found where relatively low concrete strengths (*24-26N/mm²*) are combined with high longitudinal steel (*5.6% $A_c$*) and transverse steel percentages. The more accurate method does require iteration, as a value for $\omega$ must initially be guessed to obtain *z*. After determining Eq. 6.28 and Eq. 6.30, a new value for $\omega$ is then found and the process is repeated. $V_{Rd,max}$ is typically reduced by less than 10% when compared to taking *z=0.9d*, although sections under high axial load have not been considered fully. Complete analysis and methodology is presented in Spreadsheet 6.6.

$$z = \left(\frac{2r_s}{\pi}\right) + \left(\frac{4r\sin^3(0.5\omega)}{3(\omega - \sin\omega)}\right) \qquad \text{Eq. 6.38}$$

Where $r_s$ =radius to longitudinal steel; $r$ = section radius, $\omega$ is defined in Figure 6.18(l).

### 6.5.3. Conclusions

Crushing in circular sections has been considered by using an 'equivalent rectangle' approach. An iterative procedure has been described to define the rectangular section properties, and the lever arm for the equivalent section, *z*, is given by the circular section geometry to avoid over-conservative analysis. Without experimental data the proposed equations cannot be fully verified, but theoretical analysis reveals that heavy reinforcement is required to force a crushing failure. From a practical point of view, crushing of the web is unlikely to be critical in strong-web circular sections, and it has been seen that even for web-dominated I-sections crushing does not govern under uniformly distributed loading (Hanson, 1964). Now that the lower bound truss model has been thoroughly considered, an upper bound model is developed to provide a new approach to the plastic analysis of circular sections in shear.

## 6.6. Upper bound plasticity methods

The truss analogy has been fully developed for circular sections and useful design equations have been derived. As a comparison, an upper bound plasticity approach is considered in this section, building on the introduction of §2.9. A simplified approach is initially taken, followed by a more complex rotating model where enhanced accuracy is seen. The upper bound approach of §6.6 equates a possible displacement field to the strains in the material that are possible in that condition. The failure mode chosen will provide a high, or exact, load capacity and optimisation is always required. Fuller explanations of the upper bound approach may be found in Nielsen (1984) and Calladine (1969), but essentially the method equates internal energy dissipation to external work done as shown in Eq. 6.39.

$$\sum W_i' \, u_i \leq \int_V \dot{D}^* dV \qquad \text{Eq. 6.39}$$

Where $W'_i$ is a set of loads calculated by equating external work to internal dissipation of energy, and $u^*_i$ the associated set of displacement increments giving the external work done. $D^*$ is the calculated increment of dissipation of energy per unit volume, obtained by considering the Tresca formulae for a perfectly plastic material, as given in Calladine (1969) as:

$$\dot{D}^* = Y\left|\dot{\varepsilon}^*\right|_{\max} \qquad \text{Eq. 6.40}$$

Where *Y* is the yield stress in simple tension and $|\varepsilon^*|_{max}$ is the greatest principal strain rate magnitude. *D* is derived by considering the principal strain increments in two rigid blocks of concrete, moved apart in the normal and tangential directions. The energy dissipated in the concrete is given by integrating along the length of the shear line, while the steel contribution is found by assuming that the bars yield, and thus their contribution is found by summing for the number of bars crossed by the shear line, Eq. 6.42.

$$ED = ED_{concrete} + ED_{steel} \qquad \text{Eq. 6.41}$$

$$ED = \int_l 0.5(1-\sin\alpha) f_c \, \delta b dx + \sum A_{si} f_y \delta_{si} \qquad \text{Eq. 6.42}$$

$f_c$ is the effective concrete strength (see below); $\delta$ is the resultant displacement of the concrete at an angle $\alpha$; and *b* is the sample breadth. $A_{si}$ is the area of each bar and $\delta_{si}$ gives the notional length that each bar has extended. $f_y$ is 200N/mm².

Applying plasticity theory to concrete structures is quite sensible in an under reinforced section since the steel governs and has properties similar to a perfectly plastic material. Applying a plasticity approach to over reinforced sections in which the behaviour of the concrete governs is more difficult, since concrete undergoes strain-softening (Figure 2.1) meaning that post peak load, stresses decrease with increasing strains. To account for this, the concrete is given a factored effective strength, Eq. 6.43. The factor, $\nu$, is determined analytically for only a few special cases and in general empirical methods are used. Two effectiveness factors are to be considered, the first by Nielsen (1984), Eq. 6.44, and the second by Ibell et al. (1997), Eq. 6.45. The yield strength of links ($f_y$) is to be taken as *200N/mm²*, based on experimental analysis (Ibell et al., 1997).

$$f_c = \nu f_{cu} \qquad \text{Eq. 6.43}$$

$$\nu = 0.8 - \frac{f_{cu}}{200}$$ Eq. 6.44

Where $f_{cu}$ is the compressive strength of the concrete (Nielsen, 1984).

$$\nu = 0.35 f_1 f_2 f_3 f_4 f_5$$ Eq. 6.45

Where the variables are defined in Table 6.4

*Table 6.4: Factors for Eq. 6.45.*

| Factor | Limits | Eq. |
|---|---|---|
| $f_1 = \left(0.35 + 0.32\rho_s\right)^{0.5}$ | $0.80 \le \left(\rho_s = \frac{100A_s}{bd}\right) < 4\%$ | Eq. 6.46 |
| $f_2 = \left(1 + 1.5\rho_{sv}\right)^{0.5}$ | $0 \le \left(\rho_{sv} = \frac{100A_{sv}}{bs_v}\right) < 0.6\%$ | Eq. 6.48 |
| $f_3 = \left(2.4 - 0.04 f_{cu}\right)$ | $20 < f_{cu} < 40 N/mm^2$ | Eq. 6.50 |

| Factor | Limits | Eq. |
|---|---|---|
| $f_4 \begin{cases} = \left(0.2 + 0.2 a/d\right)^{1.5} \\ = \left(2.45 - 0.7 a/d\right)^{1.5} \end{cases}$ | $\le 1.31$ for $a/d > 2.5$<br>$\le 1.00$ for $a/d < 2.5$ | Eq. 6.47 |
| $f_5 = 0.35\left(1 + \sqrt{\left(\frac{1000}{h}\right)}\right)$ | $80 < h < 700mm$ | Eq. 6.49 |

The formulae developed by Ibell et al. (1997) in general provide a lower value for the concrete effectiveness factor. It should be borne in mind that this factor was originally developed for T-beams, in which the compression zone in the top chord is thin and has a large lever arm to the tension zone. To compensate for the resulting highly effective concrete, a lower effectiveness factor was developed to ensure good correlation with experimental data.

It is now possible to apply an upper bound plastic analysis to the experimental results determined by Clarke (1993). Loading arrangements are shown in Figure 6.21, from which initial failure surface geometry will be drawn. Optimisation is carried out in subsequent sections and potential extensions to this work include bilinear or curved failure surfaces, Figure 6.22. To determine the true collapse mechanism a number of failures should be analysed, and results compared to a lower bound approach.

*Figure 6.21: Loading arrangement and overall section dimensions (Clarke, 1993).*

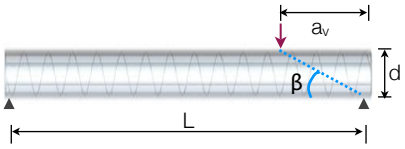


| Type | $a_v$ | Diameter | Length |
|---|---|---|---|
| 1 | 330 | 300 | 3000 |
| 2 | 660 | 300 | 3000 |
| 3 | 1200 | 500 | 3500 |

*Figure 6.22: (l-r) Potential bi-linear failure; Optimisation limits; Extensions to an upper bound approach.*

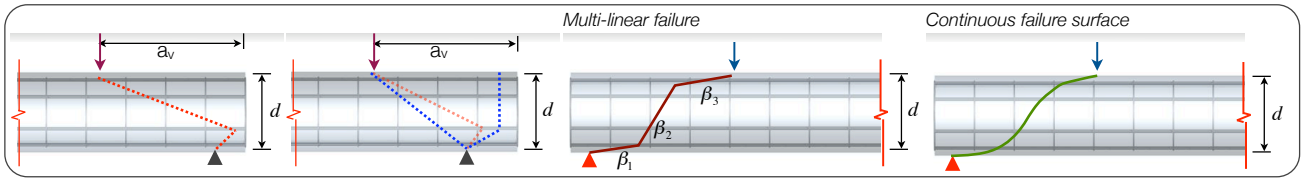


The upper bound approach is considered first for a circular section (§6.6.1) and subsequently for a rectangular section. It is hoped that by analysing the two geometries separately some kind of equivalency factor may be drawn between the two, with the aim of simplifying the plastic analysis of circular sections. The test data represents columns that have been tested with an asymmetric layout as shown in Figure 6.21. Upper bound shear analysis is generally undertaken on symmetrically loaded sections since this allows the centre to move vertically with no rotation of the ends (Shave, 2005).

In a four point bending test, the central portion moves vertically downwards with no support displacement (Figure 6.23(a, b)) whereas the three point bending failure mode (Figure 6.23(c)) must be accompanied by rotation about the supports in order to satisfy compatibility, otherwise an erroneous displacement ($\delta$) at the support location occurs as shown in Figure 6.23(d). Shave (2005) demonstrated that for web-dominated sections such as T-beams or I sections, where there is a high degree of longitudinal reinforcement such that rotation of the section occurs about the *reinforcement,* the upper bound capacity of the symmetrical and asymmetrical setups is the same, since the asymmetrically loaded section undergoes rotation at the supports in order to maintain equilibrium. In initial analysis, this assumption is assumed true for a circular section and good results are obtained. However, the strong web and distributed longitudinal steel in a circular section necessitate a more detailed analysis (§6.6.2) to obtain the true section behaviour, and the actual rotation-displacement of the section must be considered.

*Figure 6.23: Modes of failure in four- (l) and three-point (r) bending tests (after Shave, 2005).*

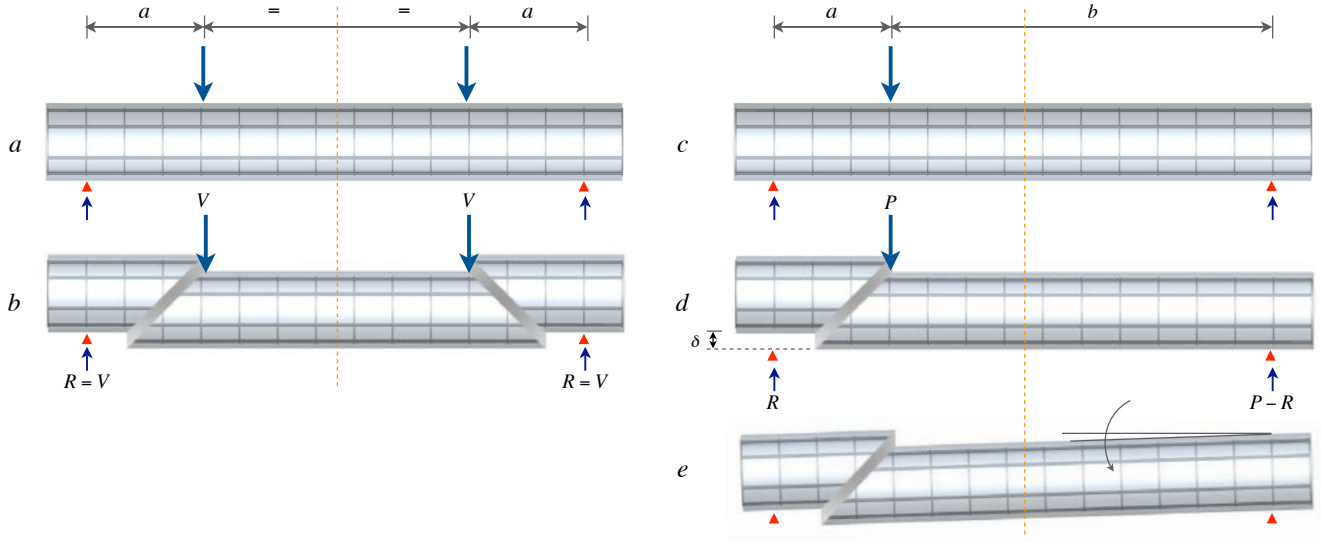


### 6.6.1. Circular section analysis

The initial analysis assumes vertical displacement of the section only, with a failure plane inclination ($\beta$) of $tan\beta = d/a_v$ (Figure 6.21). The concrete contribution requires that the area of the elliptical failure plane, inclined at $\beta$, be determined as described in Figure 6.24 and Eq. 6.53. The link component requires that the angle between the failure plane and the link is defined, which itself must be resolved into the vertical plane.

Area of ellipse = $\pi AB$ where A = half length of long axis; B = half length of short axis

$$A = \frac{D}{2\sin\beta} = \frac{2r}{2\sin\beta} \text{ and } B = r \text{ where } r \text{ is the radius of the concrete section.} \qquad \text{Eq. 6.51}$$

Therefore area of the inclined ellipse $A_e = \frac{2r}{2\sin\beta}(\pi)(r) = \frac{2\pi r^2}{2\sin\beta} = \frac{\pi r^2}{\sin\beta}$ Eq. 6.52

$$ED_c = 0.5(1-\cos\beta) f_c \delta\left(\pi r^2 / \sin\beta\right) \qquad \text{Eq. 6.53}$$

Where $r$ = radius of concrete section; $f_c$ = effective concrete strength. For this analysis Eq. 6.44 shall be used (Nielsen approach) to simplify the concrete effectiveness factor calculation.

*Figure 6.24: Area of inclined plane (l); Section definitions for upper bound analysis (r).*

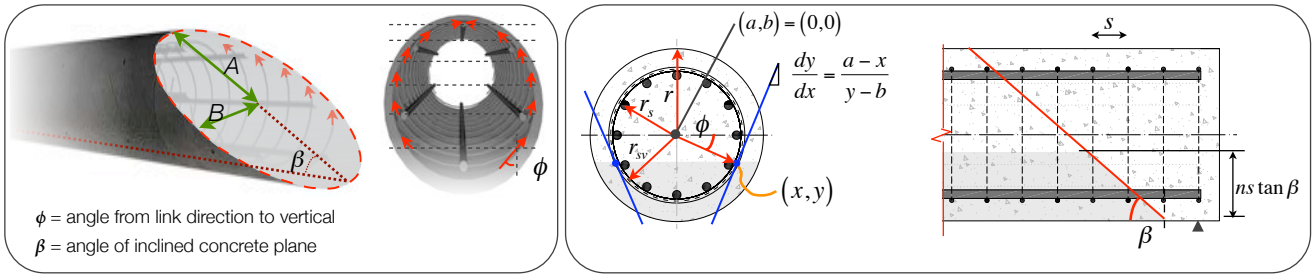


Each link crosses the failure plane at a different angle, $\phi$, (Figure 6.24(l)), defined by Eq. 6.56. The contribution of each link is then found by varying $s$ (increasing away from the inclined plane) assuming that the first link is located a horizontal distance $s$ from the start of the inclined plane as shown in Figure 6.24(r). This is a simplification, but is considered acceptable for this analysis. Other variables are defined in Figure 6.24(r). The steel contribution is determined for the links by considering Eq. 6.42 and Eq. 6.56 from which an upper bound plastic analysis for a circular section can then determined, Eq. 6.58.

The problem with an upper bound analysis is that first assumptions will usually not give the correct failure mechanism. The section will fail by the easiest mode and so only a complete analysis would find the lowest value of the upper bound analysis. Figure 6.25 shows the upper bound results of the analysis method described above. The data (from Clarke, 1993) considers only members with vertical stirrups, failing in shear: a total of 35 tests are shown. Of these, there are four different section layouts as described in Table 6.5. Longitudinal steel is assumed not to be contributing, since it has no vertical component for this simplified analysis. The influence of longitudinal steel is significant for circular sections since they have bars distributed across the height of the section and this is considered in detail in §6.6.2. The full data set is found in Spreadsheets 6.7 and 6.8.

Coordinate *y* is given by:

$$y = (n)s\tan\beta - r \qquad \text{Eq. 6.54}$$

Where *n* = number of links intersected by the plane, and:

$$n = \frac{2r\cot\beta}{s}$$

Coordinate *x* is given by

$$x = r_{sv}\cos\phi \qquad \text{Eq. 6.55}$$

Where $\cos\phi = -\frac{\sqrt{r_{sv}^{\ 2} - y^2}}{r_{sv}}$

Hence the gradient of the tangent to the circle at the location of the link-inclined plane intersection is given by Eq. 6.56.

$$\frac{dy}{dx} = \frac{a-x}{y-b} = \frac{\left(r_{sv}^{\ 2} - (ns\tan\beta - r)^2\right)^{0.5}}{ns\tan\beta - r} \qquad \text{Eq. 6.56}$$

Then, $\tan\phi = \frac{dx}{dy}$. Angles derived using Spreadsheet 6.7 (see attached CD), and: Eq. 6.57

$$ED_s = \sum A_{si} f_y \delta_{si} = \sum A_{si} f_y (\cos\phi) \qquad \text{Eq. 6.58}$$

Where *r* = radius of concrete section; $f_c$ = effective concrete strength. For this analysis Eq. 6.44 shall be used.

*Table 6.5: Data set for upper bound plastic analysis*

| Section designation | Diameter (mm) | Link Spacing (mm) | Shear span (mm) | Concrete strengths (N/mm²) | Cover (mm) | Number of specimens |
|---|---|---|---|---|---|---|
| 1 | 300 | 75 | 660 | 23.80 – 50.50 | 20 | 4 |
| 2 | 300 | 150 | 330 | 34.40 | 20 | 1 |
| 3 | 300 | 150 | 660 | 22.20 – 49.30 | 20 | 26 |
| 4 | 500 | 150 | 1200 | 32.90 – 37.80 | 20 | 4 |

*Figure 6.25: Upper bound analysis for circular section where tanβ = d/$a_v$ (l); 'Optimised' upper bound analysis (r).*

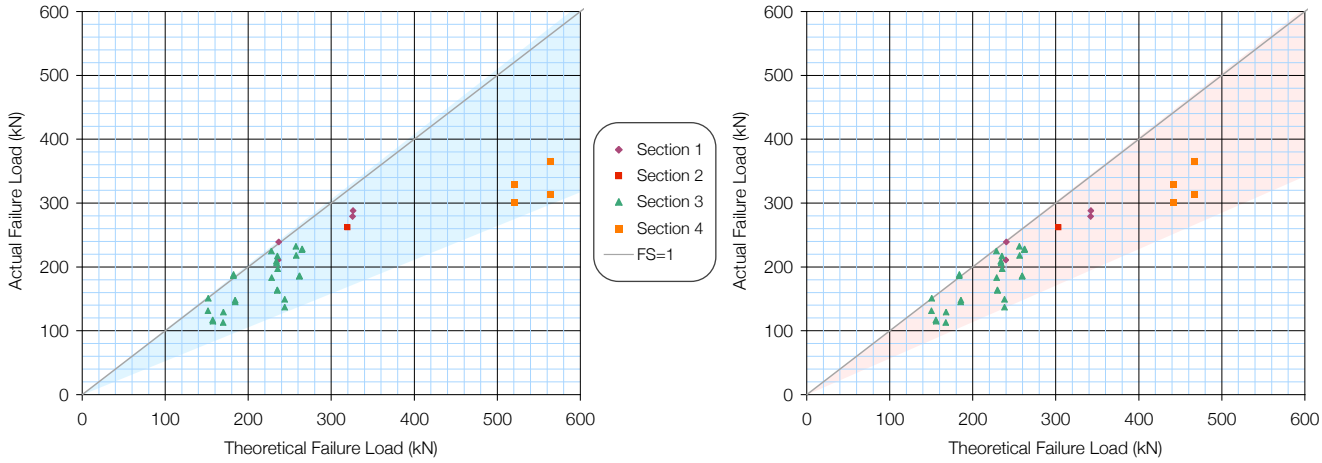


Figure 6.25(l) shows a good distribution from a relatively simple upper bound analysis method for circular sections. The results are upper bound, making them 'unsafe' so this is not a design procedure per say. Calculation of the intersection angle between link and failure plane is somewhat lengthy, but has been automated through the use of Excel. Optimisation of the results has been undertaken by varying the angle $\beta$, with the results shown in Figure 6.25(r) and summarised Table 6.6. Spreadsheet 6.7 is used to undertake this analysis, where the failure plane angle, $\beta$, can be varied to obtain the lowest failure load.

*Table 6.6: Statistical analysis for Figure 6.25.*

| | | Initial | Optimised |
|---|---|---|---|
| β (*rads*) | Section 1 | 0.43 | 0.43 |
| | Section 2 | 0.74 | 0.58 |
| | Section 3 | 0.43 | 0.41 |
| | Section 4 | 0.39 | 0.23 |

| | Initial | Optimised |
|---|---|---|
| Actual/Theoretical failure load (all sections) | 0.81 | 0.83 |
| Standard Deviation | 0.14 | 0.12 |
| COV | 18% | 15% |

The optimised failure plane angle for Section 4 (Figure 6.25(r)) is limited by the column length, suggesting that a different (bilinear) failure is actually taking place. Furthermore, a very low angle of the failure plane would be limited by crushing in the section as well as the limits set out in BS EN 1992-1-1 which would prevent this condition from being realised. The variation in capacity due to the value of $\beta$ is analysed in Figure 6.26 for the specimen designated as 'Section 2' in Table 6.5. When $\beta = 90°$ the failure plane gains capacity solely from the concrete plane (which is vertical). As $\beta$ is reduced, the concrete plane increases in area (as it becomes an ellipse, Figure 6.24) but its contribution to the section resistance reduces as the value of $\cos\beta$ increases

(Eq. 6.53). However, the failure plane now cuts a number of links, all of which provide a steel contribution as given by Eq. 6.58. The concrete contribution, in general, dominates the upper bound results. In a ductile flexural failure, the concrete contribution would typically account for *10%* of the total; here it can be up to *100%* when the failure plane does not intersect any links. The real failure plane will be rather different to, and certainly steeper than, that predicted by this method, since prior flexural cracking will change the load paths through the section, making it difficult to predict the shape of the critical failure plane.

Interpolation between points allows the failure plane angle that corresponds to the experimental failure load (*262kN*) to be estimated at *32°* (0.55rad). As discussed previously this is unlikely to represent the true failure plane since bilinear failures have not been considered. Considering photographs of test failures (for example in Capon, 1966) the actual failure mode tends to vary considerably and it is clear that the failure mode will be more complex than can be estimated using a simple linear approach. Figure 6.27 shows the one available photograph of a specimen from Clarke (1993). Although the section is under axial load, the crack distribution appears to span approximately from support to the load point. The level of axial load present on this section will also have influenced the crack pattern.

*Figure 6.26: Variation in concrete and steel capacity for Section 2.*

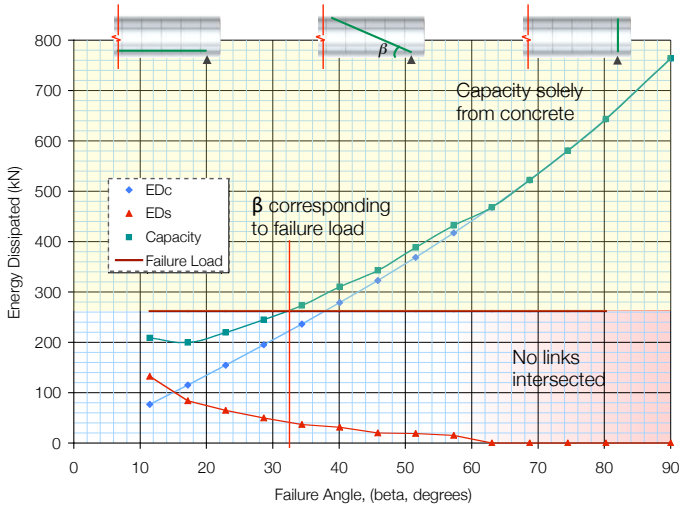


*Figure 6.27: Cracking in a circular section (Clarke, 1993).*

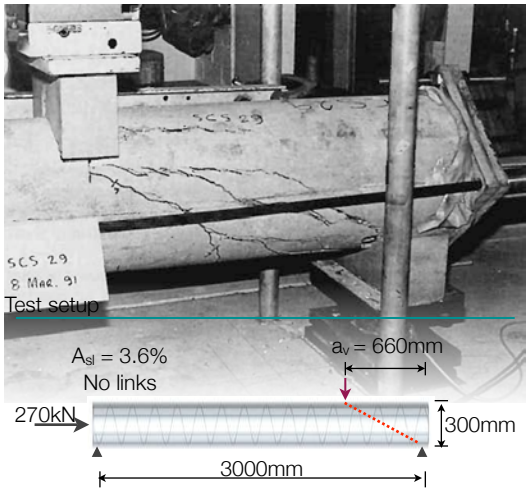


## 6.6.2. Rotation extension

The analysis of §6.6.1 has provided good results and shows that a simplified approach can be utilised in an upper bound approach for circular sections. The simplified method does not consider longitudinal steel, which is dispersed across the section and therefore requires a more detailed rotational analysis. Figure 6.28 shows the full analysis to be considered here, where *Segment I* remains stationary and *Segment II* rotates about the support. In order to provide a tension and compression zone through the section, there must be a coincident lateral displacement of the section, $U_h$. The section shall be rotated by a value of $\eta$, varying from 0 → 1; each increment will further be analysed for a lateral displacement varying from 0 → *D*, where *D* is the section diameter.

*Figure 6.28: Rotation and longitudinal displacement (l); Geometry for longitudinal steel (r).*

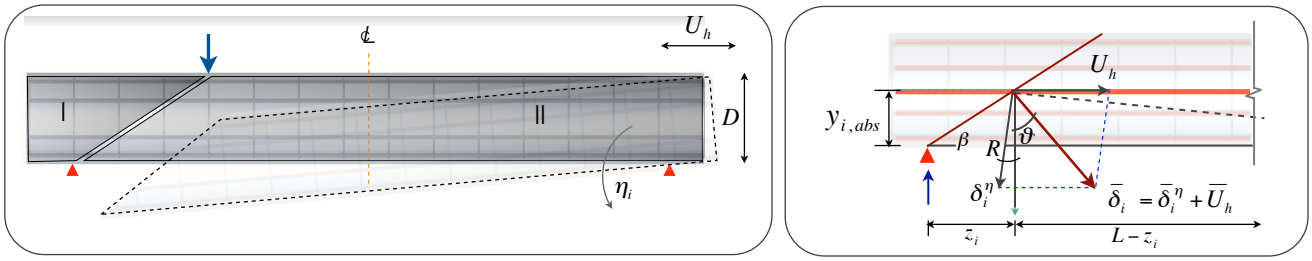


The components of displacement are now more complex, and links are resolved into the plane perpendicular to a line drawn from the rotating support to the link, Figure 6.29. The curvature of the links where they cut the failure plane is considered in the same manner as for the simplified method (§6.6.1 and Figure 6.24(l)). The longitudinal steel is considered in a similar way, with the applied longitudinal displacement ($U_h$) added to the vertical as shown in Figure 6.28(r). The angles therefore depend on variables such as the beam geometry, number of links crossing the failure plane and the angle of the failure plane itself, which may be optimised as seen in Figure 6.25(r). The point at which the failure plane crosses a longitudinal bar is defined by the

angle $\beta$, which also determines how many links are intersected. The concrete failure plane is considered as a linear surface, and to simplify analysis only the average displacement is considered, measured at the mid-height of the inclined plane and applied to the area of the inclined ellipse (Eq. 6.52). More detailed consideration of the concrete plane is given in §6.6.3.

*Figure 6.29: Full displacement mechanism.*

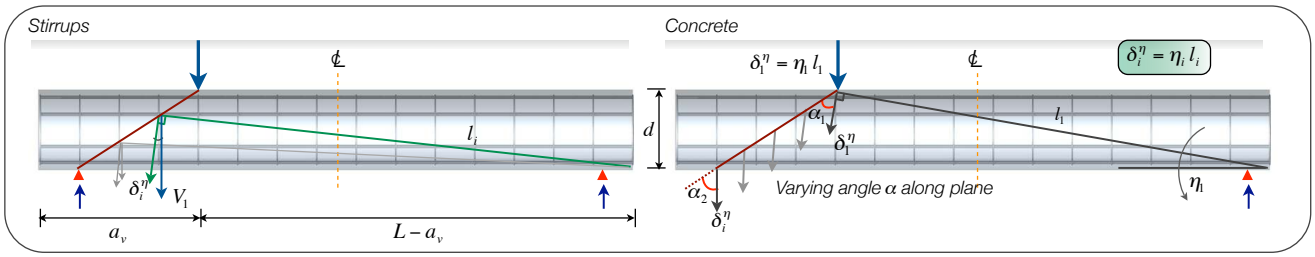


For the concrete plane, the displacement at a point on the failure surface is given by Eq. 6.59 which is then input to Eq. 6.53. The steel components are determined by considering the displacement in the relevant direction, (Figure 6.30 and Eq. 6.60). Then Eq. 6.41 is applied, and by equating the internal and external work done a failure load is predicted. The external applied load also undergoes a displacement, $u$, in the same manner as given by Eq. 6.59. Analysis then considers the combined variation in the angles $\eta$ and $\beta$ with horizontal displacement, $U_h$. The method requires considerable iteration, and is heavily influenced by the inclination of the failure plane, $\beta$.

In rotating a section with zero horizontal displacement, the longitudinal bars are put into compression. Allowing the section to move laterally produces the tension and compression zones that one would expect. This is shown in Figure 6.31(l) for a *500mm* diameter section (Section 44 in Clarke, 1993) where rotation is held constant and lateral movement extended from *0-300mm*. The advantage of the extended analysis method is that the displacements of the section ($U_h$) allow the calculation of external work done by the axial loads, whereas the simplified approach is unable to account for axial loads. However, consider that if the work done (that is, axial load multiplied by the displacement) is dependent on the value of $U_h$, then it is recommended that only *50%* of this load be used in the analysis (T. Ibell, pers comm., 09/03/09) to account for some initially elastic behaviour. Therefore, the influence of axial load is relatively small, in part due to the small values of $U_h$ used in analysis, but also due to the small axial loads (*270kN – 550kN*) applied in the experimental data from Clarke (1993).

$$\delta_i^\eta = \eta_i l_i \qquad \text{Eq. 6.59}$$

$$\bar{\delta}_i = \bar{\delta}_i^\eta + \bar{U}_h \qquad \text{Eq. 6.60}$$

Horizontal component $= \delta_i \cos\vartheta$ | Vertical component $= = \delta_i \sin\vartheta$ (see Figure 6.28)

Where $\tan\vartheta = \frac{\pi}{2} - \left(\frac{-\delta_i \sin R + U_h}{\delta_i \cos R}\right)$ and $\tan R = \frac{y_i}{L - z_i}$

*Figure 6.30: Angle definitions for links (l) and longitudinal steel (r) for extended upper bound analysis.*

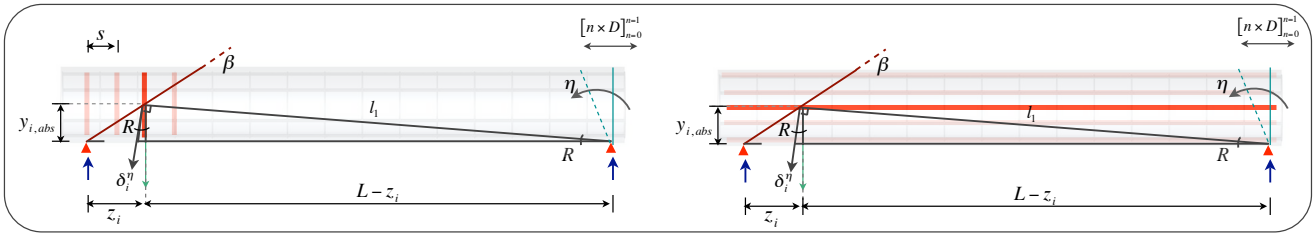


Analysis using this method shows that good predictions are made when sensible values for lateral movement and rotation are chosen. Each section is analysed for rotation in increments of *1/1000* and displacements in increments of *1mm*; a total of half a million iterations per section. Having a single line of calculations and a slider variable for rotation and displacement (Spreadsheet 6.9) solves the problem of viewing and presenting this data. Complete analysis of the *500mm* and *300mm* diameter sections is presented in Figure 6.32 and Table 6.7. Improvements over the simplified method are seen and this upper bound approach appears to be successful. However, whilst this analysis improves accuracy, it was found that the inclination of the failure plane still has a great influence on capacity predictions, which is why the simplified method is so successful. The extended analysis, where $\beta$, $\eta$ and $U_h$ are all varied, allows predictions as low as 0.99 and 1.00 to be obtained. However, similar to all upper bound analysis it is also possible to predict capacities 8 or 10 times the actual failure load, again highlighting the necessity to choose a

sensible failure mechanism. The analysis presented here is of course somewhat biased, since the failure load is known and parameters are varied for each section to provide the most accurate result.

*Figure 6.31: Bar forces under varying horizontal displacement (l); Axial load in an upper-bound analysis (r).*

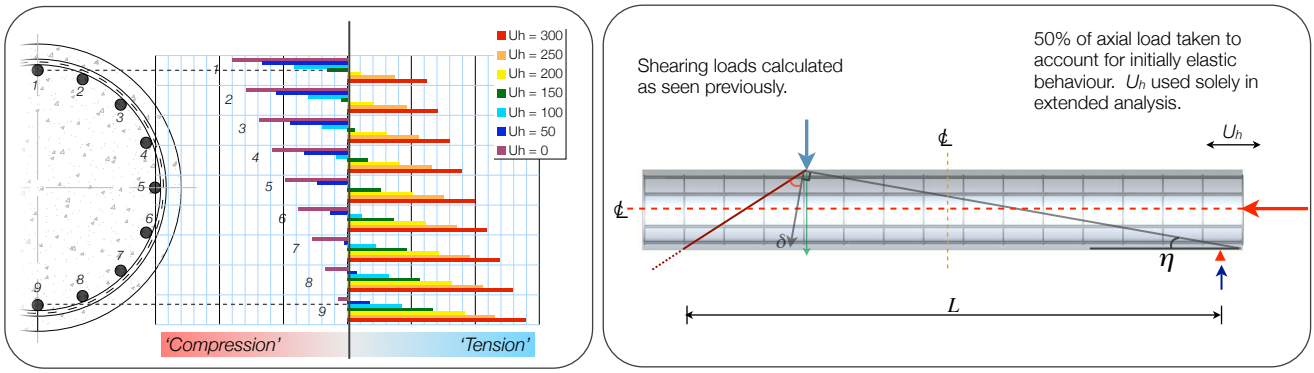


*Figure 6.32: Results of extended upper bound analysis.*

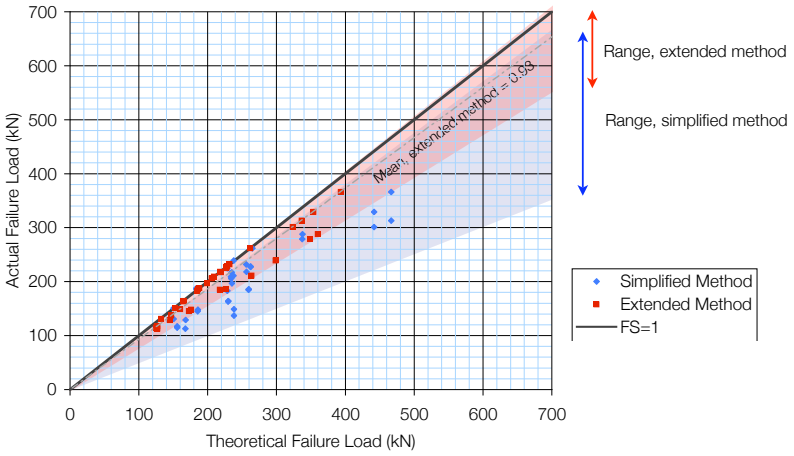


*Table 6.7: Results of improved upper bound analysis.*

| | Optimised, simplified analysis | Extended Upper Bound Analysis, optimised |
|---|---|---|
| Actual/Theoretical failure load | 0.82 | 0.93 |
| Standard Deviation | 0.12 | 0.07 |
| COV | 14% | 8% |

### 6.6.3. Concrete plane

The inclination of the failure plane has great bearing on the capacity predictions, since its inclination determines how many links are cut. §6.6.3 considers the effect of a non-linear concrete plane, and Figure 6.22 presents potential bi-linear and curved failure surfaces. Whilst the linear failure mode used in §6.6.1 and §6.6.2 is not ideal, curved failure surfaces introduce additional geometric difficulties, making mistakes more likely since the intersections with longitudinal and shear steel are now quite complex and make spreadsheets difficult to use effectively. The analysis of faceted and curved concrete surfaces is shown in Figure 6.34, taken from Spreadsheet 6.10. The simpler faceted approach defines *n* number of segments that make up the concrete plane (in this example $n = 4$, although 10 or 20 segments might be used). The angle ($\beta_i$) of each plane is then chosen, and the position of the plane on the section is determined to find its contribution to the total work done ($ED_c$). The area of each facet is taken as a rectangle whose width is given by the width of the segment at mid-height, and height by the length of the inclined plane. The approximation of the curved section edges to a rectangle leads to small errors.

An alternative approach is to define the failure plane by some equation: for example a cubic may be used, Figure 6.33(r). This simplifies intersection calculations somewhat, as each point along the plane is simply determined from the initial equation (see Spreadsheet 6.11). When calculating energy dissipation, concrete and steel terms must always be considered together, as the concrete plane will predict its lowest energy dissipation when it is very flat, but this ensures that lots of steel is activated, and thus the prediction may not be the lowest upper bound result. The use of C++ for curved and multi-linear failure surfaces would be a sensible extension to this work to properly assess the effect of a variable-shaped concrete failure plane.

*Figure 6.33: Curved failure surfaces, simple method (l); Use of equation to define failure plane (r).*

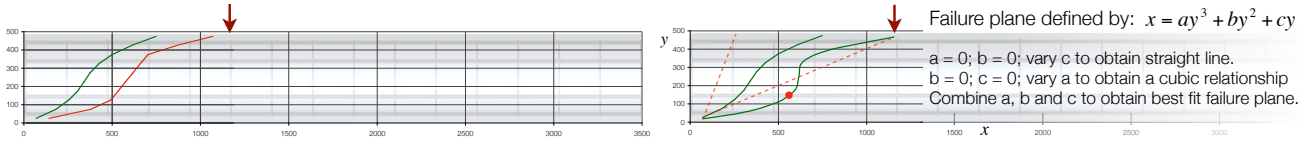

*Figure 6.34: Segment geometry. Simple faceted method (l); Equation method (r).*

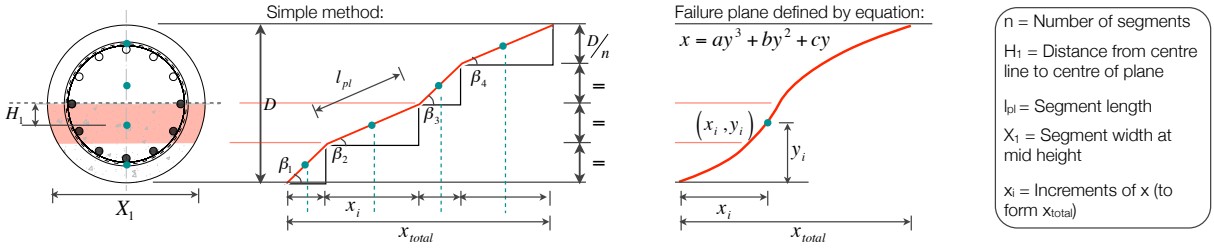


## 6.6.4. Circular analysis conclusion

Two approaches to upper bound analysis have been presented. The first is easier to apply, but is less accurate than the second, which essentially allows the correct failure load to be determined. Considerably more analysis is required however, and the method is better suited to a more powerful approach than the spreadsheets used here. Application of the upper bound theorem is relatively simple in general, and could be extended to include multiple loads along the length of the column quite easily. The major disadvantage of the simplified approach is its inability to analyse axial load (since these loads have no vertical displacement component), which for column sections is somewhat of a problem. The extended analysis is able to account for axial load, but here we see that its influence is relatively small (Figure 6.31(r)). A solution may be to propose a further concrete effectiveness factor to account for axial load. Clarke (1993) lists just 12 axially loaded tests, of which only 4 have shear reinforcement, making any potential effectiveness factor for axially loaded and shear reinforced sections difficult to determine. Further experimental data is certainly required to determine the effect of axial load (see also §4.4).

## 6.6.5. Equivalent rectangular section

The upper bound approach is now considered on an equivalent rectangular section, created by defining the effective depth, *d* as Eq. 5.1, from which the shear area is found, Eq. 5.4. The equivalent section width is given by $(A_v/d)$ and the overall rectangular section height ($h_{eff}$) is given such that ($b_{eff}h_{eff}$) equals the gross cross sectional area of the circular section, $\pi r^2$. This area is then used in the plasticity calculations. Steel areas are kept the same (in percentage terms) and whilst this may be unconservative for the stirrup steel (since the circular section can utilise only the vertical component of the link force) it is used to avoid over complication of the problem. In determining the integral (Eq. 6.39) the yield line length multiplied by the effective width gives an approximation of the result of a circular section area integrated over its depth. The approach is summarised in Figure 6.35 and the results of the upper bound analysis for rectangular sections are presented below.

*Figure 6.35: Equivalent rectangular beam section definitions.*

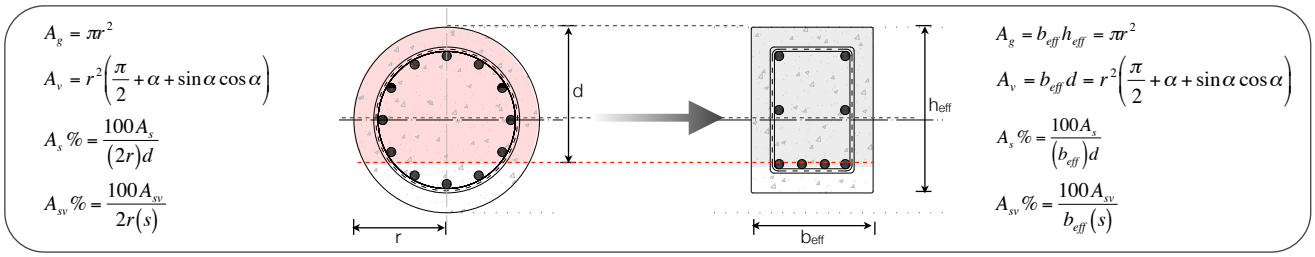


The experimental data from Clarke (1993) is again used along with the two concrete effectiveness factors from §6.6.1. Initially only those members conforming to the limits of Table 6.4 are analysed, Figure 6.36(l). It is clear that there is a much greater degree of scatter when compared to the results of §6.6.1, and this is summarised in Table 6.8. The two approaches appear to have the same overall trends, with the Ibell approach being slightly closer to the actual failure values but a coefficient of variation of between 20% and 24% does suggest an additional modification factor is required to improve the analysis.

The second analysis is undertaken for all members, including those that do not conform to the limits shown in Table 6.4. The results of this are shown in Figure 6.36(r) and again are summarised in Table 6.8. The scatter seen in this analysis, and the large coefficient of variation now obtained does indeed suggest that the limits as proposed by Ibell et al. (1997) are applicable to this analysis of circular sections. The behaviour of heavily reinforced sections with high concrete strengths appears to have altered the effectiveness of the equations. Furthermore, there are now a considerable number of 'safe' predictions (that is, less than the actual failure load), which the upper bound approach should theoretically not produce. This occurs (bar one exception) solely in those members that were previously omitted from the analysis.

*Figure 6.36: Results for members conforming to Table 6.4 (l); Results for all members (r).*

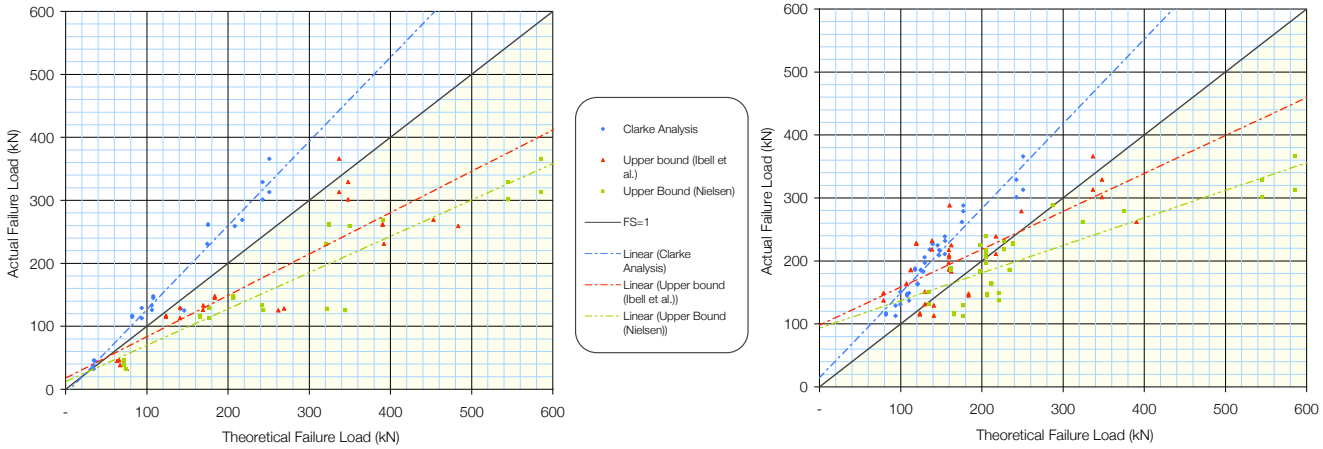


*Table 6.8: Statistical variations for Figure 6.36.*

| | Figure 6.36(l) | | Figure 6.36(r) | |
|---|---|---|---|---|
| | 'Ibell' | 'Nielsen' | 'Ibell' | 'Nielsen' |
| Average $V_a/V_{th}$ | 0.74 | 0.62 | 1.26 | 0.86 |
| Standard Deviation | 0.18 | 0.12 | 0.36 | 0.19 |
| COV (%) | 24.2 | 19.6 | 28.7 | 22.3 |

The equivalent rectangle approach analysis has been undertaken for an inclined failure plane as shown in Figure 6.21, with a straight line assumed between point of support and point of vertical load application. This approach again requires optimisation to determine the lowest upper bound value; however, as has been discussed for circular sections the possibilities of bi-linear failures make this optimisation unlikely to yield any useful results. A further analysis could include three-plane or even curved failure surfaces on the rectangular section, although the added complexity of this may not add anything if the underlying theory is failing to correctly predict the behaviour of circular sections in shear. It should be noted that the limit of Eq. 6.50 to $f_{cu} < 40N/mm^2$ accounts for the fact that the original experimental data did not include members outside this range. This highlights one of the main problems with empirically based formulae in that they must be continually reviewed to ensure that they remain applicable to modern design and construction, where perhaps higher strength concrete or higher-grade steel is used than was originally tested. The ideal design approach is therefore one which does not rely on a massive experimental database.

### 6.6.6. Discussion

The four upper bound approaches considered thus far are outlined below. The methods are compared in Figure 6.37, where a summary of the analysis methods is presented (Clarke (1993) data is used for all members, failing in shear, with closed links, see also Spreadsheet 6.12). The trends for the equivalent rectangle approach (as shown in Figure 6.36) can be compared to the circular analysis and it appears that the proposed circular method provides better results, although extrapolation beyond the small range of available test data is difficult to validate.

1) Upper bound plasticity for circular sections (proposed method);
    - Simplified method and extended angle analysis method (§6.6.2)
2) Upper bound plasticity for an equivalent rectangular section, using concrete effectiveness factors from:
    - Ibell et al. (1997) and Nielsen (1984).

The analysis shown below is most revealing when the *300mm* diameter sections (failing in shear only) are considered. Here, it is clear that the Ibell approach provides too low a concrete effectiveness factor and hence underestimates the member capacity. This has been discussed previously, and is a function of the original T-beam tests undertaken by Ibell et al. (1997). The Nielsen approach gives similar responses for both *500mm* and *300mm* diameter sections. The most consistent approach is seen in the *extended* circular analysis, where the trend lines of Figure 6.37(l) and (r) are essentially the same. The *simple* circular method shows considerable variation when *500mm* sections are included. However, for smaller diameter (*300mm*) sections a simplified approach is valid and does not require extensive optimisation.

*Figure 6.37: Comparison of four upper bound approaches. All members (l); 300mm diameter sections only (r).*

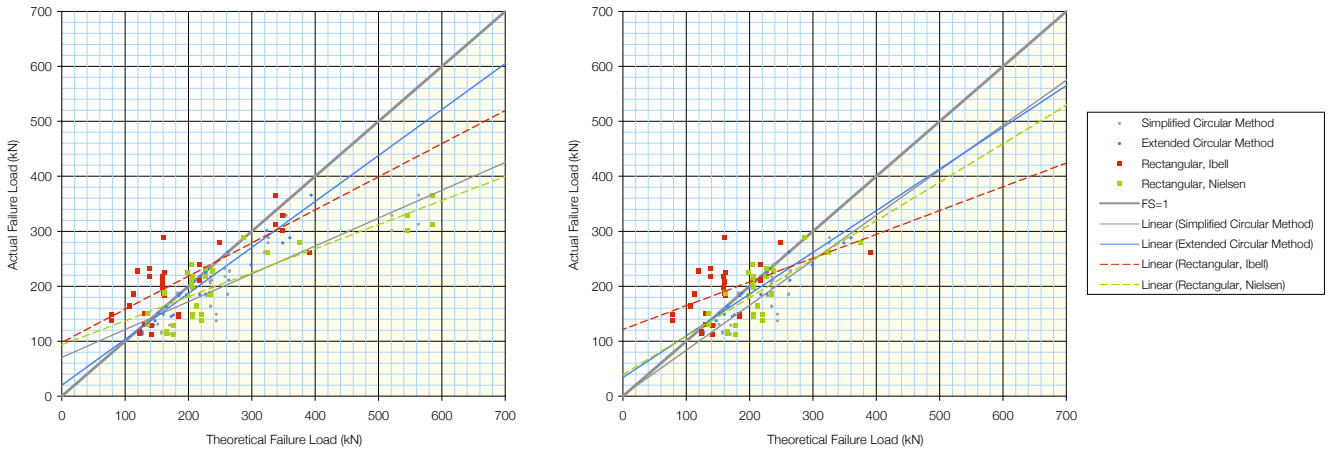


*Table 6.9: Statistical variations for Figure 6.37(r).*

| | Rectangular | | Circular | |
|---|---|---|---|---|
| | *Ibell* | *Nielsen* | *Simplified* | *Extended* |
| Average Va/Vth | 1.26 | 0.86 | 0.80 | 0.93 |
| Standard Deviation | 0.36 | 0.19 | 0.13 | 0.07 |
| Coefficient of Variation | 29% | 22% | 17% | 8% |

The limits to the truss angle, $\theta$, provided in BS EN 1992-1-1 (Eq. 4.7) should also be borne in mind when considering any further plastic analysis. Nielsen (1984) provides a simple proof that the angle of the diagonal compression field, $\theta$, analogous to the ideal strut angle in a truss model, is equal to half the angle of the failure plane, $\beta$, where $\theta$ is given by a lower bound analysis as Eq. 6.61 and $\beta$ is given for upper bound analysis as Eq. 6.62. Therefore, a limit to the angle of the failure plane can be considered as the range $\beta_{min} \leq \beta \leq \beta_{max}$ for the values shown in Eq. 6.63.

$$\tan\theta = \sqrt{\frac{\psi}{1-\psi}} \quad \text{(Where } \psi = \frac{A_s f_y}{bsf_c} \text{ } A_S \text{ = stirrup area; } b \text{ = section breadth; } s \text{ = stirrup spacing.)} \qquad \text{Eq. 6.61}$$

$$\tan\beta = \frac{2\sqrt{\psi(1-\psi)}}{1-2\psi} \qquad \text{Eq. 6.62}$$

$$\text{For } 1 \leq \cot\theta \leq 2.5;\ \frac{\pi}{2} \geq \beta \geq 0.761 \qquad \text{Eq. 6.63}$$

Applying the limits shown in Eq. 6.63 to the upper bound circular analysis requires, in general, that a steeper failure plane be taken (Table 6.11). The effect of this is to reduce the contribution of the links and increase the concrete contribution, since fewer links are cut, with the resulting analysis shown for the simplified approach (§6.6.1) in Figure 6.38 and Table 6.10. Energy contributions (as a percentage) from the Concrete and Steel terms for the simplified method, both with and without limits on the value of $\beta$, are presented in Table 6.11. These results are averaged for each of the general section definitions (Table 6.5), where the energy dissipated in the concrete is given by Eq. 6.53 and in the steel by Eq. 6.58.

*Figure 6.38: Analysis of upper bound results with $\beta$ limited by Eq. 6.63.*

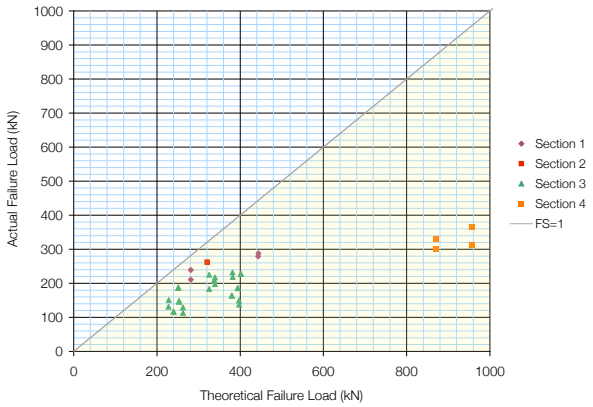


*Table 6.10: Analysis of Figure 6.38.*

| | |
|---|---|
| Average $V_a/V_{th}$ | 0.56 |
| Standard Deviation | 0.14 |
| Coefficient of variation | 24% |

Note 1:

A comparison and discussion of the upper and lower bound steel contributions is also provided on the Accompanying CD. Please see Spreadsheet 6.22 for more details.

Without limits to $\beta$, failure is predicted to occur at a flat truss angle, so by imposing the limits of Eq. 6.63 the failure planes are made steeper. Steeper failure planes then lead to a significant increase in predicted failure loads; an analysis of the *500mm* diameter sections, for example, now predicts failure loads of up to three times the actual values. Table 6.10 also shows that the method becomes more variable when these limits are imposed (although this is heavily influenced by the *500mm* diameter analysis, Section 4). It is therefore considered that these limits should not be applied in an upper bound analysis, but the influence of a limiting value for $\beta$ is interesting nonetheless. The use of a flat truss angle appears to provide better analytical results in both upper and lower bound approaches, which perhaps may warrant the use of $cot(\theta)>2.5$ to obtain the most economical design (see also §6.8). Full analysis and data is presented in Spreadsheet 6.14. The angles used in the extended approach are limited only by the geometry of the section.

*Table 6.11: Comparison of analysis when using a limited failure plane angle.*

| Section | Analysis for general failure plane | | | Analysis for limited failure plane angles | | |
|---|---|---|---|---|---|---|
| | β (§6.6.1) | $\%ED_{STEEL}$ | $\%ED_{CONCRETE}$ | $\beta_{LIMITED}$ | $\%ED_{STEEL}$ | $\%ED_{CONCRETE}$ |
| 1 | 0.48 | 34 | 66 | 0.76 | 15 | 85 |
| 2 | 0.68 | 14 | 86 | 0.76 | 6 | 94 |
| 3 | 0.41 | 26 | 74 | 0.76 | 6 | 94 |
| 4 | 0.22 | 47 | 53 | 0.76 | 6 | 94 |

### 6.6.7. Conclusions

An upper bound plasticity approach has been applied to circular sections. A simplified approach for circular sections provides acceptable results, and excellent accuracy is achieved when the extended method is used, although geometry considerations can become complex and spirally bound sections have not been considered. An 'equivalent rectangle' approach was also investigated, but provided little in the way of design simplification and is less accurate than a 'true' circular analysis. Therefore, this approach is not recommended for the upper bound analysis of circular sections, and no equivalency factor can satisfactorily be drawn between the two approaches.

The concrete contribution dominates the upper bound approach (up to 100% of total energy dissipation), suggesting that the concrete does do some work. The lower bound analysis relies solely on a steel contribution, which is generally larger than that predicted by the upper bound analysis. The principle advantage of the upper bound approach is its simplicity and ease of application. However, concrete crushing is not considered and the results are generally unsafe. It remains the aim of this dissertation to provide a suitable lower-bound model that remains in equilibrium for all applied forces. The design of non-shear reinforced sections is now briefly considered, before economic design to both BS5400-4 and BS EN 1992-1-1 are investigated.

## 6.7. Non shear reinforced design comparison

The strength of a member that is unreinforced in shear is principally dependent on the concrete strength, reinforcement ratio and depth of the member (Narayanan, 2005). Comparisons between the BS5400-4 and BS EN 1992-1-1 empirically based approaches for unreinforced sections are presented. For non shear reinforced sections, early analytical models which proposed that load was carried directly to the supports in a concrete strut, which itself was tied together across the base of the section by the tension steel are valid only when plain longitudinal bars are considered. The use of deformed bars means that the force in the tension chord must decrease towards the supports (Reineck, 1991) and so cracks form in this zone. Reineck (1991) suggests that such direct load transfer is only valid for loads applied near to the support, which in turn means that where a member does not have shear reinforcement within the Kani shear valley (Figure 2.8(r)) plasticity theory cannot be applied. Experimental work by Muttoni (1989, cited by Reineck, 1991) has supported these findings. The following sections consider the empirically based equations of both BS5400-4 and BS EN 1992-1-1 for non-shear reinforced sections.

### 6.7.1. Design approaches

The BS EN 1992-1-1 formulae for unreinforced sections are given below. Unlike previous equations, axial load is considered directly as a beneficial effect. Since BS5400-4 requires minimum links to be provided in all cases, values for $\xi_s v_c$ (Eq. 6.66) will be multiplied by *bd* to determine the equivalent concrete shear resistance, Eq. 6.67. For coexistent axial loads, the method shown in Table 5.2 for BS5400-4 is used.

$$V_{Rd,c} = b_w d\left[\left(\frac{0.18}{\gamma_c}\right)k\left(100\rho_1 f_{ck}\right)^{1/3} + 0.15\sigma_{cp}\right] \quad \text{Note: } \gamma_c = 1.5 \qquad \text{Eq. 6.64}$$

$$V_{Rd,c} \not< b_w d\left(0.035k^{1.5} f_{ck}{}^{0.5} + 0.15\sigma_{cp}\right) \qquad \text{Eq. 6.65}$$

Where: $k = 1 + \sqrt{(200/d)} \le 2.0$; $\rho_1 = \frac{A_{sl}}{b_w d} \le 0.02$; $\sigma_{cp}$ = average longitudinal stress

$$\xi_s v_c = \frac{0.27}{\gamma_m}\left(\frac{100A_s}{b_w d}\right)^{1/3}\left(f_{cu}\right)^{1/3}\left(\frac{500}{d}\right)^{1/4} \quad \text{Eq. 6.66}$$

$$V_{Rd\,BS} = \left(\xi_s v_c\right) b_w d \quad \text{Eq. 6.67}$$

*Figure 6.39: Non-shear reinforced analysis (l); Excluding partial safety factors (r) to EN 1992-1-1 and BS 5400-4.*

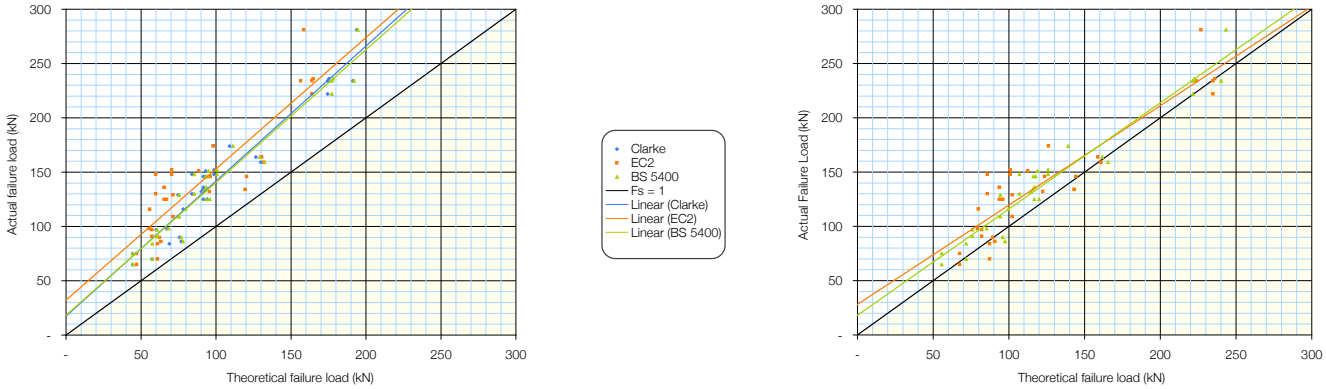


Clarke's (1993) experimental data is used for the analysis. The actual shear area, $A_v$ (Figure 6.2) replaces the *bd* term throughout, and the longitudinal steel area is taken as half the total longitudinal reinforcement. A total of 36 tests are included in the comparison (see Spreadsheet 6.15). Figure 6.39(r) shows that the two approaches are similar when partial safety factors are set to 1.0, and both are acceptably conservative when compared to the test results. When partial safety factors ($\gamma_c$ *=1.5* in BS EN 1992-1-1 and $\gamma_m$*=1.25* in BS5400-4) are included, the BS EN 1992-1-1 (Figure 6.39(l)) approach appears to be slightly more conservative than BS5400-4. The ratio of *Actual/Theoretical* failure load for the BS5400 approach is *1.43*, and in BS EN 1992-1-1 it is *1.63*. This is a relatively small difference, and broadly speaking the two methods give similar results.

Again, the scatter of data seen in shear tests is evident here, illustrating the problems of empirical formulae derivations. Developments in codified design tend to become less conservative with time, as more knowledge or increased confidence is gained in the design processes, generally supported by an increasing experimental data set. It is interesting to note therefore that the BS EN 1992-1-1 approach for non-shear reinforced sections appears to be more conservative than BS5400-4.

## 6.8. Economic considerations

This section considers the potential benefits of replacing small diameter shear-reinforced sections with larger diameter, unreinforced sections. Analysis is undertaken by firstly considering the capacity of the shear-reinforced section ($V_{Rd,s}$). Then, the diameter of an unreinforced section with the same shear capacity is determined by plotting $V_{Rd,c}$ (Eq. 6.64) against section diameter. Comparisons are provided in Figure 6.40 for a *300mm* diameter section with 8-H20 longitudinal bars and concrete cube strength of *31.20N/mm²*. Different ratios of shear reinforcement are plotted (Figure 6.40), as described in Table 6.12. As the diameter is increased, the longitudinal steel area is kept constant, and *cot(θ)=2.5* throughout. The results show that only small diameter sections are likely to be limited by $V_{Rd,max}$. Full analysis is presented in Spreadsheet 6.16.

*Table 6.12: Shear reinforcement for Figure 6.40.*

| Designation | Abbreviation | $A_{sw}/s$ | | Designation | Abbreviation | $A_{sw}/s$ |
|---|---|---|---|---|---|---|
| $V_{Rd,s}(1)$ | H12-50 | 4.52 | | $V_{Rd,s}(3)$ | H12-150 | 1.51 |
| $V_{Rd,s}(2)$ | H12-100 | 2.26 | | $V_{Rd,s}(4)$ | H12-175 | 1.293 |

| Designation | Abbreviation | $A_{sw}/s$ |
|---|---|---|
| $V_{Rd,s}(5)$ | H12-200 | 1.131 |
| $V_{Rd,max}$ = concrete crushing capacity | | |

*Figure 6.40: Relative capacities for cot(θ) = 2.5.*

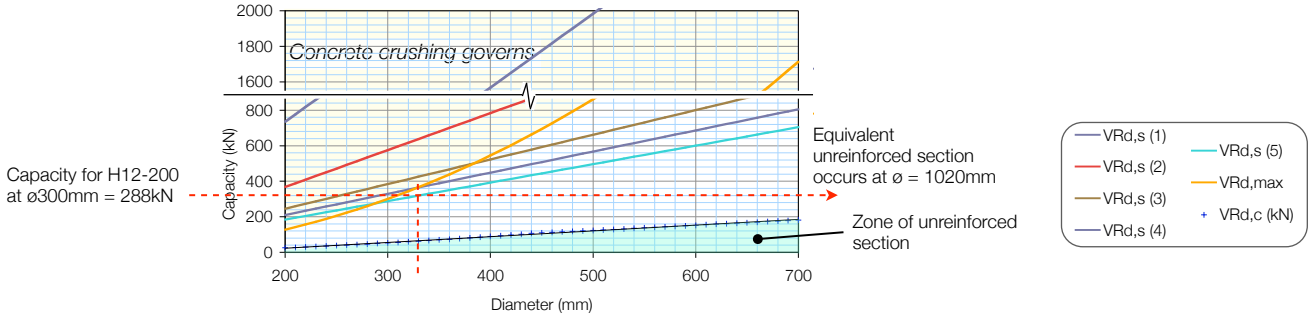

The unreinforced section capacity increases linearly in proportion to section diameter, Figure 6.40 and Eq. 6.68, allowing equivalent reinforced and unreinforced sections to be defined. To provide the same shear capacity as a *300mm* diameter section reinforced with H12-200 stirrups (*288kN* capacity, given by $V_{Rd,s}(5)$ in Figure 6.40), an unreinforced section would therefore be *1020mm* in diameter, Eq. 6.69. This is an unrealistic proposition, due to material requirement increases and space losses, both of which have negative impacts on sustainability.

$$y = 0.3232(D) - 41.56 \quad \text{Eq. 6.68}$$

Where: $y$ = capacity; $D$ = section diameter. Capacity, $y$ = *288kN*. Hence:

$$D = \frac{288 + 41.56}{0.3232} = 1020mm \quad \text{Eq. 6.69}$$

Unreinforced sections are rarely used in design, since links are required in all cases for cage stability, and large sections use up valuable floor area in building design. Since shear is a brittle failure mode, a degree of reinforcement is considered to be a good idea to improve concrete confinement, which in turn improves the ductility of the concrete. Fibre reinforced concrete may also be used, where similar improvements in ductility are seen (§2.2.2). The use of fibre-reinforced columns (without shear stirrups) could be an interesting extension to this dissertation, and may lead to a more economic unreinforced section design.

### 6.8.1. Cost comparisons to BS5400-4

Cost effective design in concrete relies to a certain extent on a parametric analysis of member size, reinforcement percentage and concrete strength. Other considerations, such as material costs, site labour and transport can also be included. Eq. 6.70 considers a simplified approach to the cost of a concrete column. Since BS EN 1992-1-1 removes the concrete contribution from stirrup requirements the relationships are more complex than in BS5400-4, although they remain interlinked since an increase in section size provides a greater lever arm, reducing link requirements. A full analysis would include the effects of axial, moment and shear forces on section design to reveal the differences between BS5400 and BS EN 1992-1-1 approaches.

Cost/column = (Concrete Cost x Area) + (Steel Cost x Area) Eq. 6.70

$$\Rightarrow C = C_c A_c \left(1 + \rho C_c / C_s\right) \quad \text{Eq. 6.71}$$

Where C = cost; $A_c$ = area concrete; $A_s$ = area steel; $\rho = A_s / A_c$

Consider the nominal section described in Table 6.13, where an arbitrary design shear capacity of *2N/mm²* has been specified for the section under consideration. Under BS5400-4, few extra stirrups are required to maintain this shear capacity when lower strength concrete is used (Table 6.14), but it may be cheaper to pour high-grade concrete and reduce time spent fixing steel. A second analysis considers the effect of varying column diameter to carry a constant design shear force of *575kN*. Under BS5400-4, there comes a point at which the concrete contribution provides enough capacity to negate the use of links entirely, Figure 6.41(r). In the BS EN 1992-1-1 approach (Figure 6.41(l)), after crushing limitations on small diameter sections, full capacity is provided solely by the links up until the point at which an unreinforced section has sufficient capacity to carry the full *575kN*. Full analysis is provided in Spreadsheet 6.17.

*Table 6.13: Design column parameters.*

| Variable | Design Value |
|---|---|
| Diameter | 600mm |
| $f_{cu}$ | 20N/mm² – 50N/mm² |
| Longitudinal Steel | 8H20 Bars |
| Transverse Steel | Varies |
| Shear | Constant 2N/mm² capacity |

*Table 6.14: Effect of concrete strength on stirrup requirements (BS5400 only).*

| $f_{cu}$ (N/mm²) | $v_c$ (N/mm²) | $A_{sv}/S_v$ required |
|---|---|---|
| 50 | 1.01 | **1.19 (H12-200)** |
| 40 | 0.93 | **1.28** |
| 30 | 0.85 | **1.38** |
| 20 | 0.74 | **1.51 (H12-150)** |

*Figure 6.41: Varying diameter for constant shear force of 565kN ($f_{cu}$ = 40MPa). EN 1992-1-1 (l); BS5400-4 (r).*

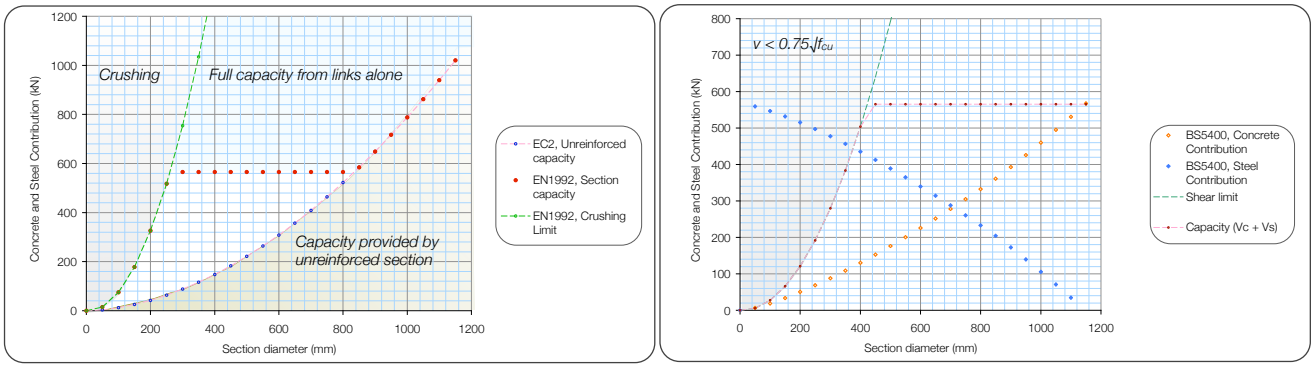

Figure 6.41(r) illustrates that the concrete contribution in BS5400 can be significant. Consider now Figure 6.42, where a constant section diameter (*1000mm*) is subject to increasing shear force, which is plotted against the required area of shear steel ($A_{sv}/s_v$). In BS5400, the concrete contribution is constant, and up until approximately *1000kN* BS5400 provides the most economical design for this section. The same analysis for a *500mm* diameter section reveals that BS EN 1992-1-1 becomes more economical at approximately *300kN* (see also Spreadsheet 6.20). Furthermore, BS EN 1992-1-1 provides much higher crushing resistances ($V_{Rd,max}$) for both limiting values of truss angle $\theta$. Whilst bridge piers may be subject high design shear loads, and will thus benefit from the reduced steel requirements in BS EN 1992-1-1, in general design little benefit may be seen when moving from BS5400-4 to BS EN 1992-1-1 and in some cases BS EN 1992-1-1 may initially require more links.

*Figure 6.42: (l-r) Section properties, Analysis showing crushing limits, Detailed analysis.*

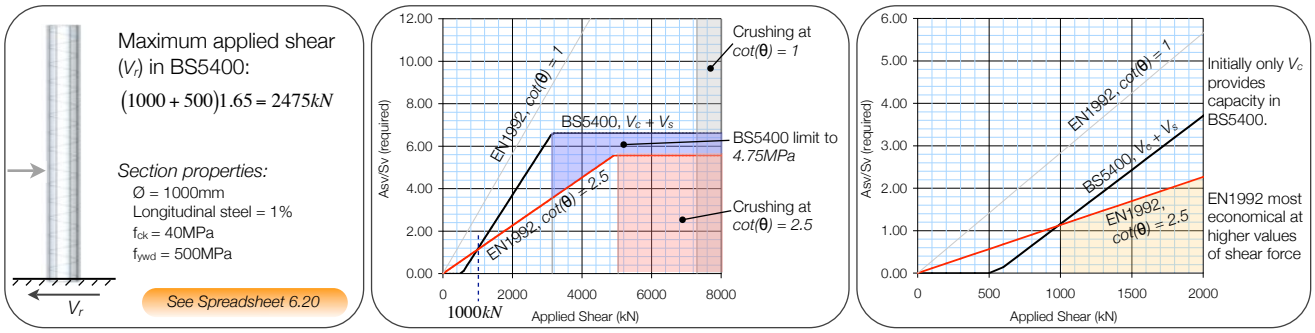


## 6.8.2. Conclusion

§6.8 provides a very brief introduction to possible comparisons between BS5400-4 and BS EN 1992-1-1. Interesting comparisons between the shear steel requirements of BS5400 and BS EN 1992-1-1 have been made by varying both the section diameter and applied loads. The proper assessment of the variable angle truss model and how its introduction will affect design is a suitable topic for further, separate work. For example, actual cost data could be incorporated into the analysis. Furthermore, axial load has not been considered, which in BS EN 1992-1-1 can potentially reduce the shear capacity of a section if an accurate definition for *z* is taken, as discussed in §4.4. Economic design to BS EN 1992-1-1 appears to be more complex than previously thought. Now that the Eurocode model for circular sections has been considered, an alternative design approach is briefly considered in §6.9, before final conclusions are presented in §7.

# 6.9. Alternative design approaches

Modified compression field theory (§2.8.3) remains an attractive design method and is assessed here using experimental data from Clarke (1993). Analysis is undertaken using Response-2000, a computerised MCFT packaged developed at the University of Toronto. Tests with closed links which failed in shear are analysed initially, although tests with axial load are not included. The results of this analysis are presented in Figure 6.43(l). Analysis to BS5400-4 by Clarke (1993) obtained an average $V_a/V_{th}$ of *1.44* for these samples, with a standard deviation of *0.13*. The MCFT approach gives a more consistent average $V_a/V_{th}$ of *1.11*, with a standard deviation of *0.11*. This suggests that 95% of the experimental results lie between *0.89* and *1.33* times the MCFT predictions. The method therefore appears to be better suited to carrying out capacity calculations for shear in circular sections. The MCFT method does present some issues of non-conservative results, but these are dealt with in design by partial safety factors.

*Figure 6.43: MCFT comparison for shear reinforced sections (l); MCFT for unreinforced sections (r).*

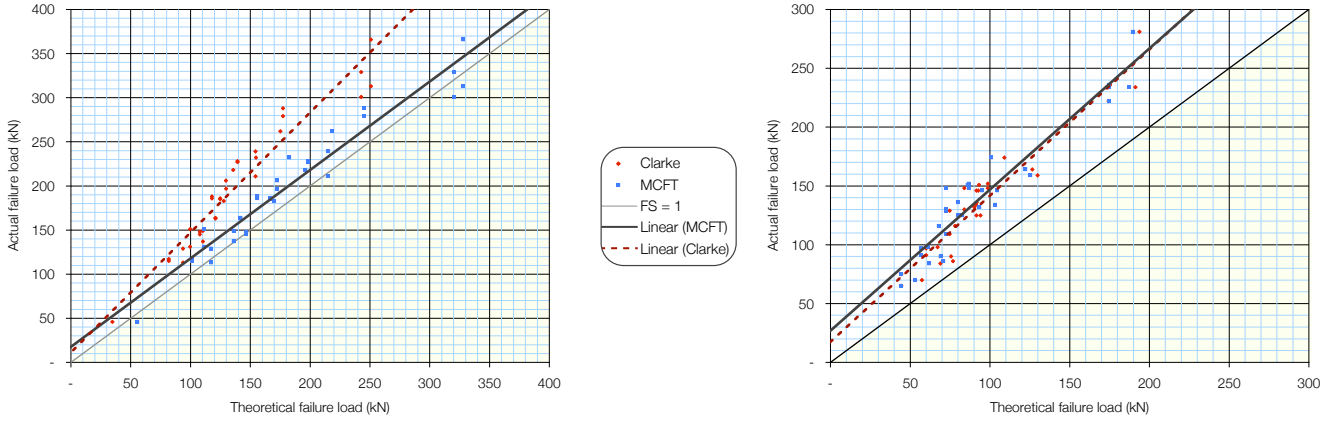

Non-conservative results using MCFT are highlighted by considering test specimen 44 (see Clarke, 1993). Here, the same section has been tested twice, and so the MCFT prediction for failure in shear remains the same for both tests (*320.4kN*). The experimental data yields failure loads of *301kN* and *329kN*, giving factors of *0.94* (unsafe) and *1.03* (just safe) on the MCFT analysis. Partial safety factors would be introduced in any codified design procedure to ensure that the predicted failure load remains safe.

Non-shear reinforced sections are also analysed, Figure 6.43(r), and again good correlation with experimental data is seen, although both MCFT and BS5400 approaches are quite conservative. The MCFT method appears to be a step in the right direction for the development of a uniform and easily applied approach to the design of members in shear. Full analysis data is presented in Appendix 4.

## 6.10. Summary

The analysis of circular sections in shear is more complex than for their rectangular counterparts. The analysis presented in §6 has shown that through geometry considerations formulae for circular sections in shear can be developed. Two truss models have been analysed, and equilibrium has been considered by applying an additional tensile force, $\Delta F$, to their compression and tension chords. A logical approach to the crushing analysis of circular sections has been presented, although experimental verification is required. The crushing approach (§6.5) may be overly conservative for spirally bound sections, where the reinforcement pitch is not considered (Eq. 6.37). Justification for the use of Eq. 4.12 in circular sections requires experimental work, as this considerably increases $V_{Rd,max}$ predictions for spirally bound sections (see also Spreadsheet 6.6).

Initial results appear to suggest that the concrete contribution is significant in circular sections (Figure 6.4(r)). This is a potentially important consideration, as other work has suggested that the flattest truss angle in BS EN 1992-1-1 more than accounts for the loss of a concrete contribution in rectangular sections. Analytical accuracy in BS EN 1992-1-1 is also more dependent on the value chosen for $f_{yk}$ than in BS5400-4 (§6.3.2). Furthermore, differences between BS5400-4 and BS EN 1992-1-1 approaches can become significant as section diameter or link spacing is increased (fewer links intersected). The concrete contribution in BS5400-4 tended to 'dampen' the influence of the stirrups; while in BS EN 1992-1-1 appreciable step changes in capacity predictions occur when fewer links are intersected.

The work undertaken in analysing the variable angle truss model is summarised in Figure 6.44 for closed and spirally bound circular sections. It is hoped that this provides a valid, logical and simple to implement extension to the Eurocode approach for the design of concrete sections in shear. The use of a flatter truss angle ($cot(\theta)>2.5$) could potentially be introduced to improve analytical results, perhaps following the DIN EN 1992-1-1 model where the truss angle has an upper limit of $cot(\theta) = 3.0$ ($18^o$).

*Figure 6.44: A truss model for circular sections. Closed links (l); Spirals (r).*

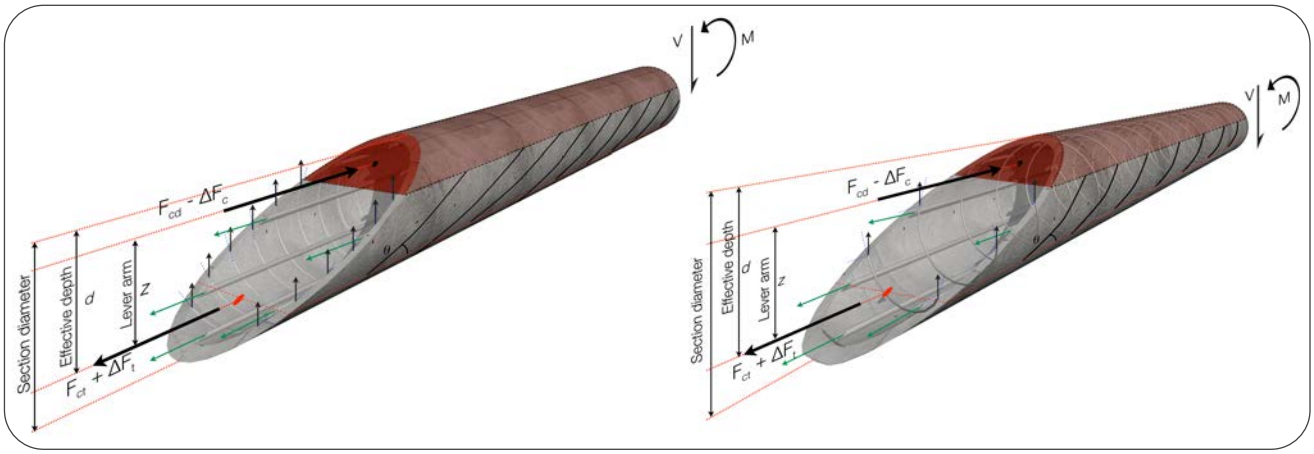


Following from work by Nielsen, an upper bound plasticity approach has been introduced and has yielded good results with a simple analysis method. The MCFT approach has also been analysed and whilst good correlations to the available experimental data have been found, this method is unlikely to be implemented in the Eurocodes in the near future. The design of non-shear reinforced sections has been considered, with comparisons drawn to the current BS5400-4 approach.

Consideration has also been given to the economics of design to the Eurocodes, and scope for further study has been identified throughout this chapter. It is hoped that more time and analysis will be given to the development of the methods presented in this dissertation before the introduction of BS EN 1992-1-1 in 2010. Concluding remarks and a set of design equations (to be read in conjunction with BS EN 1992-1-1) are presented in §7.

# 7. Conclusions

## 7.1. Conclusions

The design of concrete in shear is more complex and less well understood than flexural design. For over a century, the truss analogy has provided a simple and effective design method based on the lower bound theorem of plasticity. The 45º-truss analogy used in existing design codes requires the use of an empirically based '*concrete contribution*' to match analytical results to experimental data. The Eurocode model for shear uses a more theoretically consistent variable angle model, which assumes that once cracked the concrete provides no shear capacity. §7 presents a set of equations for the design of circular sections in shear using the variable angle truss model, which are intended to be adopted in future revisions of BS EN 1992-1-1.

Writing the new European design code has been a massive undertaking and it is well worth considering Walraven (2004) and Virlogeux (1999) who agree that new codes should be '*based upon clear and scientifically well founded theories… corresponding to a good representation of structural behaviour*' (Walraven, 2005, p. 46). Einstein (1933, p.163) said: *'It can scarcely be denied that the supreme goal of all theory is to make the irreducible basic elements as simple and as few as possible without having to surrender the adequate representation of a single datum of experience'*. In flexural design, both of these statements are, in general, satisfied by the Eurocode approach. However, the simplification of shear to a truss model arguably fails to recognise the complex nature of shear in concrete.

It should be recognised there exist more consistent and valid design approaches for concrete in shear, and that the balance between validity and simplicity is complex, depending greatly on the level of reliability and accuracy required of a specific analysis. The great advantage of the truss model is its transparency and ease of application, which allows expedient design of concrete elements that would not benefit from a more complex finite element or MCFT based analysis. Historically, analysis has relied on simplifications to save time, but with the widespread use of computer analysis, methods such as MCFT are now far more accessible. That said, the ability to verify a method by hand remains crucial to the implementation of proper and safe structural design.

## 7.2. Design equations - Stirrups

After consideration of the design approaches seen in §6, the method of Turmo et al. (2008) is presented for the design of circular sections. Dimensions used in the following are described in Figure 7.1. Where current BS EN 1992-1-1 equations and clauses are used, they will be referred to in bold type.

*Figure 7.1: Circular section dimensions, vertical links (left); spiral reinforcement (right).*

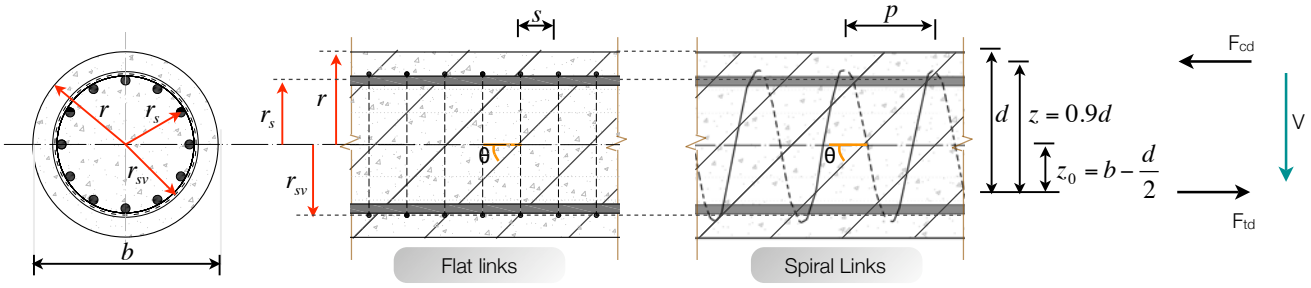


| | | | | | |
|---|---|---|---|---|---|
| $r$ | = section radius; | $r_{sv}$ | = radius to shear reinforcement; | $z$ | = the lever arm for a member with constant depth; |
| $r_s$ | = radius to longitudinal steel; | $s$ | = stirrup spacing; | $z_0$ | = lever arm from centroid of tension steel to section centroid of area |
| $d$ | = effective depth (Eq. 5.1); | $\theta$ | = concrete strut angle; | $p$ | = pitch of spiral stirrups. |

### 7.2.1. Members requiring shear reinforcement (*BS EN 1992-1-1, cl.6.2.3*).

In regions where the design shear force in the section from external loads ($V_{Ed}$) is greater than the unreinforced section capacity ($V_{Rd,c}$, §7.2.2), shear reinforcement should be provided such that $V_{Ed} \leq V_{Rd,s}$. $V_{Rd,s}$ (the design value of shear force sustained by yielding of shear reinforcement) may be given by Eq. 7.1, with $\theta$ limited by **Eq.(6.7N)**. $\theta$ may be found by equating Eq. 7.1 and Eq. 7.5, and only in sections with high design shear stresses will *cot(θ)* be less than *2.5*. Eq. 7.1 covers all possible design situations for circular columns requiring shear reinforcement, with variables as defined in Table 7.1 below.

$$V_{Rd,s} = \lambda_1 \lambda_2 \frac{A_{sw}}{s} z f_{ywd} \cot\theta \qquad \text{Eq. 7.1}$$

*Table 7.1: Variables for closed and spirally reinforced circular columns.*

| Variable | Closed Stirrups | Spirals |
|---|---|---|
| $\lambda_1$ | $\lambda_1$ = 0.85 (in general), or:<br>$\lambda_1$ = values in Table 6.2 for more detailed analysis. | $\lambda_1$ = 0.85 (in general), or:<br>$\lambda_1$ = values in Table 6.2 for more detailed analysis. |
| $\lambda_2$ | 1.0 | $\lambda_2 = \left(\left(p/2\pi r_{sv}\right)^2 + 1\right)^{-0.5}$ Eq. 7.2 |
| $s$ | Stirrup spacing | Spiral pitch (or $p$ in Eq. 7.2) |
| $A_{sw}$ | Area of transverse reinforcement | |
| $z$ | $z = 0.9d$ Eq. 7.3 | |
| $d$ | Effective depth, $d = r + \left(2r_s/\pi\right)$ Eq. 7.4 | |
| $f_{ywd}$ | Design yield strength of the shear reinforcement, as defined in BS EN 1992-1-1. | |

*Figure 7.2: Effectiveness of design equations for circular sections.*

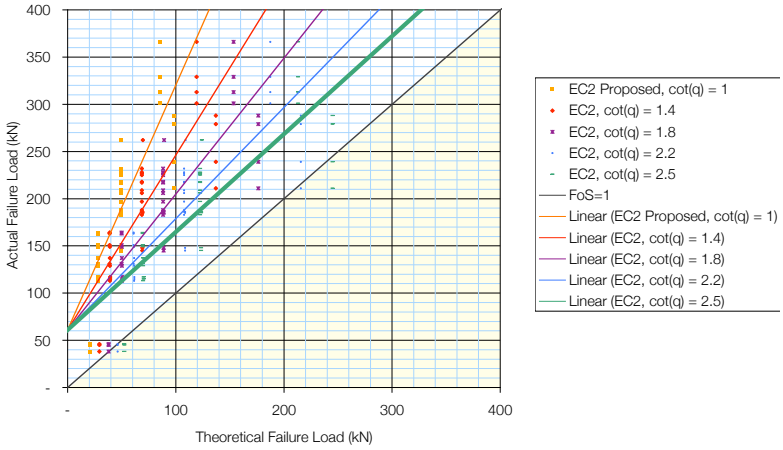


*Table 7.2: Analysis for Eq. 7.1.*

| cot(θ) | Average $V_a/V_{th}$ | Standard deviation |
|---|---|---|
| 1 | 3.77 | 1.19 |
| 1.4 | 2.69 | 0.85 |
| 1.8 | 2.10 | 0.66 |
| 2.2 | 1.71 | 0.54 |
| 2.4 | 1.57 | 0.50 |
| **2.5** | **1.51** | **0.48** |

Experimental data analysed: Clarke (1993)
For general design, cot(θ) = 2.5, unless geometry or loading dictates otherwise.

A final analysis of Eq. 7.1 is shown in Figure 7.2 and Table 7.2, for the data presented in Clarke (1993), using $f_{yk}$ = *500MPa* (see §6.3.2). The full range of *cot(θ)* is shown, and the recommended value for general design of *cot(θ) = 2.5* provides good accuracy, a suitable factor of safety and has a degree of scatter comparable to other shear analyses.

### 7.2.2. Members not requiring shear reinforcement (*BS EN 1992-1-1, cl.6.2.2*).

In regions where calculated shear reinforcement is unnecessary ($V_{Rd,c} \geq V_{Ed}$), shear capacity may be calculated as given in **Eq.(6.2a)** and **Eq.(6.2b)**. Enhancement may be applied as per **cl.6.2.2(6)**, **Eq.(6.5)** and **Eq.(6.6N)**. Detailing clauses also apply to the design of circular sections (**cl. 9.5.3**).

### 7.2.3. Additional tensile force (*BS EN 1992-1-1 cl.6.2.3(7)*).

The additional tensile force must be applied to circular sections. This additional force should be divided between the longitudinal tension bars in accordance with their geometrical arrangement as described in §6.4 and Figure 6.13.

## 7.3. Design Equations – Crushing

In general, crushing of the compression struts will not be a critical consideration for circular sections if suitable member sizes are chosen during scheme design. The circular section may be analysed by considering an equivalent rectangular section, Eq. 7.5, Figure 7.3 and Table 7.3. No crushing failures are recorded in available test data, making this approach unverified. An iterative approach is required to determine the correct value for ω. Spirally bound sections are considered in Spreadsheet 6.6.

*Figure 7.3: Equivalent rectangle section definitions for Eq. 7.5.*

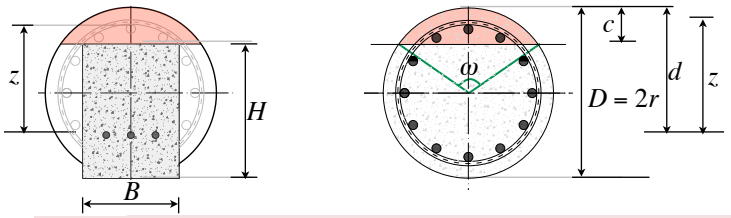


$$\left(\omega - \sin\omega\right) = \frac{2A_c}{r^2} \qquad A_c =$$

$$\cos\left(\frac{\omega}{2}\right) = \left(\frac{r-c}{r}\right) \qquad c = r\left(1 - \cos\left(\frac{\omega}{2}\right)\right)$$

$$V_{Rd,\max} = \frac{\alpha_{cw} B_w z v_1 f_{cd}}{\cot\theta + \tan\theta} \qquad \text{Eq. 7.5}$$

*Table 7.3: Variables for Eq. 7.5.*

| Variable | | | |
|---|---|---|---|
| $\alpha_{cw}$ | 1.0 for non-prestressed structures (defined in NA to BS EN 1992-1-1). | | |
| $B_w$ | = width of the effective rectangular section, $B_w = \left(\pi r^2 - 0.5r^2(\omega - \sin\omega)\right)\Big/(D-c)$ Eq. 7.6<br>Where $r$ = section radius; $\omega$ = angle to compression chord; $D$ = section diameter; $c$ = depth of compression chord (see Figure 7.3).<br>Alternatively, a sensible initial value for $B_w$ may be taken as **0.8D**, determined from analysed test data. | | |
| $z$ | Lever arm, as defined by Eq. 7.3 | | |
| $f_{cd}$ | Design value of the concrete compressive capacity. $f_{ck}$ not to be taken as > C50/60 grade (NA to BS EN 1992-1-1, Table 3.1N (**cl.3.1.2(2)P**). | | |
| $\theta$ | $1 \le cot(\theta) \le 2.5$ | **BS EN 1992-1-1** | **6.7N** |

## 7.4. Further Work

The design of members in shear has long been based on empirical data. Tests on circular sections under static loading are relatively rare and more work is required to properly verify the above equations. To retain confidence in the truss analogy for circular sections, there must be sufficient experimental data to validate it. Potential extensions to this dissertation may therefore include:

- Extension of upper bound plastic analysis to bi-linear and curved failure surfaces, utilising C++ or similar;
- Experimental work on web crushing failures in circular sections;
- Feasibility study into use of MCFT for design in BS EN 1992-1-1;
- Economic considerations and lowest cost design comparisons with BS5400-4;
- Experimental work to better determine the effect of axial load in shear reinforced columns;
- Verification of shear enhancement in circular sections;
- Shear response of high strength and fibre reinforced sections with and without shear reinforcement.

Compression field theory has provided the best analytical results for circular sections, §6.9, but incorporating the MCFT method into a Eurocode model would be a huge change in design procedure. Aside from its theoretical benefits, perhaps the best reason for adopting MCFT is that no European country currently uses it, negating any discussion over which national code clauses to incorporate. A change such as this will not come until well after the introduction of the current Eurocode in 2010.

## 7.5. Summary

The design equations presented above are the result of an analysis of the principals behind shear behaviour in concrete. By considering the underlying theories (§2), worldwide design codes (§3), Eurocode design approaches (§4) and current research areas (§5), an understanding of shear in circular sections has been developed. From this, lower bound truss equations have been formed for inclusion into BS EN 1992-1-1. The great advantage of the Eurocode approach to shear design is its ease of use and transparency in application; the equations presented here are intended to continue this as much as possible. Equilibrium considerations have led to the development of a new approach to determine the additional tensile force, $\Delta F$, in circular sections (§6.4). New equations for crushing are also presented, but require experimental verification. An upper bound approach for the analysis of circular sections has been introduced and yields consistent results, and opportunities to extend this method of analysis have been highlighted.

Throughout this dissertation, issues arising in the Eurocode design model have been identified, and are summarised below:

- The compression zone contribution to shear strength is not satisfactorily considered in the truss model;
- The design of shear reinforcement is, to a large degree, insensitive to concrete strength;
- The application of axial load has the potential to increase design stirrup requirements;
- Crushing in irregular sections is not addressed (although it may be difficult to achieve this failure mode).

The design formulae presented in §7 are intended to allow the safe design of both closed and spirally bound circular sections to the Eurocode model, but care must be taken in assumptions made for the lever arm, $z$. Further investigation is required before the true behaviour of a circular section in shear can conclusively be determined. More complex design methods also provide valid results, and may be used to verify a Eurocode based analysis.

The introduction of the Eurocodes and the variable angle truss model will change the way that shear design is approached for concrete structures. This dissertation has shown that the variable angle model can be applied with confidence to circular sections. Whilst further experimental work is recommended, it is hoped that the analysis undertaken in this dissertation will help to shape and inform future UK design practice.

# 8. Appendices

## 8.1. Introduction

The space constraints of this document necessitate that full data tables cannot be published here. Full tables are found at the relevant website addresses as listed alongside each section, and on the accompanying CD.

## 8.2. Appendix 1 – Capon and de Cossio (1966)

See http://people.bath.ac.uk/jjo20/d_a/

## 8.3. Appendix 2 – Clarke and Birjandi (1993)

See http://people.bath.ac.uk/jjo20/d_a/

## 8.4. Appendix 3 - Collins test data

See http://people.bath.ac.uk/jjo20/d_a/

## 8.5. Appendix 4 – MCFT analysis results

See http://people.bath.ac.uk/jjo20/d_a/

Also included on the CD are the relevant Response 2000 analysis files.

## 8.6. Appendix 5 – MCFT Design Equations

Full design equations are presented below, from Collins (2002), to be read in conjunction with §3.4.2.

*Figure 8.1: MCFT Design equations*

Average stresses

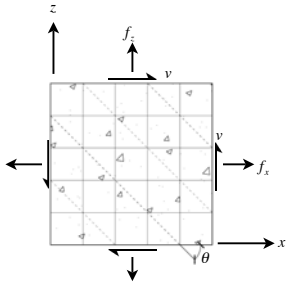


$$f_x = \rho_x f_{sx} + f_1 - v\cot\theta \quad (1)$$

$$f_z = \rho_z f_{sz} + f_1 - v\tan\theta \quad (2)$$

$$v = (f_1 + f_2)/(\tan\theta + \cot\theta) \quad (3)$$

Average strains

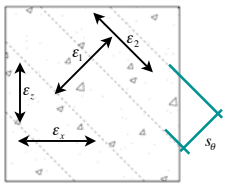


$$\tan^2\theta = \frac{\varepsilon_x + \varepsilon_2}{\varepsilon_z + \varepsilon_2} \quad (6)$$

$$\varepsilon_1 = \varepsilon_x + \varepsilon_z + \varepsilon_2 \quad (7)$$

$$\gamma_{xz} = 2(\varepsilon_x + \varepsilon_2)\cot\theta \quad (8)$$

Stress-strain relationships

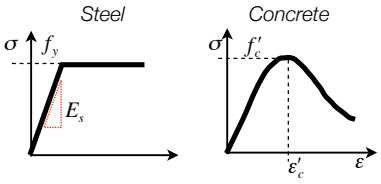


Reinforcement:

$$f_{sx} = E_s\varepsilon_x \le f_{yx} \quad (11)$$

$$f_{sz} = E_s\varepsilon_z \le f_{yz} \quad (12)$$

Concrete:

$$f_2 = \frac{f'_c}{0.8 + 170\varepsilon_1}\left[2\frac{\varepsilon_2}{\varepsilon'_c} - \left(\frac{\varepsilon_2}{\varepsilon'_c}\right)^2\right] \quad (13)$$

$$f_1 = 0.33\sqrt{f'_c}\,/\left(1 + \sqrt{500\varepsilon_1}\right) \quad (14)$$

Shear stress on crack:

$$v_{ci} \le \frac{0.18\sqrt{f'_c}}{0.31 + \frac{24w}{a_g + 16}} \quad (15)$$

Stresses at cracks

$$f_{sxcr} = \left(f_x + v\cot\theta + v_{ci}\cot\theta\right)/\rho_x \quad (4)$$

$$f_{szcr} = \left(f_z + v\tan\theta - v_{ci}\tan\theta\right)/\rho_z \quad (5)$$

Crack widths

$$w = s_\theta\varepsilon_1 \quad (9)$$

$$s_\theta = 1/\left(\frac{\sin\theta}{s_x} + \frac{\cos\theta}{s_z}\right) \quad (10)$$

# 9. Bibliography


| | |
|---|---|
| AASHTO LRFD, 2004 | *Bridge Design Specifications and Commentary*. 3rd Edition, American Association of State Highway Transportation Officials, Washington, D.C. |
| ACI 318-99 | *Building Code Requirements for Structural Concrete (1999).* ACI International. |
| ACI 318R-99 | *Commentary on Building Code Requirements for Structural Concrete (1999).* ACI International. |
| ACI-ASCE COMMITTEE 326, 1962 | Shear and Diagonal Tension. *ACI Journal Proceedings*. 59(1) pp. 1-30; (2), pp. 277-334; and (3), pp,. 352-396 |
| ACI-ASCE COMMITTEE 426, 1973 | Shear Strength of Reinforced Concrete Members (ACI 426R-74). *Proceedings, ASCE*.99(ST6), June 1973, pp. 1148-1157. |
| AMBROSE, J., TRIPENY, P., 2007 | *Simplified Design of Concrete Structures*. 8th Ed. John Wiley and Sons. |
| BA44/96 | *The Assessment of Concrete Highway Bridges and Structures.* Highways Agency, 1996 |
| BATCHELOR, W. G., BEEBY, A. W., 1989 | *Charts for the design of circular columns to BS 8110.* Berkshire: British Cement Association |
| BAZANT, P. Z., KAZEMI, M. T., 1991 | Size effect on diagonal shear of beams without stirrups. *ACI Structural Journal* 88(3) pp.268–274. |
| BAZANT, P. Z., 1993 | Scaling laws in mechanics of failure. *Journal of Engineering Mechanics*. 119(9) pp.1828 - 1844 |
| BD42/00 | *Design manual for roads and bridges: design of embedded retaining walls and bridge abutments.* HMSO, 2000 |
| BD44/95 | Highways Agency, 1995. *Design manual for roads and bridges: The assessment of concrete highway bridges and structures.* HMSO. |
| BD74/00 | *Design manual for roads and bridges: foundations.* HMSO, 2000 |
| BEEBY, A. W., 2000 | Editorial: codes of practice and model codes. Structural Concrete, 2000, 1, No. 3, 117–118. |
| BENTZ, E. C., 2000 | *Sectional Analysis of Reinforced Concrete Members*. PhD Thesis, Department of Civil Engineering, University of Toronto |
| BENTZ, E. C., 2006 | *Response-2000 References* [online]. Toronto: University of Toronto. Available from http://www.ecf.utoronto.ca/~bentz/refer.shtml (accessed 10/12/08) |
| BENTZ, E. C., VECCHIO, F. J., COLLINS, M. P., 2006 | Simplified compression field theory for calculating shear strength of reinforced concrete elements. *ACI Structural Journal*. 103-S65 pp. 614-624. |
| BHAL, N. S., 1968 | *Über den Einfluss der Balkenhöhe auf die Schubtragfähigkeit von einfeldrigen Stahlbetonbalken mit und ohne Schubbewehrung*. Dr. Ing. Thesis, University of Stuttgart, pp124. |
| BRESLER, B., PISTER, K., 1958 | Strength of concrete under combined stresses. *ACI Journal*. 55(3) pp.321-345. |
| BROOMFIELD, J., 1996 | *The Repair of Reinforced Concrete*. The Building Conservation Directory, 1996 [online]. Available from http://tinyurl.com/cw6h7e (Accessed 24/01/09). |
| BROWN, M. D., BAYRAK, O., JIRSA, J. O., 2006 | Design for Shear Based on Loading Conditions. *ACI Structural Journal.* 104(4) pp541-550. |
| BS EN 1992-1-1:2004 | *Eurocode 2. Design of Concrete Structures. Part 1: General Rules and Rules for Buildings*. |
| BS EN 1998-1:2004 | *Eurocode 8 - Design of structures for earthquake resistance. General rules, seismic actions and rules for buildings.* BSI |
| BS5400-4:1990 | *Steel concrete and composite bridges - Part 4:* |
| BS8004:1986 | *Code of practice for foundations - (formerly CP2004).* BSI |
| BS8110-1:1997 | *Structural Use of Concrete - Part 1: Code of Practice for design and construction.* BSI |
| BS8110-3:1985 | *Structural Use of Concrete - Part 3: Design charts for singly reinforced beams, doubly reinforced beams and rectangular columns.* BSI |
| BUCKINGHAM, E., 1914 | On physically similar systems; illustrations of the use of empirical equations. *Physical Review.* 2IV(4) pp 345-376. |
| BUCKINGHAM, E., 1915 | Model experiments and the form of empirical equations. *ASME*. 37, pp. 263-196 |
| CALLADINE, C. R., 1969 | *Engineering Plasticity*. Oxford: Pergamon Press. |
| CAPON, M. J. F., DE COSSIO, R. D., 1966 | Diagonal tension in concrete members of circular section. *Foreign Literature Study No.466*, Portland Cement Association, Illinois. Originally published in *Ingenieria*, April 1965. |
| CHAI, Y. H., PRIESTLEY, M. J. N., SEIBLE, F., 1990 | Retrofit of bridge columns for enhanced seismic performance. *In: Proceedings of the first US-Japan workshop on seismic retrofit of bridges*. Tsukuba (Japan): Public works Research Institute; p. 321–40. |
| CHANA, P. S., 1988 | Analytical and experimental studies of shear failures in reinforced concrete beams. *Proceedings of the Institution of Civil Engineers*. 85(4) pp.609-628. |
| CIEG, 2008 | *FAQ – Eurocode 2* [online]. Available from http://tinyurl.com/dlsmex (Accessed 03/03/09) |
| CLADERA, A., MARI, A. R., 2004a | Shear design procedure for reinforced normal and high strength concrete beams using artificial neural networks. Part I: beams without stirrups. *Engineering Structures* 26 (2004) pp. 917-926 |
| CLADERA, A., MARI, A. R., 2004b | Shear design procedure for reinforced normal and high strength concrete beams using artificial neural networks. Part II: beams with stirrups. Engineering Structures 26 (2004) pp. 927-936 |
| CLADERA, A., MARI, A. R., 2007 | Shear strength in the new Eurocode 2. A step forward? *Structural Concrete.* 8(2), pp. 57-66 |
| CLARKE, J. L., 1987 | Shear capacity of high strength concrete beams. *Concrete.* 21(3) pp.24-26. |
| CLARKE, J., BIRJANDI, F., 1993 | The behaviour of reinforced concrete columns in shear. *The Structural Engineer,* 71(5), pp73-81. |
| COLLINS, M. P., 1978 | Towards a Rational Theory for RC Members in Shear. *Proceedings of ASCE.* 104(4) pp.649-666. |
| COLLINS, M. P., MITCHELL, D., ADEBAR, P., VECCHIO, F. J., 1996 | A General Shear Design Method. *ACI Structural Journal*. 93(1) pp 36-45. |
| COLLINS, M. P., BENTZ, E. C., 2002. | *Shear Strength of Circular Reinforced Concrete Columns*. ACI Special Publication SP197-03. |
| COLLINS, M. P., MITCHELL, D., BENTZ, E. C., 2008 | Shear Design of Concrete Structures. *The Structural Engineer*. 86(10) pp32-39. |
| CP110: PART 3: 1972 | *Structural use of concrete - Part 3: Design charts for elements.* BSI |
| CP110:PART 1:1972 | *Structural use of concrete - Part 1: Design, materials and workmanship.* BSI |
| CSA COMMITTEE A23.3, 2004 | *Design of Concrete Structures (CSA A23.3-04*). Canadian Standards Association: Mississauga. |
| CSA S6-06 | *CAN/CSA-S6-06, Canadian Highway Bridge Design Code*. Canadian Standards Association: Mississauga. |
| CSA S6-06-R | *Commentary on CAN/CSA-S6-06, Canadian Highway Bridge Design Code*. Canadian Standards Association: Mississauga. |
| DD ENV 1992-1-1:1992 | *Eurocode 2. Design of Concrete Structures. Part 1: General Rules and Rules for Buildings.* BSI |
| DE COSSIO, R. D., ROSENBLUETH, E., 1961 | Reinforced Concrete Failures During Earthquakes. *Journal of the American Concrete Institute.* 58(11) pp571-590 |
| DS411, 1984 | Code of Practice for the Structural Use of Concrete (in Danish). Denmark: Danskbyggeri. |
| DUTHINH, D., CARINO, N. J., 1996 | *Shear Design of Concrete Beams: A review of the state of the art.* Gaithersburg: Building and Fire Research Laboratory |
| EINSTEIN, A., 1933 | *On the Method of Theoretical Physics.* The Herbert Spencer Lecture, published in *Philosophy of Science,*1(2) pp. 163-169. |
| FELTHAM, I., 2004 | Shear in reinforced concrete piles and circular columns. *The Structural Engineer*. 84(11) pp.27-31 |
| FIB, 2007 | *fib bulletin 40: FRP reinforcement for concrete structures.* Fédération internationale du béton: Task Group 9.3. |
| FRITZ, C., NAAMAN, A. E., REINHARDT, D.H.W., 1992. | *Sifcon Matrix in RC Beams*. Proceedings of the RILEM-ACI International Workshop, held June 23-26, 1991, Mainz, Germany; Ed. by H. W. Reinhardt and A. E. Naaman, E & FN Spoon, London, pp. 518-528. |
| GHEE, A. B., PRIESTLEY, M. J. N., PAULAY, T., 1989 | Seismic Shear Strength of Circular Reinforced Concrete Columns. *ACI Structural Journal.* 86(6) pp. 45-59 |
| GUPTA, P. R., COLLINS, M. P., 2001 | Evaluation of Shear Design Procedures for Reinforced Concrete Members under Axial Compression. *ACI Structural Journal*. 98(4) pp. 537-547 |
| HANSON, J. M., HULSBOS, C. L., 1964 | Ultimate shear tests of prestressed concrete I-beams under concentrated and uniform loadings. *Prestressed Concrete Institute – Journal.* 9(3), pp.15-28 |
| HAWKINS, N.M., KUCHMA, D. A., MAST, R. F., MARSH, M. L., REINECK, K-H., 2005 | *NCHRP Report 549: Simplified Shear Design of Structural Concrete Members.* Transportation Research Board: Washington DC. |
| IBELL, T. J., 1992 | *Behaviour of anchorage zones for prestressed concrete.* PhD Thesis. Cambridge: University of Cambridge |

| | |
|---|---|
| IBELL, T. J., MORLEY, C. T., MIDDLETON, C. R., 1997 | A plasticity approach to the assessment of shear in concrete beam and slab bridges. *The Structural Engineer.* 75(19) pp 331-338 |
| JACKSON, P., SALIM, S. W., 2006 | Web crushing in EN 1992. *The Structural Engineer.* 84(23) pp.50-57 |
| JOHNSON, O. M., COUTURE, A., 2007 | *Commission of Inquiry into the Collapse of a Portion of the de la Concorde Overpass: Report*. Quebec: Government of Quebec. |
| JSCE, 1986 | *Specification for Design and Construction of Concrete Structures: Design, JSCE Standard, Part 1*. Japan Society of Civil Engineers: Tokyo |
| KANI, G. N., 1964 | The Riddle of Shear Failure and its Solution. *Journal of the American Concrete Institute.* 61(4) pp441-468 |
| KANI, G. N., 1967 | How safe are our large reinforced concrete beams? *ACI Structural Journal* 64(3) pp.128-141 |
| KHALIFA, J. U., COLLINS, M. P., 1981 | Circular reinforced concrete members subjected to shear. *University of Toronto, Department of Civil Engineering, Publication 81-08*, December 1981. |
| KIM, J. H., MANDER, J. B., 2005 | Theoretical shear strength of concrete columns due to transverse steel. *Journal of structural engineering.* 131(1) pp 197-199. |
| KIM, J. H., MANDER, J. B., 2007 | Kim, J.H., Mander, J. B., 2007. Influence of transverse reinforcement on elastic shear stiffness of cracked concrete elements. *Engineering Structures*. 29(2007) pp.1798-1807 |
| KOTSOVOS, M. D., 1983 | Effect of testing techniques on the post-ultimate behaviour of concrete in compression. *Materials and Structures*. RILEM 16(91) pp.3-12 |
| KOTSOVOS, M. D., 1988 | Compressive Force Path Design: Basis for Reinforced Concrete Ultimate Limit State Design. *ACI Structural Journal*. 85(1) pp. 68-75. |
| KOTSOVOS, M. D., LEFAS, I. D., 1990 | Behaviour of RC Beams Designed in Compliance with the Concept of Compressive-Force Path. *ACI Structural Journal* 87(S14) pp.127-139 |
| KOTSOVOS, M. D., NEWMAN, J. B., 1981 | Fracture mechanics and concrete behaviour. *Magazine of Concrete Research*. 33/115, pp. 103-112 |
| KOTSOVOS, M. D., PAVLOVIC, M. N., 1995 | *Structural concrete: finite element analysis for limit-state design*. London: Thomas Telford. |
| KOTSOVOS, M. D., PAVLOVIC, M., 2001 | The 1999 Athens earthquake: Causes of damage not predicted by structural-concrete design methods. *The Structural Engineer*. 79(15) pp.23-29. |
| KOTSOVOS, M. D., PAVLOVIC, M., 2004 | Size effects in beams with small shear span-to-depth ratios. *Computers and Structures* 82(2004) 143-156 |
| KOTSOVOS, M. D., PAVLOVIC, M., 2006 | Shortcomings of code methods for shear design of RC structures and the possible role of fibres. *The Structural Engineer*. 84(23) pp.44-49 |
| KOWALSKY, M. J., PRIESTLEY, M. J. N., 2000 | Improved Analytical Model for Shear Strength of Circular Reinforced Concrete Columns in Seismic Regions. *ACI Structural Journal*. 97(42) pp 388 – 396. |
| KOWALSKY, M. J., PRIESTLEY, M. J. N., SEIBLE, F., 1995 | *Shear behaviour of lightweight concrete columns under shear seismic conditions.* Structural Systems Research Project Report 95/10. California: University of California. |
| KUPFER, H., 1962 | *Erweiterung der Mörschschen Fachwekanalogie mit Hilfe des prinzips vom Minimum der Formänderungsarbeit*. In: Nach einem Vortrag auf fem Schub-Kolloquium. Stuttgart. |
| KUPFER, H., HILSDORF, H. K., 1969. | Behaviour of Concrete under Biaxial Stresses. *ACI Structural Journal*. 66-52, pp. 656 - 666. |
| LAMBERT, P., 2002 | *Reinforced Concrete – History, Properties and Durability.* Surrey: Corrosion Prevention Association. |
| LEONHARDT, F., 1970 | Shear and Torsion in Prestressed Concrete. *Proceedings 6th FIP Congress,* Prague: June 1970. |
| LEONHARDT, F., WALTHER, R., 1961 | Contribution to the Treatment of Shear Problems in Reinforced Concrete. *Beton- und Stahlbetonbau* (Berlin). 56(12). |
| MACGREGOR, J. G., HANSON, J. M., 1969 | Proposed Changes in Shear Provisions for Reinforced and Prestressed Concrete Beams. *ACI Journal Proceedings*. 66(4) , pp. 276-288 |
| MANDER, J. B., CHENG, C. T., 1995 | Renewable hinge detailing for bridge columns. In: *Proceedings of pacific conference on earthquake engineering.* p. 197–206 |
| MANDER, J. B., KIM, J. H., LIGOZIO, C. A., 1996a | Seismic performance of a model reinforced concrete bridge pier before and after retrofit. *Technical report NCEER-96-0009*. New York: National Center for Earthquake Engineering Research, State University of New York at Buffalo. |
| MANDER, J. B., MAHMOODZADEGAN, B., BHADRA, S., CHEN, S. S., 1996b | Seismic evaluation of a 30-year old non-ductile highway bridge pier and its retrofit. *Technical report NCEER-96-0008*. New York: National Centre for Earthquake Engineering Research, State University of New York at Buffalo; |
| MINELLI, F., VECCHIO, F. J., 2006 | Compression field modelling of fibre reinforced concrete members under shear loading. *ACI Structural Journal.* 103(2) pp.244-252 |
| MITCHELL, D., COLLINS, M. P., 1974 | Diagonal Compression Field Theory - A Rational Model for Structural Concrete in Pure Torsion. *ACI Structural Journal.* 71(8) pp.396-508 |
| MÖRSCH, E., 1908 | *Der Eisenbeton, seine Theorie und Anwendung* (Reinforced Concrete, theory and practical application. Stuttgart: Wittwer. |
| MOHAMMAD, F. A., MERRONY, B., 1995 | Design charts for reinforced circular concrete columns in accordance with Eurocode 2. *Proceedings of the Institute of Structural Engineers*. 110, pp. 410-416. |
| MORETTI, M. L., TASSIOS, T. P., 2006 | Behaviour and Ductility of Reinforced Concrete Short Columns Using Global Truss Model. *ACI Structural Journal.* 103(3) pp.319-327. |
| NA TO BS EN 1992-1-1:2004 | *UK National Annex to Eurocode 2: Design of concrete structures - Part 1-1: General rules and rules for buildings.* BSI |
| NAGATO, Y., 1990 | Shear strength of reinforced concrete members with circular cross-section, *Federal University of Rio de Janeiro.* |
| NARAYANAN, R. S., BEEBY, A., 2005 | *Designers' Guide to EN1992-1-1 and EN1992-1-2. Eurocode 2: Design of concrete structures. General rules and rules for buildings and structural fire design.* London: Thomas Telford |
| NIELSEN, M. P., 1984 | *Limit Analysis and Concrete Plasticity*. New Jersey: Prentice Hall |
| NZS 3101:1982 | *Code of practice for the design of concrete structures.* Standards Association of New Zealand. |
| PARK, R., PAULAY, T., 1975 | *Reinforced Concrete Structures.* USA: John Wiley and Sons. |
| PD 6687: 2006 | *Background paper to the UK National Annexes to BS EN 1992-1*. BSI |
| POPOV P. P., BALAN, T. A., 1998 | *Engineering mechanics of solids*. NJ (USA): Prentice Hall |
| PRIESTLEY, M. J. N., SEIBLE, F., VERMA, R., XIAO, Y., 1993 | *Seismic shear strength of reinforced concrete columns. Structural systems research project.* California: University of California. |
| PRIESTLEY, M. J. N., VERMAM R., XIAO, Y.,1994 | Seismic shear strength of reinforced concrete columns. *Journal of Structural Engineering,* 120(8) pp.2310-2329. |
| PRIESTLEY, M. J. N., CALVI, G. M., KOWALSKY, M. J., 2007 | *Displacement based seismic design of structures.* California: IUSS Press. |
| REGAN, P. E., 1993 | Research on shear: a benefit to humanity or a waste of time? *Structural Engineer.* 71(19) pp.337-347 |
| REINECK, K-H., 1991 | Ultimate shear force of structural concrete members without transverse reinforcement from a mechanical model. *ACI Structural Journal*. 88(5) pp.592-602 |
| RITTER, W., 1899 | *Die bauweise hennebique (Construction techniques of Hennebique).* Schweizerische Bazeitung. Zurich. |
| SHAVE, J. D., 2005 | *Shear assessment of concrete bridges: Anchorage effects and use of plasticity*. PhD Thesis. Bath: University of Bath. |
| SPPD, 2003 | University of Washington, 2003. *The Structural Performance Database.* [online]. Available from http://nisee.berkeley.edu/spd (Accessed 03/11/08) |
| STRATFORD, T., 2008 | *The Shear of Concrete with Elastic FRP Reinforcement.* Bath: University of Bath. |
| TALBOT, A. N., 1909 | Tests of Reinforced Concrete Beams: Resistance to Web Stresses Series of 1907 and 1908. *Engineering Experiment Station, Bulletin 29,* Urbana: University of Illinois. |
| TAYLOR, H. P. J., 1970 | *Investigation of the Forces Carried Across Cracks in Reinforced Concrete Beams in Shear by Interlock of Aggregate*. 42(447), Cement and Concrete Association. London: UK. |
| TURMO J., RAMOSB, I., APARICIO, A. C., 2008 | Shear truss analogy for concrete members of solid and hollow circular cross section. *Engineering Structures* doi:10.1016/j.engstruct.2008.09.002 |
| VECCHIO, F. J., COLLINS, M. P., 1986 | The Modified Compression Field Theory for Reinforced Concrete Elements Subjected to Shear. *ACI Structural Journal*. 83(22) pp.219-231 |
| VIRLOGEUX, M., WALRAVEN, J. C., 1999 | *The development of an international codification for structural concrete with the CEB-FIP Model Codes*. Concrete Model Code for Asia, IABSE |
| WAGNER, H., 1929 | Ebene Blechwandtrager mit sehr dunnem Stegblech (Metal beams with very thin webs) *Zeitschrift für Flugtechnik und Motorluftschiffarht.* 20(8-12) |
| WALRAVEN, J. C., 1981 | Fundamental Analysis of Aggregate Interlock, Journal of the Structural Division. *Proceedings of the American Society of Civil Engineering.* 107(11) pp.2245-2269. |
| WALRAVEN, J. C., 2004 | Thinking about codes. *Structural Concrete*, *Journal of the fib*. 5(3) pp.93-100 |
| WALRAVEN, J. C., 2005 | *Towards a new model code for concrete structures.* African Concrete Code Symposium. Delft University of Technology: The Netherlands. |
| WALRAVEN, J. C., 2008 | *Symposium Eurocodes: Backgrounds and Applications.* Brussels, 18-20 February 2008. |
| WITHEY, M. O., 1907 | Tests of Plain and Reinforced Concrete Series of 1906. *Bull. University of Wisconsin, Engineering Series.* 4(1) pp1-66 |
| ZISOPOULOS, P. M., PAVLOVIC, M. N., KOTSOVOS, M. D., 2004 | A contribution to the study of the mechanical properties of plain and fibre-reinforced shotcrete. *Concrete Engineering International,* 8(2), pp. 44-46 |
| ZIA, P., AHMAD, S., LEMING, M., 1994 | *High performance concretes. A state of the art report (1989-1994).* FHWA-RD-97-030, U.S. Department of Transportation. |